ICE ACCRETION ON WIND TURBINE BLADES

ANALYSIS OF HEATING SYSTEMS TO MITIGATE ICE ACCRETION ON WIND TURBINE BLADES

By PETER SUKE, B.ENG.

A Thesis Submitted to the School of Graduate Studies in Partial Fulfilment of the Requirements for the Degree Master of Applied Science in Engineering

McMaster University MASTER OF APPLIED SCIENCE IN ENGINEERING (2014) Hamilton, Ontario

TITLE: Analysis of Heating Systems to Mitigate Ice Accretion on Wind Turbine Blades

AUTHOR: Peter Suke, B.ENG. (McMaster University)

SUPERVISOR: Stephen Tullis, Ph.D

NUMBER OF PAGES: xiv, 115

Abstract

Ice forming on wind turbine blades can cause loading imbalance and reduce power production of the turbine. Heating systems that prevent or remove ice on wind turbine blades are one of the more promising solutions to mitigate ice accretion. Methods to apply heat include direct application through electro-thermal resistance heaters mounted on the external surface of the blade or by indirect heating by forcing hot air through a channel along the leading edge of the blade. Heating systems for aircraft blades have become standardized and in some cases compulsory on aircraft to preserve human life; however, the technology is not directly transferable to the blades on wind turbines. The relative power of the anti-icing or de-icing system is critical to providing a cost benefit of having the system.

This thesis investigates the heat transfer involved for electro-thermal and hot air heating strategies. An appropriate range of operating conditions and blade constructions are considered in order to characterize the effectiveness of both systems. A numerical model is developed to solve the one dimensional, differential heat transfer equations. The heater power required to prevent ice accumulation (anti-icing) on wind turbine blades is determined for electro-thermal heating. Anti-icing with hot air is shown to be unrealistic for a practical range of operating conditions.

The low conductivity of the blade core creates a bottleneck for the de-icing system. It is shown that alternative core materials (Nomex/aluminum honeycomb) can reduce this effect. Electro-thermal and hot air de-icing each have their advantages and cannot be equally compared. In this thesis the suitability of each system has been analysed for a range of operating conditions and wind turbine constructions; the designer can then implement the most suitable strategy for their individual application.

Acknowledgements

I really have to acknowledge my supervisor, Dr. Stephen Tullis for his support and guidance. I would also like to thank the members of my defense committee, Dr. Ching and Dr. Judd for taking their time to review my thesis. To all of the friends that I have made throughout my time at McMaster and to the McMaster Climbing Club for helping me maintain a healthy balance while at Mac. I would especially like to thank Hillary Williamson for persevering by my side through good times and bad. Last but not least, I would like to thank my family for their love and unwavering support. If I failed to mention you, yet you are still taking the time to read the acknowledgements section of my thesis, then I would like thank you as well.

Table of Contents

List of Figures

Table of Tables

Nomenclature

α_1	Collection efficiency of subcooled droplets
α_2	Sticking efficiency of subcooled droplets
α_i	Thermal diffusivity of ice [m^2/s]
α_s	Thermal diffusivity of substrate [m^2/s]
A	Planar area [m^2]
C	Chord length [m]
C_f	Drag coefficient
C_{ice}	Heat capacity of ice [J/kgK]
C_{liq}	Heat capacity of water [J/kgK]
Δh_{fl}	Change in enthalpy [J/kg]
Δt	Time step [s]
ΔT	Temperature difference [K]
δ	Surface roughness [μm]
D_{hyd}	Hydraulic diameter [m]
h_{fl}	Latent heat of fusion [J/kg]
h_{hotair}	Internal heat transfer coefficient [W/m^2K]
h_o	External heat transfer coefficient [W/m^2K]
h_x	Local heat transfer coefficient based on the distance from the leading edge [W/m^2K]

i	Index number
inf	Inflation factor
k	Conductivity [W/mK]
k_h	Conductivity of the hot air [W/mK]
k_{heater}	Conductivity of the heater material [W/mK]
k_{ice}	Conductivity of ice [W/mK]
L	Domain length [m]
L_{blade}	Blade length [m]
L_C	Characteristic length [m]
L_{core}	Core thickness of the blade [m]
L_{conv}	Approximation of ice thickness required for convection to be considered negligible [m]
L_h	Length of heater wrap area [m]
L_{heater}	Heater thickness [m]
L_{ice}	Ice thickness [m]
L_{skin}	Fibreglass skin thickness of the blade [m]
LWC	Liquid water content [g/m^3]
$\dot{m}_{local}$	Mass flow rate of impinging subcooled droplets [kg/s]
n	Freezing fraction of subcooled droplets
N	Number of nodes

Nu_d	The Nusselt number based on a representative cylinder diameter
Nu_h	The Nusselt number on the hot air side of the blade wall
Nu_x	The Nusselt number based on the length from the leading edge
μ	The dynamic viscosity of air [kg/ms]
μ_f	The dynamic viscosity of air based on the film temperature [kg/ms]
Pr	Prandtl number
Pr_h	Prandtl number on the hot air side of the blade wall
Q	Energy density required to melt the adhesion layer of ice [J/m^2]
q''_c	Heat flux due to convection [W/m^2]
$q''_{A/I}$	Heat flux due to convection with the surface temperature specified at 0°C [W/m^2]
q''_f	Heat absorbed due to the release of latent heat of fusion form the impinging droplets [W/m^2]
q''_{min}	Minimum heat flux required for de-icing [W/m^2]
q''_{mod}	Approximation of the heat flux required for convection to be considered negligible [W/m^2]
q''_w	The heat lost from the surface due to the absorption of impinging water droplets [W/m^2]
Re	Reynolds number
Re_C	Reynolds number based on chord length
Re_d	Reynolds number based on a representative diameter

Re_h	Reynolds number on the hot air side of the blade wall
Re_x	Reynolds number based on length from the leading edge
R_h	Thermal resistance between the hot air and inner blade wall [m^2K/W]
R_i	Thermal resistance of the ice [m^2K/W]
R_o	Thermal resistance between the ambient air and the outer surface [m^2K/W]
R_{wall}	Thermal resistance of the blade wall [m^2K/W]
ρ_{air}	Air density [kg/m^3]
ρ_{ice}	Ice density [kg/m^3]
ρ_f	Air density based on film temperature [kg/m^3]
σ_{cent}	Force per unit area from centrifugal loading [N/m^2]
t	Blade thickness [m]
τ_{aero}	Shear stress due to aero-loading [N/m^2]
t_f	Time for the ice to refreeze [s]
T_h	Hot air temperature [°C]
θ	Angle from the stagnation point [degrees]
T_{melt}	Melting temperature [°C]
T_o	Ambient temperature [°C]
T_s	External surface temperature [°C]
t_{sens}	Time required to raise the ice to 0°C [s]
t_{tot}	Total time required to de-ice the blade [s]

V_h	Velocity of hot air [m/s]
V_{rel}	Relative velocity, as seen by the blade [m/s]
V_w	Wind velocity [m/s]
V_t	Tangential velocity due to the rotation of the blade [m/s]
x	Length from the leading edge [m]
$x(i)$	Node coordinate position [m]

1 Introduction

In 2012, 2.5% of the global electricity was supplied by wind energy [1]. Canada is the ninth largest producer of wind energy in the world and in 2012 our wind energy capacity grew by 20%, to reach a capacity of approximately 6500 MW [2]. This figure is expected to increase in the future with improvements in design and reliability of wind turbines combined with tax incentives and other subsidies for electricity generated from renewable sources. This enables wind electricity generation at competitive prices, where wind conditions are favourable. Wind energy produces electricity for both large urban centres and remote rural communities. Remote communities in Canada that are separated from main electrical grids often rely on grossly inefficient diesel generators. In these communities, where good wind sources are located, wind energy is an attractive method to supplement diesel generated electricity.

Unfortunately, the best locations for wind turbines are often areas that are subject to icing. Ridge lines, hill tops and geographical positions of higher elevation experience greater than average wind speeds. At higher elevations icing is more common because temperatures are typically colder and precipitation is more frequent than the surrounding region. Near-shore and off-shore wind turbine locations often have consistent, greater than average wind resources. Where temperatures can go below freezing, icing is prevalent in near-shore and offshore regions. Consequently, many areas that would be prime locations for wind turbines experience ice build-up on the blades of the turbines.

Ice accretion on the blades can effect both the production of energy and the lifetime of the wind turbine. Accumulation of ice on the blade reduces power produced by the wind turbine due to increased surface roughness, which disrupts the flow of air around the airfoil [3]. In worse conditions ice accretion on the blades may cause the wind turbine to come to a complete stop and may not be operational again for days or weeks at a time [4]. An imbalance of icing load can cause increased wear on components of the turbine which can increase the maintenance costs and effectively reduce the lifetime of the wind turbine

[4]. In areas where ice accumulation is a concern, an icing mitigation strategy is required for wind turbines in order to prevent production losses. In North America and northern European countries, icing mitigation strategies are being pursued, so far with limited success.

Currently, heating the blade of the wind turbine is the most promising method to mitigate against ice accretion. Anti-icing is the application of heat to prevent ice from forming on the surface of the blade. De-icing is an alternative strategy that allows ice to from on the blade before heat is applied in order to melt a thin film between the ice and the blade surface. Heat can either be applied electrically with resistance heaters mounted on the surface of the blade, or by forcing hot air through a channel on the inside of the blade. The operating limitations and the effectiveness of heat application strategies for wind turbine blades are not yet fully understood.

Methods to protect aircraft wings from ice accretion have been developed since the early 1940's. However icing mitigation technology used in the aeronautical industry is not directly applicable to wind turbines. The blades of wind turbines are hard to access from the ground, cover a large surface area and only a limited amount of power is available for de-icing. Icing mitigation strategies that melt ice on the wind turbine blades must be efficient so that the benefit of heating the blade exceeds the energy required. Successful hot air heating systems for aircraft are able to quickly heat the wing surfaces through a relatively thin layer of aluminum. However, the skin of modern wind turbine blades are commonly constructed of poorly conductive fibreglass composites and low density core materials. This makes it harder to heat the wind turbine blades from the inside, where the heating system would be protected from the environment. On the outside of the blade any icing protection system is vulnerable to the environment, blade flexing and lightning strikes. Currently, there is yet to be a proven icing mitigation strategy for wind turbines in different icing climates [5].

The emerging field of de-icing wind turbines is slowly gaining momentum as new wind turbine construction in icing prone areas increases. In order to design an effective heating

strategy for removing ice from wind turbine blades, an understanding of the heat transfer involved must be developed. The purpose of this thesis is to investigate different heat application strategies using electro-thermal resistance heaters and forced hot air. Initially, the simple scenarios that can be investigated analytically will be explored. When the heat transfer becomes more complex, the heat conduction equation will be solved numerically for a range of expected icing conditions. This thesis will investigate the effectiveness of electro-thermal and hot air heating strategies to determine their operating limitations and parameters in order to successfully mitigate against ice accretion.

Thesis Outline

In the second chapter of this thesis, the necessary background information and literature review are provided. The third chapter presents the analysis and results of the electro-thermal anti-icing and de-icing system. Hot air anti-icing and de-icing are analysed in chapter four. The fifth and final chapter is a summary of the operating limits and the effectiveness of electro-thermal and hot air heating strategies for wind turbines.

2 Background and Literature Review

In this chapter the background information and literature review pertaining to icing of wind turbine blades is provided. Icing of wind turbine blades is a relatively new area of research, hence little published information exists while much new research needs to be done. The current knowledge base of icing on wind turbine blades is a synthesis of experience gained by the aerospace industry, the power utility industry and the wind turbine industry. Research taken from the aeronautical industry is based on experience with icing mitigation on airplane blades over the last 70 years. The power utility industry and meteorological societies, particularly in the northern hemisphere have cumulated experience from icing on power lines and structures. The first documented case of a wind turbine to experience severe icing conditions in Canada was on Haeckel Hill in the Yukon in 1993 and the years following [6]. A lot of the previous icing research has been summarized by IEA, Task 19, in a series of BOREAS conferences held by the Finnish Meteorological society [5,7].

There is a growing awareness of the gap in our understanding of issues relating to icing of wind turbines; including the effect of ice accretion on the performance of the airfoil, environmental conditions for icing to occur, mapping of icing severity and research into potential mitigation strategies for wind turbines. The aim of this thesis is to contribute to the knowledge and understanding of potential icing mitigation strategies for wind turbines.

2.1 Wind Energy in Cold Climates

Ice accretion on wind turbine blades is a characteristic that is often associated with cold climates. Consequently, prediction of the severity of icing at a particular site is frequently wrongly correlated to the average daily temperatures; cold temperatures are only a pre-requisite for icing to occur. The average daily temperature for a region is easy to measure and the data is widely available while the frequency of atmospheric icing in a region is highly variable and more difficult to measure. Atmospheric icing is the most common

type of icing to be encountered and occurs when water droplets in the atmosphere freeze when they come into contact with a structure such as a wind turbine blade. A site is categorized as being in a cold climate if the average daily temperature remains below the rated operating temperature of the turbine for a certain number of days [7]. In parts of the Canadian Arctic, winter temperatures can often reach below the standard operating temperature range however icing conditions are rarely encountered. On the contrary, the yearly temperatures along the east cost of Canada are moderated by the Atlantic Ocean and wind turbine sites here encounter frequent icing conditions. Therefore sites that experience cold temperatures and those that experience icing conditions should be categorized separately. The conditions for which a wind turbine experiences significant production losses due to atmospheric icing can be defined as the number of icing days per year. The Swiss Meteorological Society [9] has classified the severity of icing at a given site using this criteria (Table 2.1). Table 2.1 provides a simple yet somewhat arbitrary

Days with atmospheric icing/year	Icing Severity
>60	Heavy
31-60	Strong
11-30	Moderate
3-10	Light
0-5	Occasional

Table 2.1: Classification of sites according to the severity of icing [9]

evaluation of the icing severity in a particular area. A more accurate evaluation of the icing severity at a potential site can be estimated through measurements of the duration of ice accumulation, persistence of ice, frequency distribution of icing, temperature, wind speed, wind direction, and cloud height observations [5]. However these parameters are notoriously difficult to obtain.

Meteorological communities across the globe, including Canada have published national climactic data maps. A map of the average number of days with freezing precipitation (freezing rain) is available from the National Archives and Data Management Branch of the Meteorological Society of Canada (Figure 2.1). Similarly the Finnish Meteorological Institute provides a map of the average number of icing days for Europe (Figure 2.2).

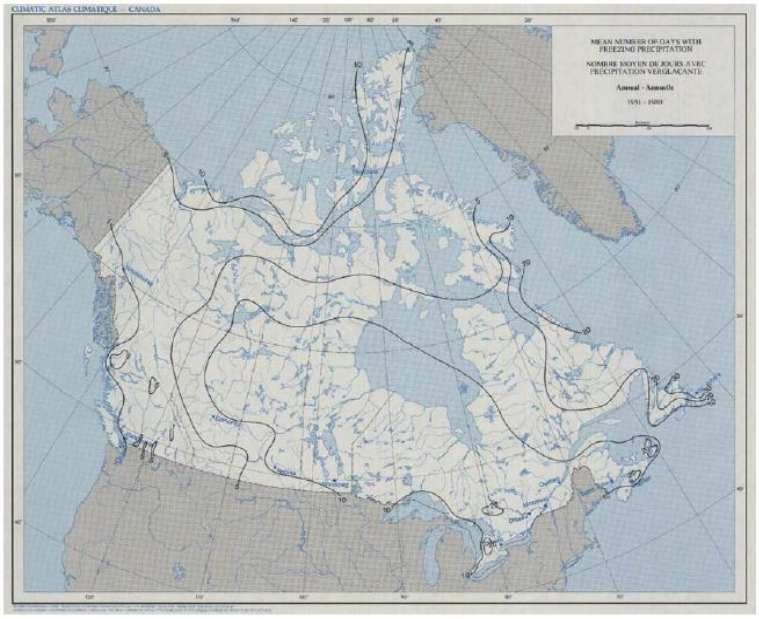

Figure 2.1: Number of days with freezing rain during one year in Canada, averaged from 1951-1980 [7]

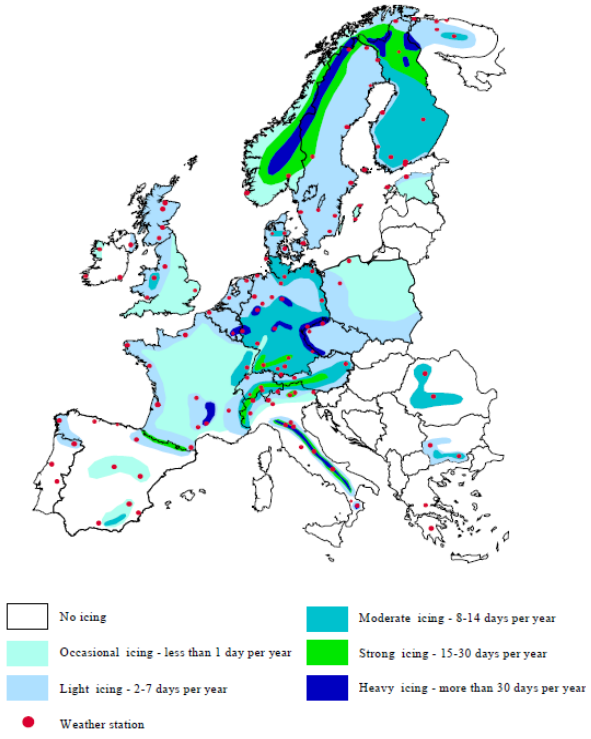

Figure 2.2: Icing map of Europe. Estimated number of days with icing conditions, determined numerically [8]

Figure 2.1 and 2.2 would not provide sufficient accuracy for determining the risk of icing at a given site. This map is made for such a large area that the resolution of the data available can only be considered indicative of the local icing. Icing frequency and severity are sensitive parameters that change with local conditions such as topography and average cloud height. Localized icing measurements and prediction models that take into account the local topography must be used in order to get a better estimate of the severity of icing at a particular site.

A refined icing map was developed in 2013 by Perron [10] for the Gaspé Peninsula, along the east coast of Canada. Figure 2.3 is an icing severity map of the St. Lawrence region in Canada.

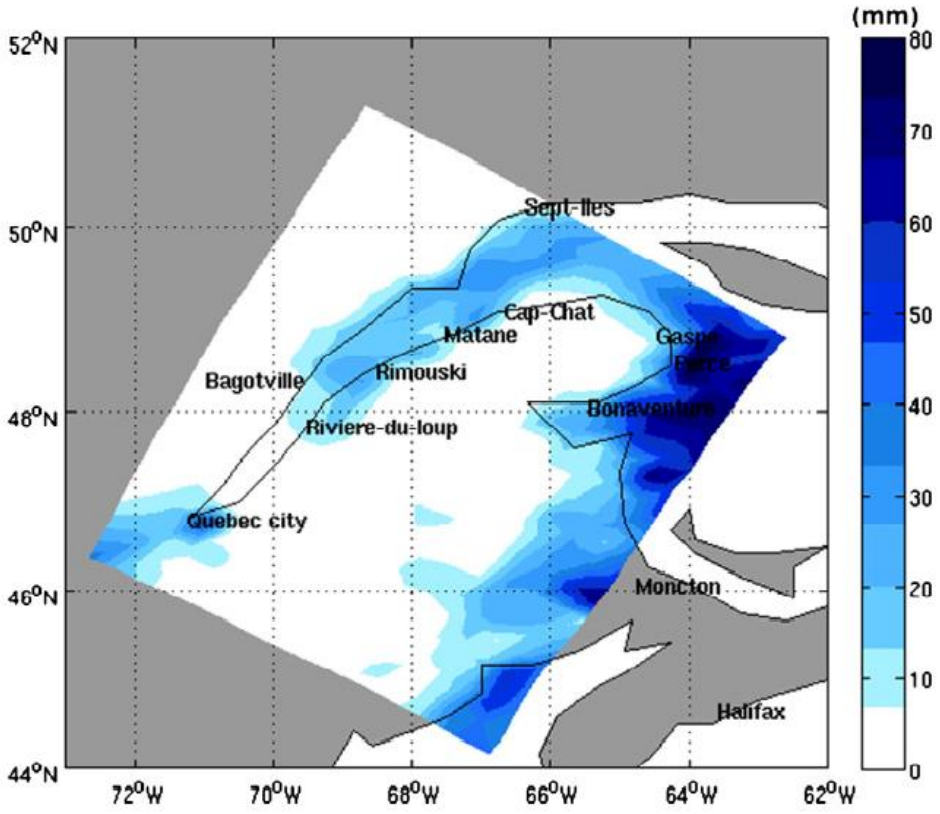

Figure 2.3: Icing severity index map. Average amount of ice accretion is averaged for the month of January between the years, 1979 and 2010 [10]

The resolution of Figure 2.3 is 32 km by 32 km. This resolution would be sufficient for locating offshore turbines which from Figure 2.3 shows significantly increased ice accretion amounts. However for siting a wind turbine in mountainous areas and on ridgelines this resolution is insufficient and would tend to underestimate the severity of the icing. Consequently an icing severity map with sufficient accuracy is difficult to obtain and will require decades of experimental observation at various sites across Canada.

2.2 Ice Types

Atmospheric icing is generally classified as either precipitation icing, which includes freezing rain and wet snow or by in-cloud icing, which is also referred to as rime/glaze icing. Freezing rain typically begins as snow first, passing through an inversion layer of warmer air where it melts, then a subsequent colder air layer, below freezing where the water droplets are subcooled. On impact with a surface, the subcooled rain will refreeze, forming what is known as glaze ice. Historically freezing rain has had devastating effects on power transmission lines. However freezing rain is relatively infrequent when compared to the occurrences of in-cloud icing on wind turbine blades. A cloud or fog consists of small water droplets that can remain in the liquid state below freezing. Upon contact with a crystallization site, such as an airfoil blade, the subcooled droplets will freeze, typically on the leading edge. If the flux of water droplets impinging on the airfoil surface is less than the freezing rate, each droplet will freeze before the next impact and the ice growth is said to be dry. Once the flux of water droplets is greater than the freezing rate, the ice growth will tend to be wet since the droplets do not have the necessary time to freeze, before the next droplet impinges. Dry ice growth results in trapped air bubbles forming rime ice while wet ice growth form solid, clear glaze ice.

The form and thermal properties of the accreted ice are important in formulating an icing mitigation strategy. Glaze ice typically forms at temperatures slightly below freezing, when there is high liquid water content in the air. Glaze ice is identified by having a

smooth surface and a transparent appearance. Glaze ice forms slower than rime ice and consequently is of much higher density. Often glaze ice will form icicles, rivulets and will freeze further from the leading edge than rime ice.

Rime ice typically forms at colder temperatures than glaze ice and consequently more air is trapped when the ice forms. The result is ice with a rougher surface and an opaque appearance (Figure 2.4). The properties of rime ice are highly dependent on the volume fraction of solid ice and the trapped air.

Figure 2.4: Rime ice formation on the leading edge of a 150 kW wind turbine blade, Grenchenberg, Switzerland [5]

The type of ice formation is dependent upon the ambient temperature, liquid water content in the air and the relative wind speed. At lower wind speeds glaze ice is more likely to form and at higher wind speeds rime ice is more likely to form. The relationship between ambient temperature and relative wind speed is presented in Figure 2.5:

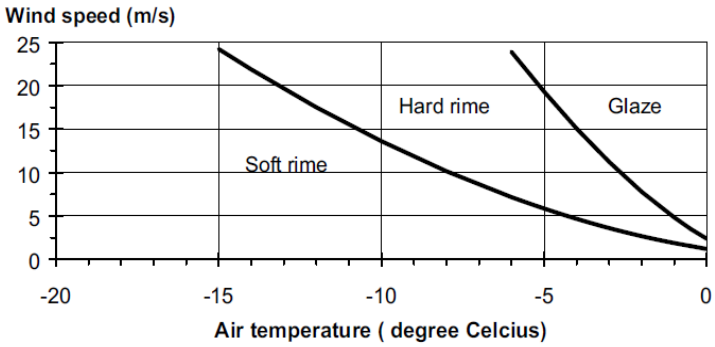

Figure 2.5: Type of accreted ice as a function of wind speed and air temperature Cost 727 [9]

At temperatures below -10°C icing events are less common. As the temperature of the air decreases so does the humidity that the air can hold. Below -20°C, the potential liquid water content that the air can hold is so low that icing is not a concern. The majority of icing on turbine blades occurs between 0°C and -10°C [11]. This is shown for a specific site in Figure 2.6.

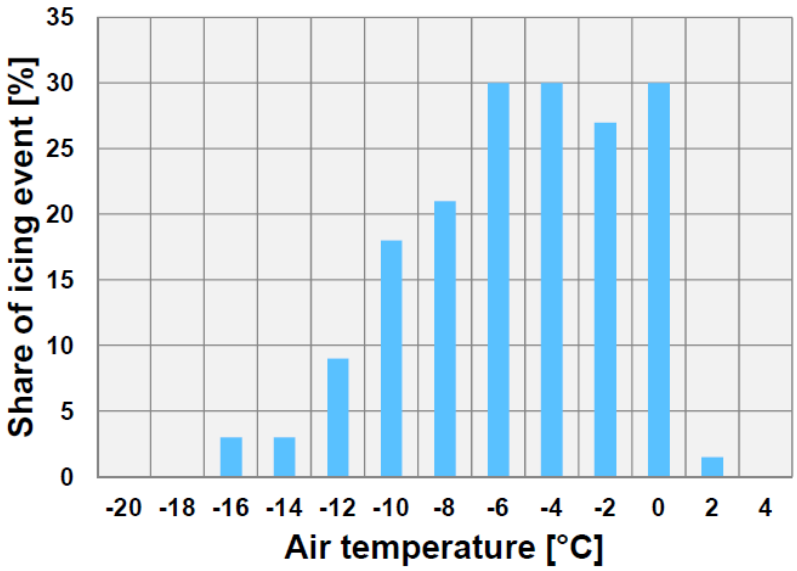

Figure 2.6: Icing distribution for different ambient temperatures at a specific site [11]

The properties of ice depend upon the volume fraction of trapped air and can be related to the density of the ice. For the purpose of our analysis two cases where considered, a dense form of glaze ice and a low density form of rime ice. The thermal properties are outlined in Table 2.2 below:

Property:	Glaze Ice	Air	Rime Ice
Density (kg/m^3)	920	1.292	333
Thermal Conductivity (W/mK)	1.88	.0236	0.696
Heat Capacity (J/kgK)	2040	1006	1380

Table 2.2: Thermal properties of glaze ice, air and rime ice at 0°C [12, 13]

The properties of pure glaze ice and air are relatively consistent, with a variance of about 10% over the anticipated temperature range. Glaze ice that is contaminated with air bubbles, but is still considered glaze ice has a density in the range of 900-920 kg/m^3. Rime ice has a density between 333 – 900 kg/m^3[9]. Two case scenarios, pure glaze ice and a low density rime ice are considered as the worst and best case scenarios, respectively. These two case scenarios represent the range of potential ice accretions. The volume fraction of the rime ice is determined based on the assumption that the lowered density is directly caused by pockets of air. The thermal conductivity and heat capacity of the rime ice is then determined from the volume fraction and the thermal properties of pure glaze ice and air. This calculation is based on the reasonable assumption that the conductivity and heat capacity of rime ice is linearly dependent upon the volume fraction of air.

2.3 Production Losses due to Icing

The general effects of ice accumulation on airfoils are well understood and several studies have documented the results [14, 15, 16]. However predicting the power loss is complicated due to the variability in ice formation.

Accretion of ice on the airfoil will increase the surface roughness, increasing the drag and decrease the lift that the airfoil produces. Roughening of the leading edge will have the

most drastic affect due to the early transition into the turbulent regime. The response of the airfoil to icing is highly dependent upon the design of the airfoil as well as the shape and lateral position of the accumulated ice.

Light ice accumulation on the airfoil may go unnoticed since there is no ice detection system capable of reliably detecting thin ice accretions. In many cases airfoils are quite tolerant to leading edge icing. In 1997, Seifert [16] performed a detailed study on the performance of a NACA 4415 airfoil with different severities of accretion. The study found that a sharper leading edge was able to tolerate more severe icing while an airfoil with a higher t/c ratio (thickness/chord length) would be more sensitive to icing.

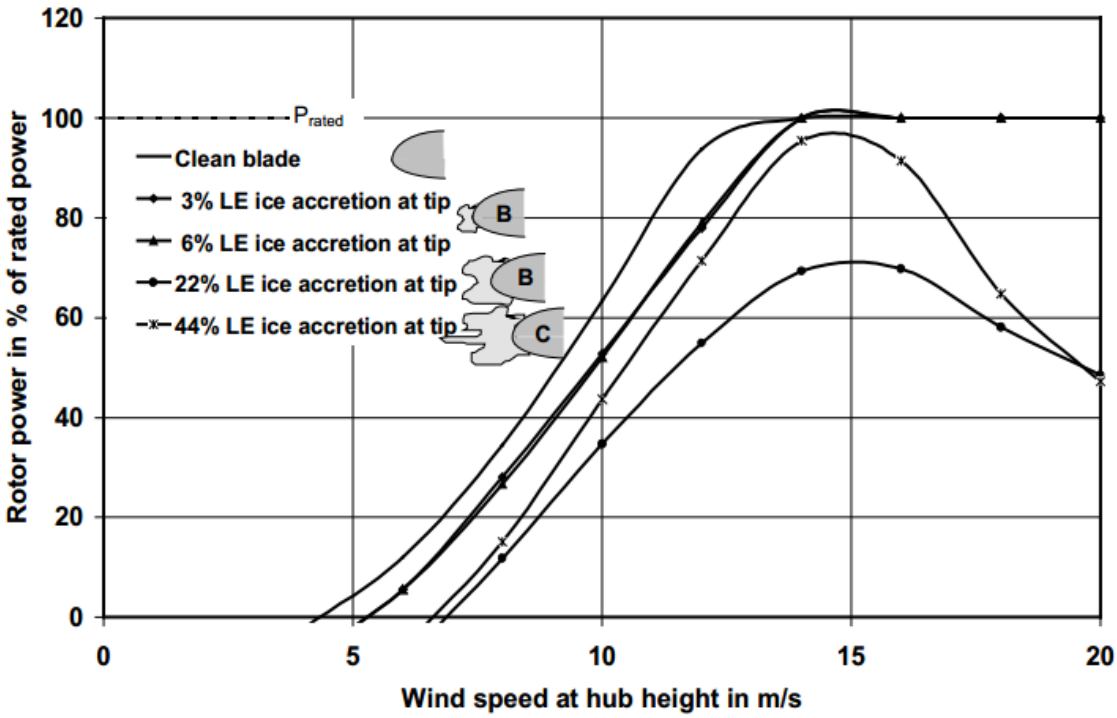

Figure 2.7: Performance of a variable pitch wind turbine using a NACA 4415 airfoil with different levels of ice accretion severity [16]

Figure 2.7 shows that for a leading edge ice accretion thickness equal to 3% of the chord length that the power output of the turbine is only reduced marginally, by about 15% at a wind speed of 10 m/s. In Figure 2.7, the projected power increased when the ice accretion increased from 22% to 44% (Seifert [16] based this on an increase in lift

produced by the now larger airfoil shape). The deviation of power during standard operation is typically greater than 15% for a given wind turbine, making it difficult if not impossible for the power curve comparison method to detect a thin layer of ice.

Indirect methods of detecting ice such as the power curve comparison method lack reliability. Alternative indirect ice detection methods typically utilizes sensors that are mounted on the nacelle of the turbine, avoiding the complications associated with a blade mounted sensor. The sensors are used to detect ambient conditions (humidity, temperature, wind speed) or a change in the dielectric constant that would occur when ice forms on the sensor. Direct methods of ice detection use capacitance, inductance, resistance or a combination of these to detect the ice on the blade and are mounted directly at the location where the ice is expected to form. For reliable and accurate detection, a capacitance or inductance direct detection method is the most promising [17]. With improved ice detection technology, moderately severe icing cases can be recognized and protected against using an icing mitigation system. Current ice detection technology can identify severe icing occurrences however a proven de-icing technology is required to remove the accreted ice.

2.4 Ice Strength and Surface Adhesion

In order to remove ice from the blade, the adhesive force must be overcome. Both the adhesive strength and tensile strength of the ice must be considered in order to determine whether the ice will break off at the adhesive bond or cohesively under a given degree of force. In 1952 Loughborough [18] found that the adhesion strength of ice linearly increases by approximately 8.5 psi per centigrade decrease in temperature. This translates to an adhesion strength of 8.5 psi (58.6 kPa) at -1°C and 85 psi (586 kPa) at -10°C.

In 1989 Xian [19] studied the tensile strength of impact ice in the NASA icing wind tunnel and found that the tensile strength increases with decreasing temperature until about -12°C after which it is relatively constant at 1.1 MPa (Table 2.3). Impact ice is

differentiated from generic ice because it is formed by accumulation on a surface and can be simulated in an icing wind tunnel.

Test Temperature (°F)	Test Temperature (°C)	Mean Ultimate Tensile Strength (MPa)
-10	-23.3	1.172
0	-17.8	1.137
10	-12.2	1.161
20	-6.7	0.896
25	-3.9	0.827

Table 2.3: Ultimate tensile strength of impact ice. Results are the calculated mean from multiple tests [19]

These results are consistent with the adhesion tests performed by Gouni in 2011 [20] who observed that beyond -20°C the test samples would break cohesively rather than at the adhesive bond, indicating that the adhesive strength is equal to or greater than the cohesive strength of the ice. Therefore active de-icing systems that rely on removing ice mechanically will have a difficult challenge below temperatures of -20°C since this cohesive breakage will result in only partial de-icing of the blade.

The structural strength of ice test samples is dependent upon the microstructure of the ice which will change depending upon the environmental conditions in which it is formed. Glaze ice and rime ice will have significantly different structural properties. Additionally the thickness of the test sample will influence the result of the tensile strength. Xian [19] found that for a thicker section of ice the ultimate tensile strength decreases. A larger test sample will have a higher probability of developing a weakness in the microstructure. Therefore the tensile strength of accreted ice should be treated as a range of values.

Similarly, the adhesion strength of ice is dependent upon a number of variables and is not rigidly constrained to the linear relationship proposed by Loughborough [18]. Even within a laboratory environment, the adhesion strength of ice has a 30% scatter [21]. Figure 2.8 presents the results of three different studies that measured the adhesion strength of ice.

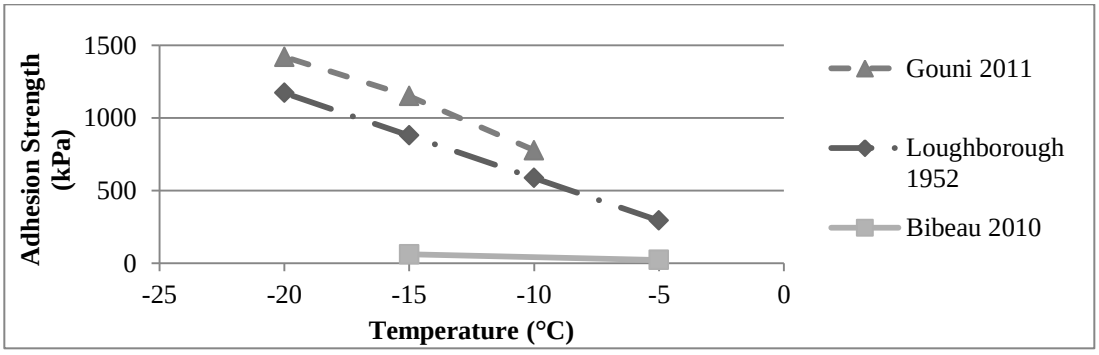

Figure 2.8: Proposed adhesion strength of ice [18, 20, 22]

The low values of adhesion strength recorded by Bibeau 2010 [22] can be attributed to the large test section analysed. Conventional adhesion strength tests use a small test section, typically a few mm^2 in area. However Bibeau [22] directly tested the adhesion strength of the ice on the airfoil, which likely allowed significant stress concentrations to develop.

Typically low density rime ice has lower adhesion strength than glaze ice due to the contamination of trapped air within the adhesion layer. At higher wind speeds and temperatures below -5°C hard rime ice is likely to form. At the interface of hard rime and the substrate, the adhesion is similar to that of glaze ice. There is no surface material known that can completely resist ice formation. However the average adhesion strength for different materials varies considerably (Table 2.4).

	Adhesion Strength (kPa)
Smooth concrete	600
Smooth steel	500
Epoxy paint, thinned with solvent	450
Carbon Fibre paint	440
Glass	430
Elastomer “Inerta 400”	420
Inerta 160	350
Polyurethane with silicon layer	330
Wearlon® F-1 (Silicone-epoxy)	150
PVC	90
Teflon (smooth)	40

Table 2.4: Ice adhesion strengths for different materials at a temperature of -10°C [23]

From Table 2.4 the dependence of adhesion strength on substrate type can be realized. Typically high strength adhesive bonds with ice will be made with ice and surfaces with a higher surface roughness (concrete). Smooth surfaces (Teflon) will reduce the adhesion strength. Several "innovative" surfaces that depend upon silicon coatings offer a reduced surface roughness however it has been found that with prolonged exposure to the environment, the silicon based coatings would wear away leaving a surface that is rougher than the original surface. The ultimate result is a stronger ice bonding [18, 24, 25]. Surface coatings that are both smooth and durable have been the subject for research both in the wind industry and the aeronautical industry for decades. A robust coating that is truly ice phobic has not yet been developed. Therefore an alternative, active ice removal strategy is required for wind turbines in icing prone areas.

The underlying molecular reasons for the strength of adhesion remains unclear [26] however several notable trends can be observed:

- Decreasing temperature increases the adhesion strength linearly [18, 27].
- Relative velocity at which the ice was formed will affect the adhesive strength. At higher wind speeds the density of the accreted ice will increase, strengthening the adhesive bond [9].
- Increased surface roughness will increase the strength of the adhesive bond [28].
- Trapped impurities within the bond will reduce the adhesive strength, notably trapped air along the bond surface, such as with low density rime ice [29].
- The relative difference between the thermal expansion coefficients of the substrate and the ice will affect the adhesion strength. A low thermal expansion coefficient for the surface material matched with a high thermal expansion coefficient of the ice will create tension at the bond surface, reducing the adhesion strength [27].
- The longer the ice has been left on the blade the higher the strength of the adhesive bond [29]. Particularly soft rime ice hardening with time.
- The structure of the accreted ice affects the ice strength. The shape of the ice formation influences the stress distribution within the ice [22, 30].

2.5 Forces on the Blade

In order for ice to separate from the wind turbine blade, the separation forces must overcome the adhesion force at the blade/ice interface. If only a section of ice is to be removed (i.e. the outer third of a blade length), then the tensile strength of the ice must be overcome in order for the ice to separate from the neighbouring ice. Forces during normal operation include aero-loading, centrifugal loading, gravitational forces, and bending stress. In order for a mitigation strategy to be successful the separation forces must be greater than the adhesion and tensile strength.

The magnitude of the shear stress due to aerodynamic loading can be approximated using a simple formula:

$$\tau_{aero} = \frac{1}{2}\rho_{air}{V_{rel}}^2 C_f \qquad \text{Eq. 2.1}$$

The magnitude of the stress due to the rotation of the blade can be calculated simply as:

$$\sigma_{cent} = \rho_{ice} L_{ice} \Omega^2 r \qquad \text{Eq. 2.2}$$

The shear stress due to gravitational forces is approximately:

$$\sigma_{gravity} = L_{ice}\rho_{ice} g \qquad \text{Eq. 2.3}$$

V_{rel} is the relative velocity as seen by the blade, L_{ice} is the thickness of the ice accretion and Ω is the rotational speed of the turbine.

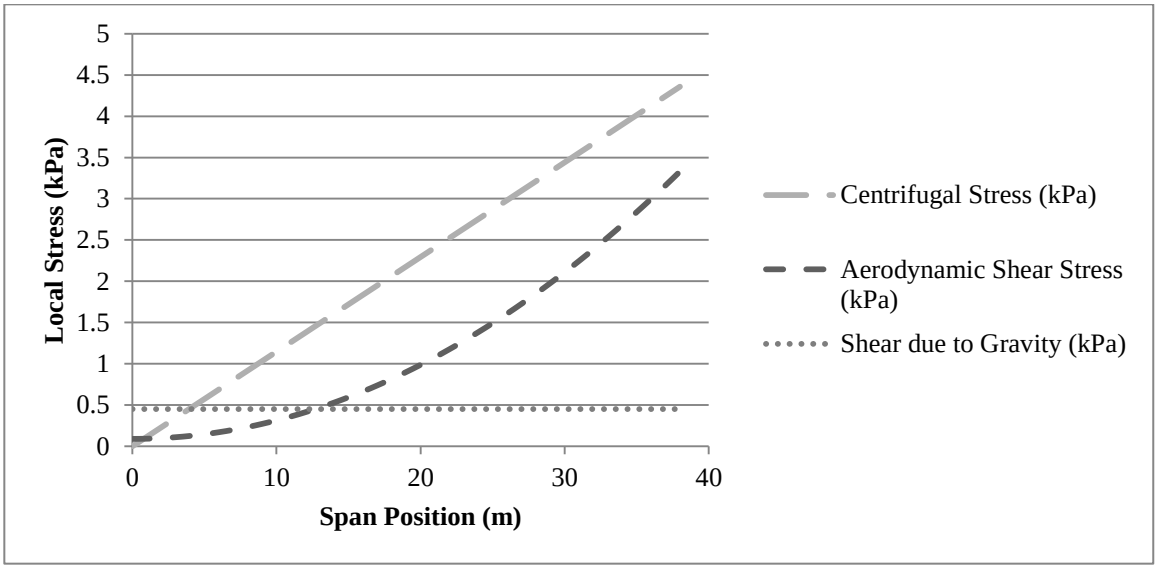

Figure 2.9: Local shear stress during normal operation for a generic 1.5 MW, 38m blade radius wind turbine. Wind speed is 10 m/s and the tip speed ratio is 6. Icing on the blade is severe, with 5 cm of glaze ice

In comparison with the adhesion strength of ice (Figure 2.8), Figure 2.9 shows that the loads encountered during normal operation are typically one or two orders of magnitude smaller. Therefore ice removal is not likely to occur due to the normal operation of the blade.

During one revolution of the turbine the blade undergoes a slight loading and de-loading through the shadow of the tower for both upwind and downwind turbines. Turbine blades are mainly comprised of fibreglass, which is quite flexible allowing the blade to deform significantly throughout each revolution. In cold climates turbine operators have been known to attempt to take advantage of this phenomenon. Operating the blade at a rotational speed that approaches a flap-wise natural frequency of the blade increases the bending of the blade. This process is referred to as "blade shake". Under certain conditions bending the blade can create stresses at the adhesion interface sufficient enough to remove the ice from the blade. However blade shake has not proven to be reliable to de-ice the blade [31]. Often only part of the ice is removed resulting in fragmented adhesion of the ice [26].

2.6 Icing Mitigation Systems

2.6.1 Aircraft Experience

Preventing ice accretion and removing it once it has accumulated has long been a subject of concern in the aeronautical industry. Classical icing mitigation systems for aircraft include:

- Applying anti-icing fluids to the wings before takeoff
- Using a "weeping wing" system
- Pneumatic boots that are installed along the leading edge that can inflate in order to break of the ice
- Re-routing bleed air from the engines to heat the leading edge of the blade

However icing mitigation systems used in the aeronautical industry are not directly transferrable to wind turbines.

Anti-icing fluids are too difficult to apply to wind turbines due to the large surface area and the unpredictable nature of icing on wind turbine blades [8]. Weeping wing systems that secrete anti-icing fluid through holes in the blades are also not practical for wind turbines. The total amount of de-icing fluid required for wind turbines would be prohibitively high [25].

Flexible pneumatic boots used in the aeronautical industry inflate to break ice. The boots are mounted along the leading edge of the wing where ice is expected to form. Initially the boots lay relatively flat against the wing. Once 6-13 mm of ice has accumulated on the wing the boots are inflated with compressed air, causing the ice to crack and de-adhere [32]. The broken ice is carried away by aerodynamic forces. Several difficulties are encountered when adapting pneumatic boots for wind turbine blades. The centrifugal forces of the rotating blades can cause the boots to automatically inflate [25, 33], which would require them to be partitioned in sections. Also the boots may increase the drag on

the airfoil which would reduce the annual energy production of the wind turbine, counter-productive to the purpose of the de-icing system.

Aircraft have the benefit of being able to extract thermal energy from their engines and use it to de-ice. In wind turbines this is not possible. De-icing aircraft is a matter of safety whereas the main concern with de-icing wind turbine blades is increased annual energy production. Common in-flight aircraft de-icing strategies heat the wings whenever there is ice detected on the blades, ensuring the maximum level of safety. If the same strategy applied to heating wind turbine blades, the supplied energy would at times exceed the production benefits of heating the blades. In this thesis, the operating limitations of heating systems are investigated in order for wind turbine operators to have a guideline for the selection and operation of heating systems.

2.6.2 Passive Icing Mitigation Strategies

Potential icing mitigation systems for wind turbines are classified as either passive or active. Passive systems that depend upon hydrophobic and icephobic coatings would replace the need for an active de-icing system. A successful ice-phobic coating would have numerous applications beyond wind turbines, including aircraft, shipping vessels and structures in cold climates. Previous studies have shown that the strength of the adhesive bond can be reduced using different coatings (Table 2.4). However all coatings that have so far been developed are susceptible to leading edge erosion and pitting. This causes the surface to become rougher, reducing the effectiveness of the coating, often resulting in higher than normal adhesion strength of the ice. For ice repellent coatings to be successful they must be durable or at least be re-applicable.

Multiple turbine operators have experimented with black coloured coatings for the turbine blades in order to increase the temperature of the blades in an attempt to delay ice accumulation and enhance de-icing [6, 34]. Two wind turbines situated in the Yukon had their blades painted with a low adhesive, black coating, StaClean©, in an effort to

mitigate against icing [34]. The result of the experiment showed minimal solar gain in windy areas [35].

2.6.3 Active Icing Mitigation Strategies

Active heating strategies for the removal of ice from wind turbine blades can be subdivided into two main categories; anti-icing and de-icing. Heat is supplied to the blades by forced hot air through channels inside the blades or by electro-thermal heating mats mounted on the outside of the blades.

Anti-icing heats the surface of the blade to be above zero so that impinging subcooled droplets do not have a chance to freeze. Heat is supplied throughout the duration of the icing event. Typically the power consumption is minimized by only heating the critical areas. The result is a heater that is positioned at the leading edge, slightly offset to the pressure side of the airfoil [32]. The drawback of only heating the leading edge is the risk of runback icing that can occur from the impinging droplets freezing further down the blade. Trailing edge heaters can be used to keep the trailing edge ice free if desired. An anti-icing system allows the critical areas of the airfoil to remain ice free throughout a de-icing cycle; however this comes at the cost of much greater energy expenditure.

Active de-icing strategies remove the ice at a predetermined threshold. This can be once a certain amount of ice has accumulated, when the power production falls below a certain percentage of the expected power generation or after a certain amount of time from the beginning of the icing event. De-icing strategies melt a thin layer of ice proportional to the surface roughness at the adhesion layer. This eliminates the adhesive bond of the ice to the blade, allowing the ice to be removed by external forces (section 2.5).

2.6.3.1 Hot Air Anti-Icing and De-Icing

Currently no proven de-icing or anti-icing system exists for wind turbines in all climates. Enercon has developed and tested a hot-air de-icing system at two sites in Sweden. The system was analysed by a third party contracted by Enercon. The analysis showed that

over two winter seasons the de-icing system improved the overall energy output of the wind turbines [36]. Despite the promising results, hot-air de-icing has not been widely implemented into the designs of wind turbines experiencing production losses due to icing. Reasons for the systems short-falls have not been published. It is expected that the hot-air de-icing system loses efficiency as the scale of the blades increase due to increased thickness of the blade wall.

Gray et al. (1952) [37] and Thomas (1953) [38] investigated the heating requirements of a hot air heating system for a turbojet transport airplane. The icing protection system was able to operate in an anti-icing and de-icing function. Heat was supplied from hot-gas bleed back. Consequently the type of icing protection imposed a severe penalty on engine performance. A hot air heating system for a wind turbine blade would require a separate heating system installed in the blade. The performance of this system in a wind turbine blade would be significantly different due to differences in blade construction and the amount of power available.

Battisti et al. (2006) [39] performed a one-dimensional numerical analysis, comparing hot air anti-icing and de-icing for a 450 kW wind turbine blade. The analysis solved the heat diffusion differential equations using finite differencing. A predictor-detector method was used in order to tackle the phase change problem. The analysis performed by Battisti [39] was representative of a section at the tip, with a 1 cm thick glaze ice accumulation. The thickness of the blade wall was 1 cm of relatively conductive, polymeric material, with a thermal resistance of only 0.02 m^2K/W. For most wind turbine blade designs, the wall thickness and consequently the thermal resistance of the airfoil wall will vary considerably from the root of the blade to the tip. Larger diameter wind turbines will have thicker walls in order to support the weight of the turbine blade. In order to most effectively support the bending loads of a wind turbine blade, the wall is the thickest at the blade root and tapers toward the tip. Therefore, in the de-icing analysis performed by Battisti [39], the heat transfer is only representative of a portion of the blade length. This thesis will expand upon the work performed by Battisti [39] by examining the heat transfer analysis of hot air de-icing and anti-icing for a range of blade wall thicknesses.

2.6.3.2 Electro-Thermal Anti-Icing and De-Icing

Several companies and researchers have developed and tested electro-thermal de-icing and anti-icing systems [40-44]. Despite the promising thermal efficiency of electro-thermal mitigation systems they have not moved beyond the prototype and testing stage. In recent years, electro-thermal heating systems have been developed and prototyped for the aeronautical industry. The Therma-wing© system developed by Kelly Aerospace [42] has been certified for small, single engine aircraft. A comprehensive numerical heat transfer analysis could provide insight into the effectiveness of electro-thermal de-icing as it is applied to wind turbine blades. It is expected that difficulties will arise adapting this mitigation strategy to commercial scale wind turbines due to the large surface area and consequently large power requirements.

2.7 Design of Modern Wind Turbine Blades

An understanding of the construction of modern commercial wind turbine blades is essential before the individual mitigation systems can be analysed. Standard wind turbine blades are designed with either one or two spars to increase the structural integrity of the blade.

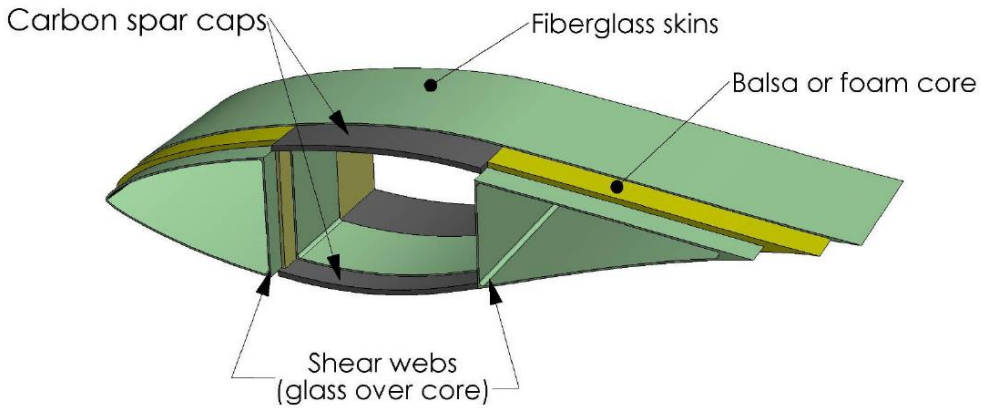

Figure 2.10: Blade construction of modern wind turbine blades [45]

Figure 2.10 is a cross section of a modern wind turbine blade with two spars. The skin of the blades is made of two skins of fibreglass that sandwich a foam core. For this study a range of blade constructions are considered based on a survey of common blade materials and geometries. A typical case is considered that was used previously in a study performed by Severino (2012) [46]. The geometry and thermal properties of this example case are available in Appendix A.

2.8 Summary of The Background and Literature

Wind turbines located in areas prone to ice accumulation face a significant disadvantage in terms of energy production. Methods of preventing or removing ice once it has formed are necessary to ensure the cost effectiveness of wind turbines in these locations. Due to the thin and structurally weak nature of ice accretions on wind turbine blades, the key to ice removal is reducing the adhesion strength of the ice to the blade. Coatings for structures and airfoils in icing prone regions have so far not proven to be durable or reliable enough to be considered as a viable icing mitigations strategy. Thermal heating systems have promise but need to be analysed before they can be deemed useful for de-icing wind turbine blades. Previous studies have only investigated the operation of heating systems for individual scenarios. The power requirements of a heating system will depend upon the environmental conditions, the type and thickness of ice formation, the power available and the properties of the blade. In this thesis both electro-thermal and hot air heating systems are investigated for a range of typical operating conditions. The objective will be to determine the operating characteristics and limitations of both heating systems.

3 Electro-Thermal Heaters

Electro-thermal anti-icing and de-icing systems are one proposed mitigation system for ice accumulation on wind turbine blades. In an icing scenario, an anti-icing system would heat the leading edge of the blade in order to prevent ice from accumulating. A de-icing system allows ice to accumulate to a certain thickness before heat is applied. Within the first section of this chapter, the heating power density required for anti-icing systems is investigated. The second section of this chapter will analyse an electro-thermal de-icing strategy. The benefit of insulating the heater from the blade in order to reduce the de-icing time is also investigated. The performance of both the anti-icing and de-icing systems are evaluated based on a range of expected icing conditions.

3.1 Electro-Thermal Anti-Icing Analytical Analysis

In order to effectively apply anti-icing or de-icing, it is first necessary to attain an understanding of the heat transfer balance associated with the icing phenomenon in order to approximate the correct amount of heating required. Previous numerical models [47 – 51] have developed ice accretion codes to simulate ice growth on airfoils and other structures. LEWICE and TURBICE are two such ice codes; LEWICE was developed by NASA [47] and TURBICE [49] was developed specifically for wind turbine applications. The basis of the ice accretion codes is an energy balance at the surface of the blade, initially described by Messinger [52]. The heat transfer analysis of ice accretion described here has been adapted directly from Messinger (1953) [52], Poinsatte (1990) [53] and Meier (2010) [54]. As an aircraft passes through an area of cool air with high moisture content (often subcooled droplets), a fraction of the subcooled droplets will impinge on the leading edge of the airfoil. If the cooling from the surface of the blade is sufficient to overcome the latent heat that is released from the freezing droplets, then ice may form on the surface. For wind turbine applications the significant modes of heat transfer are outlined below:

$$q"_c + q"_w = q"_f \quad \text{Eq. 3.1}$$

Other modes of heat transfer such as evaporation, frictional heating, and kinetic energy absorbed due to impinging droplets, radiation from the blade surface and conduction through the air are relatively insignificant. The individual terms of Equation 3.1 represent

(1) the heat lost from the surface due to convection:

$$q"_c = h_o(T_s - T_o)$$

(2) the heat lost from the surface due to the absorption by impinging water droplets:

$$q"_w = \dot{m}_w C_w(T_s - T_o)$$

(3) the heat absorbed due to the release of latent heat of fusion from the impinging droplets:

$$q"_f = n \cdot \dot{m}_w h_{fl}$$

In the above equations, T_s is the surface temperature of the blade, T_o is the ambient temperature and n is the freezing fraction of ice. The mass flux of impinging subcooled droplets, $\dot{m}_w$ can be estimated with equation 3.2:

$$\dot{m}_w = \alpha_1 \alpha_2 \cdot LWC \cdot V_{rel} \quad \text{Eq. 3.2}$$

This mass flux is proportional to the efficiency of the blade at striking suspended droplets and the efficiency of those droplets sticking to the leading edge. α_1 is the collection efficiency, α_2 is the sticking efficiency, LWC is the liquid water content of suspended, subcooled droplets in the air and V_{rel} is the relative velocity of air impinging on the blade. The efficiencies of the mass flow rate have values between 0 and 1. Flow around the airfoil diverts impinging droplets away from the blade. The thinner the airfoil blade, the higher the collection efficiency [54]. Meier (2010) [54] proposes a handbook method to calculate the collection efficiency based on the thickness of the airfoil, t and the relative velocity, V_{rel}:

$$\alpha_1 = 0.00324 \left(\frac{V_{rel}}{t}\right)^{0.613} \quad \text{Eq. 3.3}$$

The sticking efficiency, α_2 is less than one when impinging droplets bounce off of the blade. The sticking efficiency and the freezing fraction, n are both equal to one for the case of rime icing [55].

The external heat transfer coefficient, h_o is discussed in detail later in the chapter. For a typical anti-icing or de-icing scenario, the relative magnitude of heat lost due to convection when the blade surface is brought up to 5°C is compared to the latent heat released, q_f and the cooling due to the absorption of subcooled droplets, q_w in Figure 3.1.

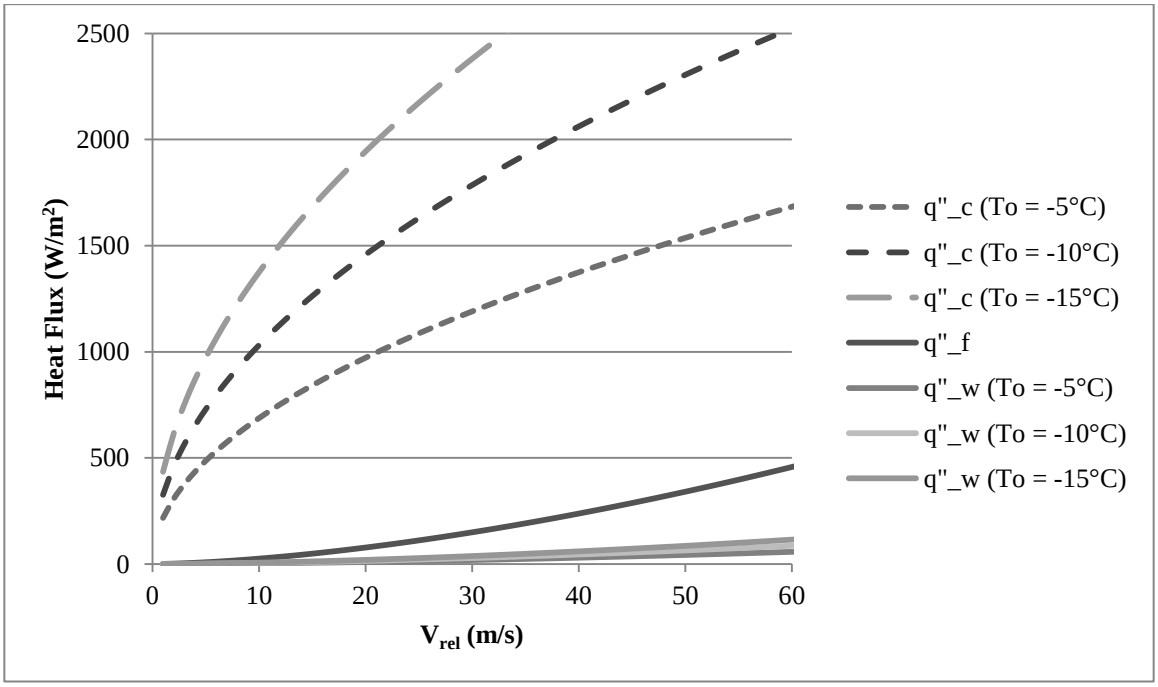

Figure 3.1: Comparative heat flux between convection losses and cooling due to impinging droplets. The surface temperature (Ts) is maintained at 5°C. Liquid water content is 0.2 g/m3, the blade thickness is 0.18 m and the droplets are assumed to form rime ice (α2 = n = 1).

The ambient temperature has little influence on the cooling of impinging droplets due to the relative magnitude of the latent heat of fusion. Figure 3.1 shows that for the representative case scenario, convection losses are the dominant form of cooling, hence the importance of the external heat transfer coefficient, h_o.

3.1.1 External Heat Transfer Coefficient

The external heat transfer coefficient, h_o varies down the length of the blade and in the position on the airfoil. The heat transfer coefficient is dependent upon the relative velocity, blade geometry, boundary layer development and the properties of the air. Buildup of ice on the leading edge will also affect the external heat transfer coefficient depending on the nature of the buildup. Formation of ice on the leading edge can cause either a simple increase in roughness, a trip for laminar to turbulent transition to occur or a more complicated effect (for significant buildup). In this section, a range of external heat transfer correlations are examined to identify the most appropriate external heat transfer treatment for the analysis of commercial wind turbine anti-icing and de-icing.

Variation of the heat transfer coefficient along the span of the blade is caused by the changing blade profile and the relative velocity of the air. The relative velocity, V_{rel}, is the velocity as seen by the blade, due to the ambient wind speed, $V_{w,}$ and tangential velocity, $V_{t,}$ caused by the rotation of the blade and is approximated as:

$$V_{rel} = \sqrt{{V_w}^2 + {V_t}^2} \qquad \text{Eq. 3.4}$$

If the blade is stationary, the relative wind speed will be equal to the ambient wind speed along the span of the turbine blade. If the wind turbine is operational, the relative wind speed can be quite large due to the rotation of the blade. A typical range of relative velocities for wind turbine applications is then between 0 and 70 m/s.

The heat transfer coefficient h_o varies significantly from the leading edge to the trailing edge as a result of the boundary layer developing. The local heat transfer coefficient along an airfoil has been determined by treating the leading edge region as the front half of a cylinder and the remaining section of the upper and lower surfaces as flat plates parallel to the flow [56]. The flow regime of the fluid is dependent upon the Reynolds number, which is the ratio of inertial forces to viscous forces in the fluid:

$$Re_L = \frac{\rho_f V_{rel} L_c}{\mu_f} \quad \text{Eq. 3.5}$$

ρ_f and μ_f are the film density and dynamic viscosities, respectively, which are calculated at the film temperature, $T_f = \frac{T_s + T_o}{2}$ (although in de-icing applications the range of temperatures considered is usually small). L_c is the characteristic length of the geometry, which is either the representative diameter of the leading edge or the length along the chord of the airfoil. At a Reynolds number of approximately $5x10^5$ the flow transitions from laminar flow to turbulent flow although this can be affected by blade shape, roughness and surface contamination. For a 38 m blade radius wind turbine, the range of Reynolds numbers across the outer third of the blade is approximately 10^5 to $4x10^5$ at stand-still and $4x10^5$ to $4x10^6$ if the wind turbine is operating.

The Nusselt number represents the enhancement of heat transfer through a fluid layer as a result of convection relative to conduction across the same fluid layer.

$$Nu_L = \frac{h_o L_c}{k} \quad \text{Eq. 3.6}$$

For a 38 m blade radius wind turbine the Nusselt number on the outer third of the blade ranges from approximately 250-1000, when the wind turbine is at stand-still to 1000-5000, when the wind turbine blades are rotating.

For slender bodies such as airfoils the Nusselt number can be determined from empirical correlations derived for heated flat plates. Initially the flow is laminar, for this section the Nusselt number can be approximated as

$$Nu_x = \frac{h_x x}{k} = 0.332 {Re_x}^{0.5} Pr^{1/3} \quad \text{Eq. 3.7}$$

where x indicates the length from the leading edge. At a Reynolds number of approximately 10^5, the flow begins to transition to laminar flow. At a Reynolds number of 10^6, the flow is turbulent and can be approximated with the equation:

$$Nu_x = \frac{h_x x}{k} = 0.0296 {Re_x}^{0.8} Pr^{1/3} \quad \text{Eq. 3.8}$$

Theoretically the heat transfer coefficient at the leading edge, calculated from Equation 3.7, would reach infinity. Since this is physically unrealistic, an alternative method to estimate the heat transfer coefficient at the very tip of the leading edge is required. Commonly, the impingement point on an airfoil is treated as a cylinder in a cross flow. Frössling (1940) [57,58,59] developed an empirical correlation to estimate the Nusselt number for the leading edge of a cylinder.

$$Nu_d = \left[0.945 - 0.7696\left(\frac{x}{d}\right)^2 - 0.3478\left(\frac{x}{d}\right)^4\right] {Re_d}^{0.5} \qquad \text{Eq. 3.9}$$

where x is the distance from the stagnation point and d is the diameter. Equation 3.9 is valid up to the separation point, which is typically about 80° from the stagnation point. Spalding (1961) [60] compared seventeen alternative correlations for predicting the Nusselt number on the front face of a cylinder and found similar results. The difficulty with adapting this approximation for airfoils is in choosing a representative diameter for the leading edge. The chord thickness of the airfoil is one possibility; however airfoils are typically slender outboard of the hub attachment on wind turbines. A more appropriate representative cylinder would be a fraction of the maximum blade thickness that is proportional to the curvature at the leading edge. Poinsatte (1990) [58] found that the equivalent diameter for a NACA 0012 airfoil was 26% of the blade thickness.

The local heat transfer coefficient for an example airfoil is calculated for a range of conditions, using the method previously described and is later presented in Figure 3.5. A representative diameter equal to 25% of the blade thickness is chosen for comparison of the local heat transfer coefficient with available experimental data.

Gelder and Lewis (1951) [40] measured the convective heat transfer coefficient across a NACA 65, 2-016 airfoil at a high Reynolds number ($Re_c = 1.145x10^7$), representative of a large aircraft wing and presented the results in Figure 3.2:

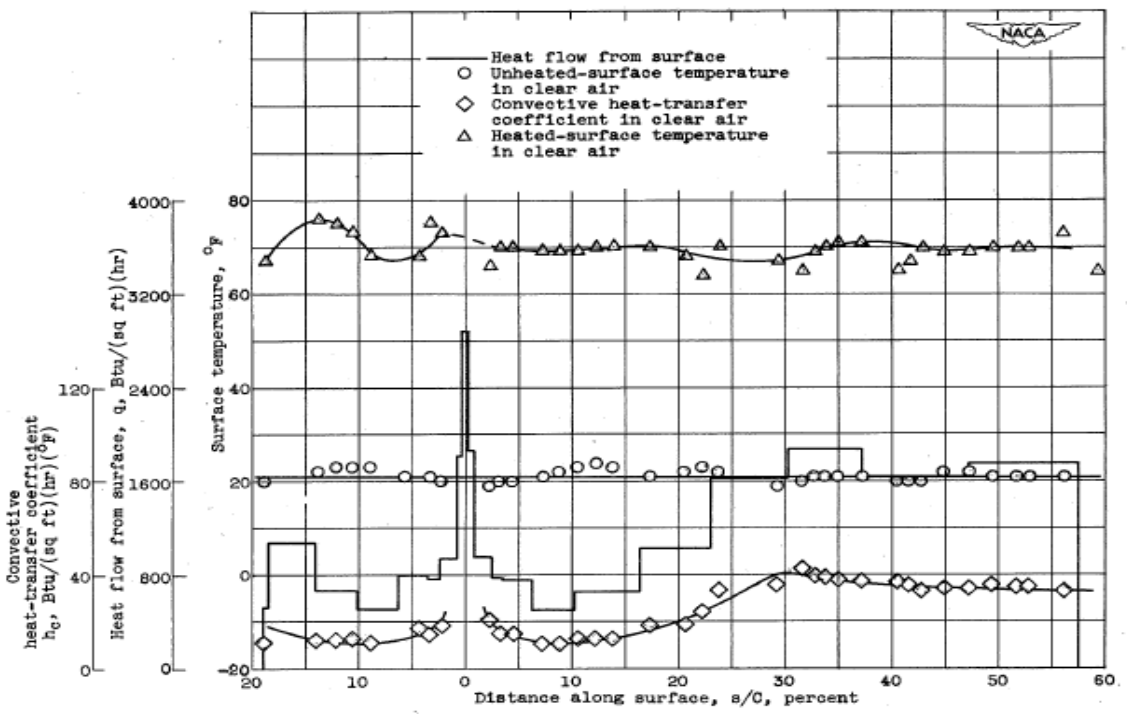

Figure 3.2: Tunnel heating distribution on NACA 65,2-016 electrically heated airfoil, zero degree angle of attack. The Reynolds number is 1.145×10^7, free stream velocity is approximately 62 m/s and the chord length is approximately 2.44 m [40].

It can be observed that local maximums exist both at the stagnation point and at the onset of fully turbulent flow. The surface heat applied by Gelder [40] is proportional to the convective heat transfer from the surface. Alternative studies have simply applied a constant heat flux across the entire surface [6, 61]. The required heater power in the study performed by Ilinca [61] ($Re_c = 6 \times 10^5$) is calculated based on the average heat transfer coefficient for turbulent flow over a flat plate where the average Nusselt number can be approximated as:

$$Nu_L = \frac{hL}{k} = 0.037 Re_L^{0.8} Pr^{1/3} \qquad \text{Eq. 3.10}$$

where L represents the heated length.

Poinsatte (1989) [58] investigated the heat transfer in flight and in the NASA Lewis icing research tunnel over a symmetrical, NACA 0012 at a range of Reynolds numbers closer to those expected for a wind turbine blade. The chord length was 0.533 m and the range

of Reynolds numbers for the tests were in the range of 1.20×10^6 to 4.52×10^6. The results of the tunnel and in-flight experiments are presented in terms of the Frössling number which is calculated as:

$$Fr = \frac{Nu}{\sqrt{Re}} = \frac{hC/k}{\sqrt{\rho VC/\mu}} \qquad \text{Eq. 3.11}$$

In the icing wind tunnel, the heat transfer coefficient was measured with and without spray air in order to measure the effects that spray air would have on turbulence levels and airfoil heat transfer (the conclusion was that spray had did not have a significant effect on the results). Poinsatte [58] compared the Frössling numbers that were determined experimentally to the analytically predicted Frössling number, calculated using empirical correlations. The representative cylinder method was compared at the leading edge and flat plate correlations were compared past a dimensionless surface distance, x/chord of 0.02. The heat transfer from the blade surface was measured up to a dimensionless surface distance up to 0.083 and the results are presented in Figure 3.3.

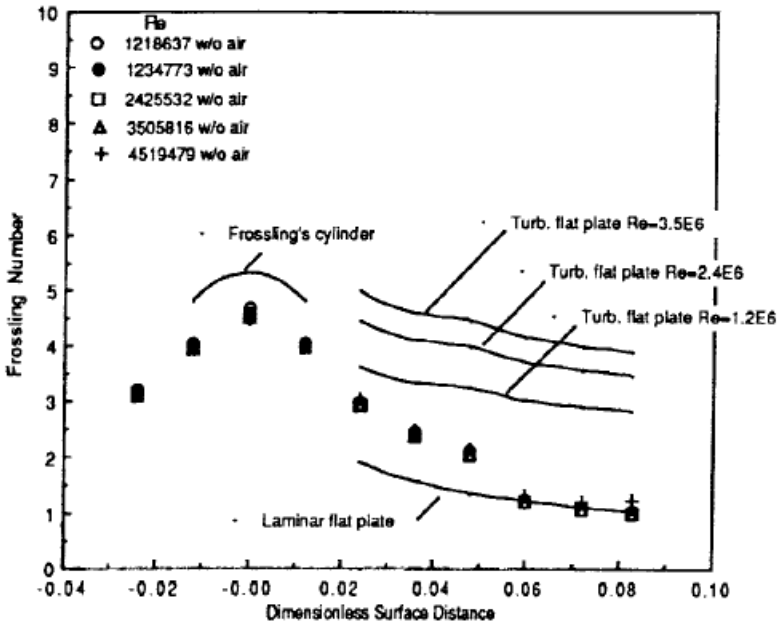

Figure 3.3: Frössling number comparison for a smooth NACA 0012 airfoil, chord length = 0.533 m with a 0° angle of attack. Measured in an icing wind tunnel, without spray. Positive numbers represent the suction surface and negative numbers indicate the pressure surface [58]

Poinsatte's results show that the maximum Frössling number occurs at the stagnation point and decreases away from the leading edge. However the heat transfer was only measured for a short section, where the flow was still laminar. Further from the leading edge, the flow will transition from laminar to turbulent flow and the heat transfer will increase. In the laminar region the Nusselt number is proportional to the square root of the Reynolds number. In this region the Frössling numbers will collapse for a smooth airfoil, independent of the Reynolds number.

Poinsatte [58] also investigated the effects of angle of attack and increased surface roughness. For higher angles of attack it was observed that separation of flow from the airfoil occurred much closer to the leading edge, resulting in higher turbulence and greater heat transfer. At the impingement point the Nusselt number and consequently the Frössling number also increased with angle of attack. Adding roughness elements to the smooth airfoil showed an increase in the Frössling number.

Wang (2007) [41] analysed the heat transfer of the entire surface of a NACA 63421 airfoil, comparable to Poinsatte [58], at a lower range of Reynolds numbers, between $Re=1.9x10^4$ and $Re=1.3x10^6$. The Nusselt numbers at different span locations were measured and are presented in Figure 3.4.

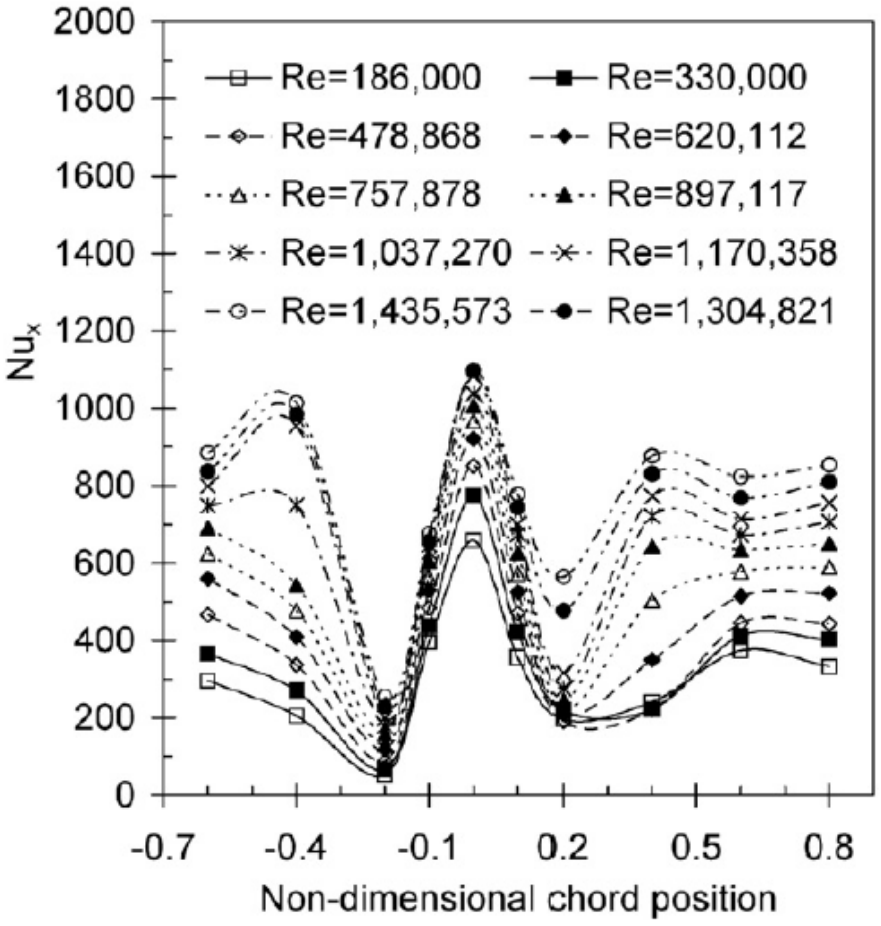

Figure 3.4: The local Nusselt number at varying non-dimensional chord positions. The airfoil is an asymmetrical NACA 63421 airfoil with a chord length of 0.5 m. The suction surface is represented by positive chord positions and the pressure side is represented by negative chord positions [41].

The results of Wang [41] illustrate the Nusselt number dependence on Reynolds number over a laminar, turbulent and transition regime. In the laminar regime it is shown that the Nusselt number is proportional to $Re^{0.389}$, comparable to flow over a flat plate, which has a Reynolds number dependence of approximately $Re^{0.5}$. In the laminar regime Poinsatte [58] found that the Nusselt number was approximately proportional to $Re^{0.5}$. In the turbulent regime, Wang [41] found that the Nusselt number was proportional to $Re^{0.636}$ (for this airfoil), comparable to flow over a flat plate which has a Reynolds number dependence of $Re^{0.8}$ in the turbulent regime. Figure 3.4 confirms that a secondary

maximum occurs at the onset of turbulent flow; however the overall maximum is nearly always located at the stagnation point.

In the work of both Wang [41] and Poinsatte [58], the local Nusselt numbers presented are dependent upon the local heat transfer coefficient, but not the local span position. The advantage of this method is that the Nusselt number can be represented at the stagnation point based on the chord length. However the local heat transfer coefficient is not dependent upon the chord length at the impingement point, but is dependent upon the sharpness of the leading edge. Further from the impingement point, the heat transfer coefficient is dependent upon the surface distance due to the development of the boundary layer.

The chord length used in the experiments of Poinsatte [58] and Wang [41] are similar, 0.533 m and 0.5 m, respectively. The simplest method to compare the experimental data is to consider specific Reynolds numbers of interest (i.e. typical sizes and relative velocities for wind turbine applications) and look directly at the local heat transfer coefficient. Figure 3.5 presents the local heat transfer coefficient of the previously mentioned experimental data along with the empirical correlations for a representative Frössling cylinder and flat plate.

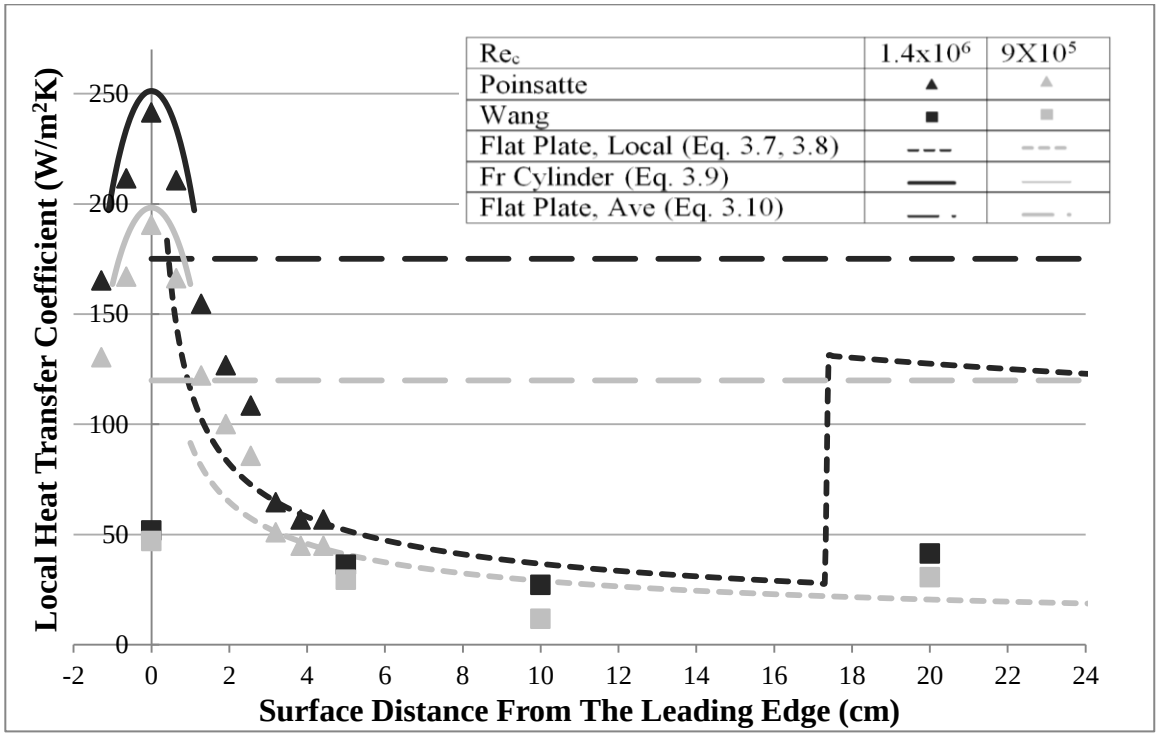

Figure 3.5: Local heat transfer coefficient across an airfoil with a chord length of 0.5 m. The results dependent on $Re_c = 1.4x10^6$ are presented in dark grey and the results dependent on $Re_c = 9x10^5$ are presented in light grey. The empirical correlations are represented by lines and the experimental data is labelled by markers. The data by Poinsatte [58] is represented by triangular markers and the data by Wang [41] is represented by square markers. The average turbulent, flat plate heat transfer coefficient is based on a heated length that is one quarter of the chord length. The Frössling cylinder correlation is based on a representative cylinder diameter that is 25% of the blade thickness.

The experimental results presented by Poinsatte [58] agree with flat plate and Frossling cylinder correlations with a close $Re^{0.5}$ dependence. Wang's data has a much lower leading edge impingement heat transfer coefficient (~1/4 – 1/5), with little Reynolds number dependence (see Figure 3.4). Downstream of the leading edge, Wang's data agrees with Poinsatte and the laminar flat plate correlation. Wang's data shows that the transition is initiated close to a Reynolds number of $5x10^5$ however has not yet become fully turbulent (hence only a small increase in the heat transfer coefficient). The transition from laminar to turbulent flow over an airfoil is not the same as a flat plate due to the presence of adverse and favourable pressure gradients.

For icing applications, the point of maximum heat transfer (i.e. the impingement point) and the heat transfer over the leading ¼ chord of the blade are of concern. The heat transfer coefficient at the impingement point for a typical wind turbine blade can be based on cylinder correlations, where the representative cylinder diameter can be taken as approximately 0.25 of the max blade thickness. A NACA 64(3)-618 blade profile is representative of wind turbine blade profiles, as used in the work by Severino [46]. The chord length of the outer third of a large scale wind turbine is typically between 0.8 and 1.4 m. The local relative velocity, as seen by the blade is between 1 and 25 m/s when the wind turbine is at standstill and between 20 and 70 m /s when the wind turbine blades are rotating. The range of impingement heat transfer coefficient values can then be plotted versus the relative velocity, as seen by the blade. From Figure 3.6 it can be observed that a reasonable range of heat transfer coefficients is between 30 and 250 W/m^{2}K.

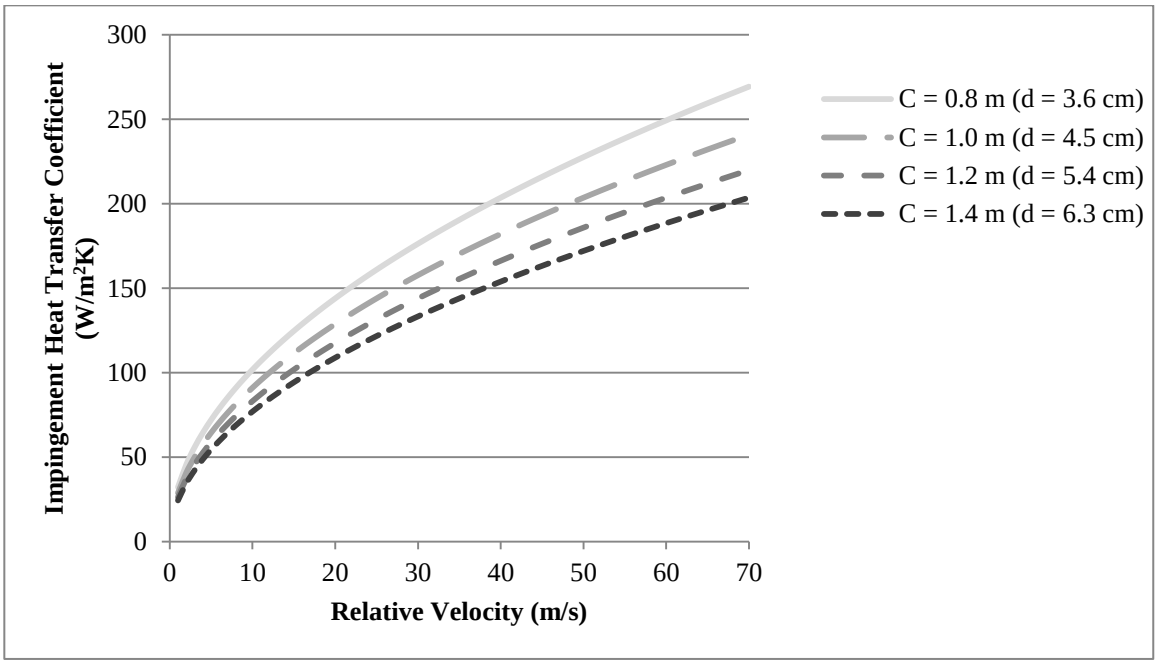

Figure 3.6: Local heat transfer coefficient at the impingement point, calculated from the Frössling cylinder correlation (Eq. 3.9) for a NACA 64(3)-618 blade profile

The heat transfer coefficient is variable across the surface of the blade and is dependent upon the Reynolds number (i.e. wind speed and turbine operation), the flow transition point and the geometry of the blade. Given this variability and the discrepancies of airfoil

experimental data with simplified geometry correlations, it was decided to retain the use of the external heat transfer coefficient, h_o as an independent variable in the subsequent analysis. Results are then provided for the range of heat transfer coefficients from 0 – 250 W/m^{2}K, letting a designer choose the appropriate heat transfer coefficient value for their application.

3.1.2 Heater Area

The size of the heater wrap area in de-icing literature has so far been arbitrarily chosen [9, 61, 62]. It is well documented that ice accumulates along the leading edge of the blade; therefore the heater should be large enough that at the very minimum, the leading edge is covered. For this analysis, the heater area is chosen based on a representative geometry of a cylinder at the leading edge with a diameter equal to a quarter of the blade thickness, followed by a section that is one quarter the length of the chord. The length of the heater from the leading edge is calculated as:

$$L_h = \frac{\pi}{16}t + \frac{1}{4}C \qquad \text{Eq. 3.12}$$

where t is the chord thickness and C is the chord length. A representation of this geometry is presented in Figure 3.7.

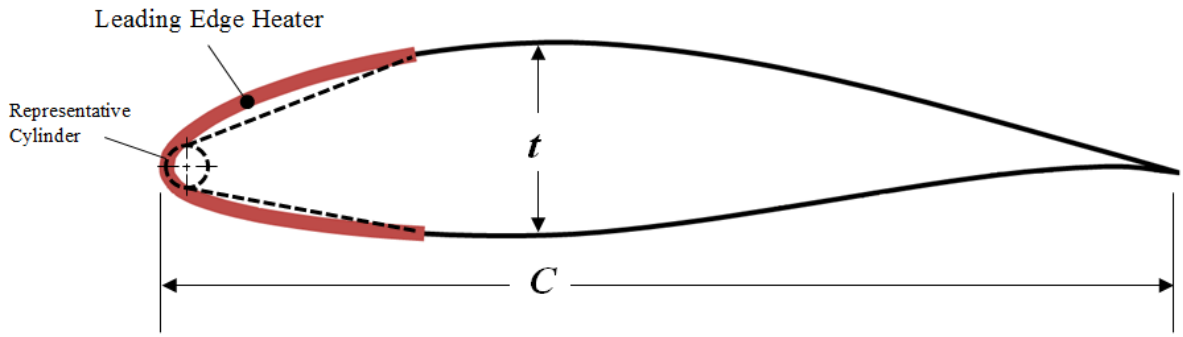

Figure 3.7: Approximate size of a leading edge, electro-thermal wind turbine blade heater. C is the chord length and t is the blade thickness. The airfoil is a NACA 64(3)-618.

For simplicity it is assumed that the heater length is equal on both the top on the bottom. The total area is calculated by multiplying the total length of the heater by the span width. At different angles of attack the distribution of icing will change. Higher angles of attack will result in a wider accumulation of ice on the pressure side of the airfoil [9, 61]. Conversely, negative angles of attack will result in more ice accumulation on the suction side. Additionally, the trailing edge of the airfoil may also want to be protected in the event of run-back icing [32]. Therefore Equation 3.12 is only an approximation of the required heater area used to estimate the power required for anti-icing. Alternative heater configurations are possible, dependent on the requirements of the wind turbine operator.

3.1.3 Anti-Icing Power Required

The power required for a wind turbine blade anti-icing system is dependent upon a number of variables. The size of the turbine, geometry of the blade, ambient temperature, arrangement of heaters and ambient wind speed are all important factors. For a range of turbine diameters (Table 3.1), the anti-icing power requirements can be compared at

	Wind Turbine Summary				
W.T. Description	G.E., 1.5 MW	Siemens, 2.3 MW	Siemens, 3 MW	Siemens, 4 MW	Siemens, 6 MW
Diameter (m)	77	82	108	120	154
Swept Area (m^2)	4700	5300	9100	11300	18600
Blade Length (m)	37	40	53	58.5	75

Table 3.1: Description of wind turbines of varying size

varying wind speeds. The geometry of each wind turbine is geometrically scaled based on the geometry outlined in chapter 2 and the respective blade lengths. The size of the heater area is calculated from Equation 3.12 in order to maintain consistency. The heater power density is based on the average Nusselt number over the domain of the heater (Equation 3.1). This assumes that the heater power density is matched to the local heat transfer coefficient. A constant heater power can be applied, however this will require a

higher overall power input in order to prevent ice accretion. For the 1.5 MW wind turbine, the parameters to calculate the anti-icing power required at a wind speed of 7 m/s are presented in Figure 3.8:

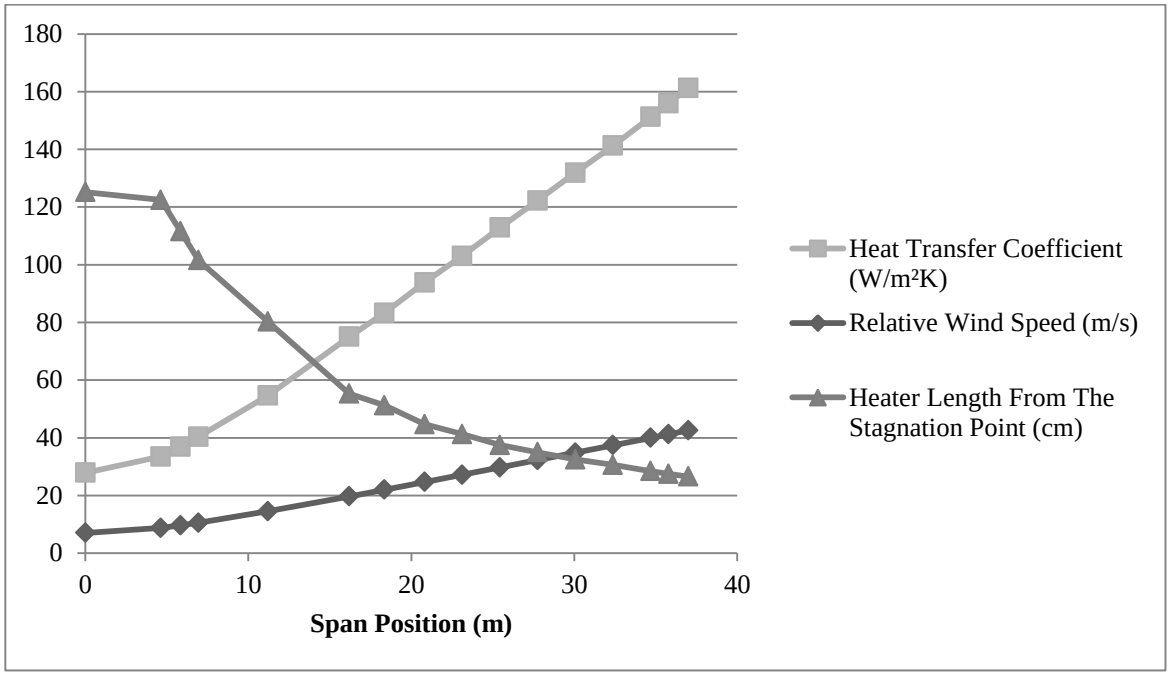

Figure 3.8: Parameters of an example 1.5 MW, 37 m blade radius wind turbine used to calculate the anti-icing power. Ambient wind speed is 7 m/s, tip speed ratio is 6 and the temperature difference between the ambient and the surface is 10°C.

From the root of the turbine to the tip, the length of the heater will decrease but the local, spanwise heat transfer coefficient will increase along with the required heater power density. The equation used to calculate the power requirements of a wind turbine can be combined:

$$P_{req} = \sum_{r}^{L_{blade}} (T_s - T_o)[h_o]A$$

where h_o is determined from Equation 3.10, A is area of each section and (T_s – T_o) is the temperature difference between the surface and the ambient (assuming the thickness of the water film is small). Expanding h_o and A gives:

$$P_{req} = \sum_{r}^{L_{blade}} (T_s - T_o) \left[\frac{0.037 {Re_L}^{0.8} Pr^{1/3} k_{air}}{L_h} \right] 2 L_h \Delta x$$

where Δx is the span length of each section and L_h is the heater length from the stagnation point, determined from Equation 3.12. The Reynolds number is dependent upon the wind speed, span location, tip speed ratio and length from the stagnation point. Expanding Re_L gives:

$$P_{req} = \sum_{r}^{L_{blade}} (T_s - T_o) \left[0.037 \left(\frac{\rho_{air} L_h \sqrt{{V_w}^2 + \left(\frac{\lambda V_w r}{L_{blade}} \right)^2}}{\mu_{air}} \right)^{0.8} Pr^{1/3} k_{air} \right] 2 \Delta x$$

where L_{blade} is the blade length, λ is the tip speed ratio and V_w is the ambient wind velocity. The properties of the air ρ_{air}, k_{air}, μ_{air} and the Prandtl number, Pr are dependent upon the film temperature $T_f = (T_s - T_o)/2$. Therefore the equation above can be further reduced:

$$P_{req} = (T_s - T_o) C \cdot {V_w}^{0.8} \sum_{r}^{L_{blade}} \left[1 + \left(\frac{\lambda \cdot r}{L_{blade}} \right)^2 \right]^{0.4} {L_h}^{0.8} \Delta x \qquad \text{Eq. 3.13}$$

where C is a constant that is determined based on the properties of air at the film temperature. The total power required can be approximated by accumulating the power of each span section. From the equation above, the combination of linear dependence on blade length, temperature difference and almost linear dependence on wind speed and heater length can be seen clearly. For example, if 100 kW is required to keep the blade at 5°C at an ambient temperature of -5°C, 200 kW of power will be required to keep the blade at 5°C when the ambient temperature is -15°C. The total power generated by the wind turbine is proportional to the cross sectional area, the ambient wind speed cubed, and the coefficient of performance, C_p. For a range of ambient wind speeds, the total power required for anti-icing of three different wind turbines is presented in Figure 3.9.

As expected the required anti-icing power to keep the blade ice free increases linearly with ambient wind speed and turbine size.

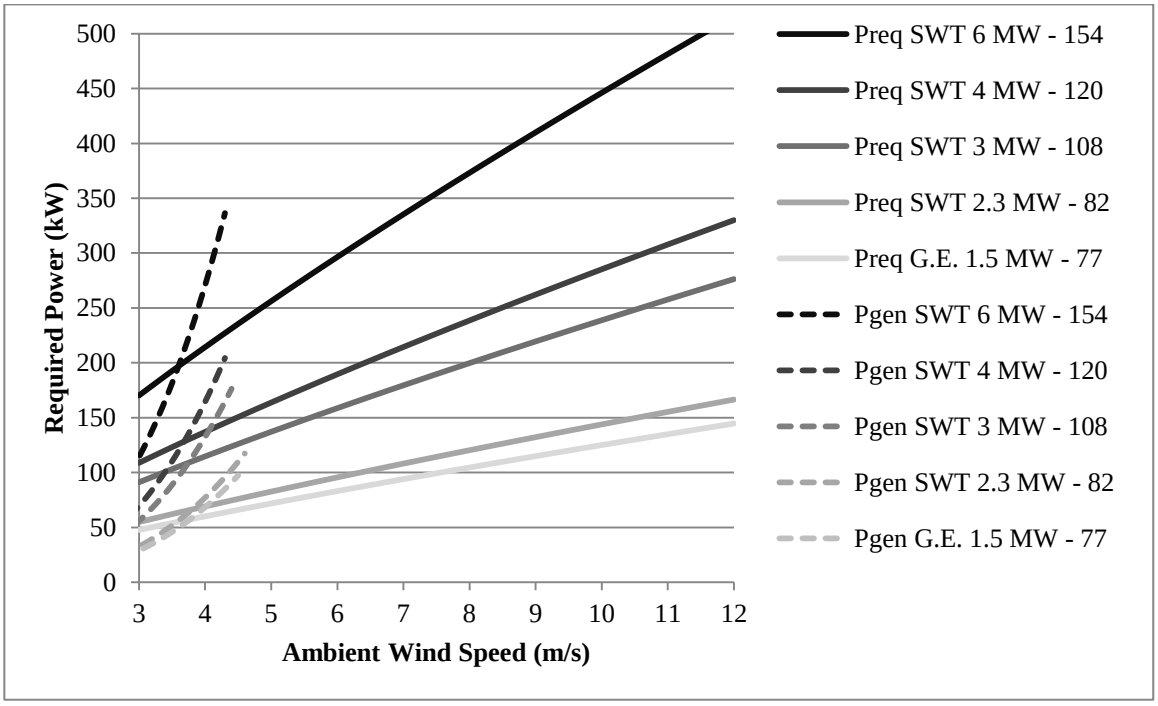

Figure 3.9: Anti-icing power required for a range of commercial wind turbines. Required power is indicated by a solid line and the power generated is indicated by a dotted line. The coefficient of performance is assumed to be 0.35 and the tip speed ratio is 6. The temperature difference between the blade surface and the ambient used here is $T_s - T_o = 10°C$.

3.2 Electro-Thermal De-Icing Analysis

The design of an icing mitigation system should minimize the total amount of energy input. An anti-icing system is required to be in operation for the entire duration of the icing event and so can result in a very large overall energy input. An alternative strategy to anti-icing is to allow ice to accumulate along the turbine blade and then to heat the interface, creating a thin film of water which will allow the ice to de-adhere. This strategy is termed de-icing. Previous studies focusing on the development of de-icing systems of car windshields and aircraft wings have measured the required power density

[43, 54, 63]. However, wind turbines face a significant challenge due the large surface that is required for de-icing.

De-icing of the blades is a transient heat transfer problem with phase change and convection at the ice/air interface. In order to solve this problem, a numerical model is developed using a one dimensional finite volume approach. The first two subsections explain the setup of the physical and numerical models. The numerical model is used to evaluate the time required to remove ice from the blade for a range of conditions. The effect of insulation thickness, ambient temperature, heater power density, external heat transfer coefficient, ice type and thickness are all explored. Additionally, possible methods of power application are explored that will most effectively de-ice the blade. In scenarios where the heater can be considered perfectly insulated and the ice semi-infinite, the analytical solution can be used. For these limited cases the numerical results are validated with the analytical solutions and provided in Appendix B.

3.2.1 Model Basis and Numerics

The heater of a de-icing system is positioned on the outside of the blade so that when ice accumulates, the heater can be turned on which will melt a thin layer of ice next to the blade. The thermal electric heater used in this analysis is based on the heater used by the Kelly Aerospace icing protection system for aircraft and marketed for wind turbine blades. The heating element of the thermal electric heater is manufactured out of metal coated carbon fibre [42]. Carbon fibre heaters are typically less than 1 mm and for leading edge application incorporate a thin but durable erosion resistant coating. A representation of the de-icing system is presented in Figure 3.10.

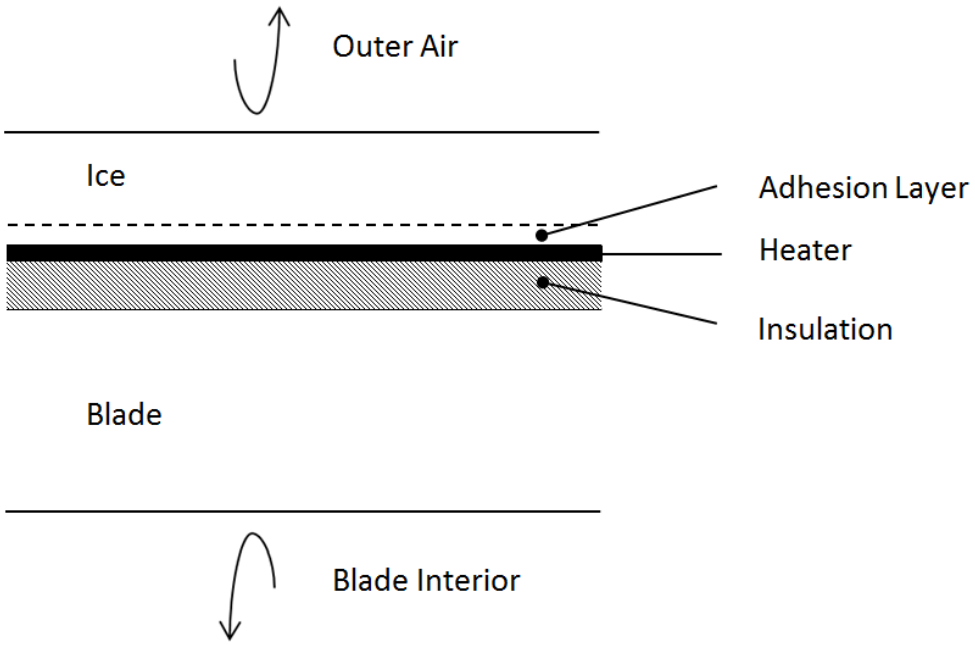

Figure 3.10: Graphical representation of the electro-thermal de-icing system. Note: figure not to scale.

The heater is mounted on the blade and can be backed with an insulation layer to minimize the amount of heat lost into the blade. When the heater is turned on, heat will diffuse into the ice and into the insulation. If the ice is thin enough and the heater is on long enough, the heat will penetrate to the outer surface of the ice where convection due to moving air will carry heat away from the blade. On the blade side, typically it will be seen that the diffusion of heat does not significantly penetrate through the fibreglass blade skin (B.1). Therefore the blade can be assumed to be a semi-infinite medium.

Under conditions of constant thermophysical properties, no heat generation and uniform initial temperature, the one-dimensional transient diffusion of heat can be expressed as:

$$\frac{\partial T}{\partial t} = \alpha \frac{\partial^2 T}{\partial x^2} \qquad \text{Eq. 3.14}$$

A formal non-dimensionalization of the de-icing process is not possible but the results will be presented in terms of convective losses and conduction through the ice. The numerical model developed here is based upon a fully implicit, finite volume approach

(Patankar 1980 [64]), that solves the one dimensional transient conduction equation. The time marching scheme is first order accurate and the length of the time step is chosen to be small enough that the numerical results are unaffected.

Within the boundaries of the heater, the transient conduction equation also incorporates heat generation. The temperature and energy stored by the heater are negligible due to the high conductivity and thin thickness (0.5 mm). Heat then diffuses into the ice and the substrate material (insulation, if present, blade skin and core). Due to the thickness of the blade wall, the effects of convection at the inner blade wall are not significant, as shown in Appendix B.1. However convection at the ice/air interface cannot be neglected. Therefore this is incorporated into the numerical model by a convection boundary condition at the ice/air interface node. At each interface of dissimilar materials, an additional boundary node is allocated in order to satisfy the energy balance for each time step.

The grid spacing is fine enough to ensure that the solution is not dependent upon the grid size. Discussion of the grid independent study is presented in Appendix B.3. For computational efficiency the grid is refined at areas where the temperature gradients are expected to be larger, i.e. near the heater.

Once the ice reaches 0°C, the phase change begins and the ice starts to melt. Previous phase change models [43, 39, 65] have incorporated the latent heat of melting using an "equivalent heat capacity", in which the heat capacity of the ice/water is modified over a specified temperature range about the melting point. An advantage of this method is that the temperature of the water can be modelled past the phase transition. The disadvantage is that the phase transition occurs over a temperature range, which for water is physically unrealistic. If the temperature range is made small, the equivalent heat capacity spikes sharply and numerical errors are likely to occur.

When the adhesion layer is thin, the temperature of the portion of ice that is melted will not increase significantly above 0°C throughout a de-icing cycle [43]. For the analysis in this thesis, the adhesion layer is assumed to be proportional to the surface roughness of

the substrate. This assumption was validated by the experimental research performed by Petrenko [43]. A conservative estimate of blade roughness is taken as 100 μm. Since we only need to model the heat transfer up to melting of the adhesion layer, the thickness of this layer can be predefined and resolved using a single control volume, which contains either ice at a temperature less than or equal to 0°C or an ice/water mix at 0°C. Once the temperature of ice that forms the adhesion layer reaches the melting point, it is held constant for the duration of the phase transition. Over each time step, the cumulative change in enthalpy is calculated from an energy balance over the adhesion layer as:

$$\Delta h_{fl} = \sum_{\substack{time \\ steps}}^{t_{tot}} \frac{\Delta t}{\delta \rho_{ice}} \left(k_{heater} \left. \frac{\Delta T}{\Delta x} \right|_{heater/adh\ layer} - k_{ice} \left. \frac{\Delta T}{\Delta x} \right|_{adh\ layer/ice} \right) \quad \text{Eq. 3.15}$$

where δ is the thickness of the adhesion layer. The ratio of total enthalpy change to latent heat of melting, gives the fraction of melted ice. Once the adhesion layer has fully melted, the external forces (gravity, aerodynamic loading, and centrifugal loading) are able to remove the ice from the blade.

3.2.2 Results

In this section the parameters that effect de-icing are explored using the numerical model described previously. The effect of heater power density, ambient temperature, convection from the surface of the blade, ice thickness, ice type and thickness of the insulation layer are investigated. These results are presented in comparison to a base case scenario.

3.2.2.1 Base Case Results

An electro-thermal de-icing base case is initially considered. The heater is assumed to be directly mounted to the fibreglass blade, without insulation. Appendix B.4 describes a method to approximate the proportion of useful heat that diffuses into the ice based on the blade and the ice as a semi-infinite media. However for longer de-icing times the heat

can penetrate through the ice and the effects of convection at the ice surface cannot be ignored. For this reason the results cannot be non-dimensionalized and must be considered for a range of operating conditions.

An electro-thermal base case is considered in which the ambient temperature is -5°C, the external heat transfer coefficient is 180 W/m^2K, the ice layer is 1 cm of glaze ice and the heater power is 5000 W/m^2. The power of the heater is expressed in W/m^2, which is the power generated (W/m^3) multiplied by the heater thickness (0.5 mm). Presenting the heater power in terms of W/m^2 allows for a direct comparison to the heat flux due to convection and conduction. The full conditions for the base case are listed in Table 3.2:

q"	5000 W/m^2	$\delta_{adhesion\ layer}$	100 μm
L_{ins}	0 mm	h_o	180 W/m^2K
T_o	-5°C	L_{ice}	10 mm (glaze)
k_{skin}	0.18 W/mK	k_{ice}	1.88 W/mK
ρ_{skin}	150 kg/m^3	ρ_{ice}	920 kg/m^3
C_{skin}	1600 J/kgK	C_{ice}	2040 J/kgK

Table 3.2: Conditions of the electro-thermal de-icing base case scenario

The temperature profiles for the base case scenario are presented in Figure 3.11:

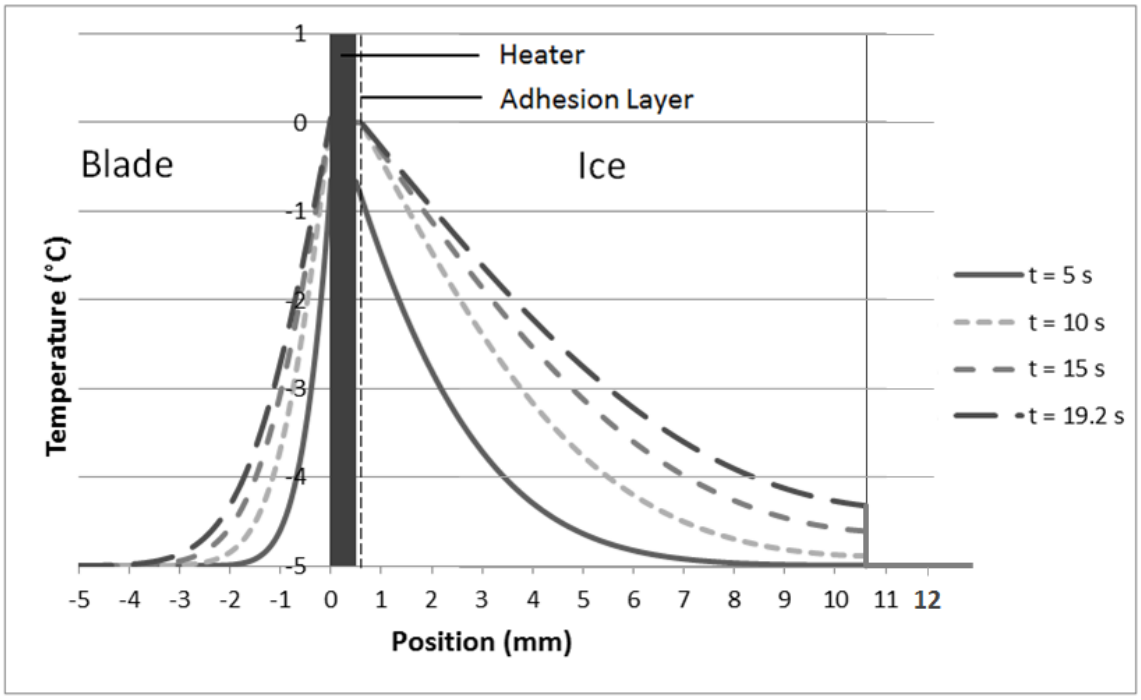

Figure 3.11: Temperature profiles through the ice and the blade skin, determined using numerical simulation. Base case conditions, see Table 3.2 for details.

The heater is resolved by several control volumes, however due to the high conductivity and small thickness of the heater, it can be shown that the temperature through the heater is relatively constant. Figure 3.11 shows that heat penetrates faster into the ice than it does into the blade. At the time required for the adhesion layer to melt (19.2 s), significant penetration of heat does not reach the blade core through the 5 mm thick blade skin and the majority of the energy from the heater diffuses into the ice. The outer surface of the ice reaches a temperature of -4.3°C, only a 0.7°C rise, after 19.2 seconds.

The total time to de-ice the blade is defined as the time required for the adhesion layer to be heated up to 0°C and then melted. The adhesion layer of ice warms up to 0°C after 6.6 seconds. The fraction of the adhesion layer that is melted throughout the simulation of the base case is presented in Figure 3.12. After 19.2 seconds the adhesion layer has been fully melted and the ice is free to be removed by centrifugal and aerodynamic forces.

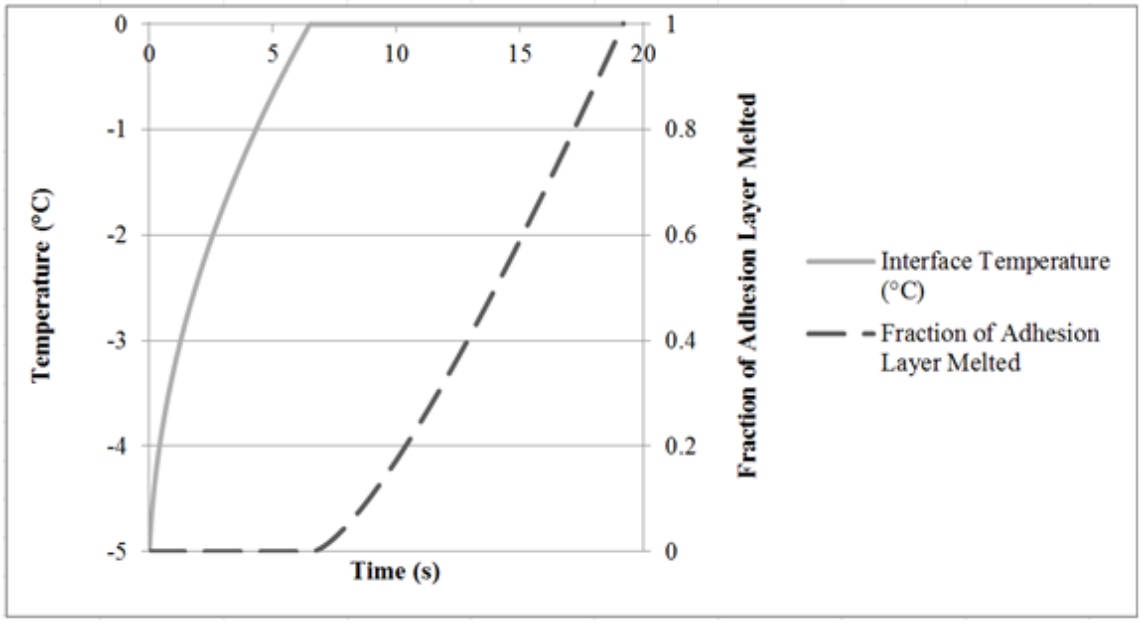

Figure 3.12: Simulation of the interface temperature and fraction of adhesion layer melted with time. Base case conditions, see Table 3.2 for details.

3.2.2.2 Effect of Heater Power Density and Ambient Temperature

The power density of the heater and the ambient temperature are critically important parameters when considering the time required to de-ice the turbine blade. Lower ambient temperatures will increase heat loss due to conduction through the ice and convection at the ice surface; this will increase the total time to de-ice the blade. The limitations of a de-icing system can be determined from a simple steady state analysis; the governing equation for one dimensional conduction through the ice of uniform conductivity is:

$$\frac{d^2T}{dx^2} = 0$$

at the heater/ice boundary, the heat flux from the heater, q" is considered to be equal to the conduction into the ice (although there will be losses into the substrate)

$$-k_{ice}\frac{dT(0)}{dx} = q"$$

and at the ice/air interface the heat flux due to conduction is equal to convection to the ambient temperature, T_o

$$-k_{ice}\frac{dT(L_{ice})}{dx} = h_o[T(L_{ice}) - T_o]$$

The minimum heat flux required for the adhesion layer to reach T_{melt} = 0°C is therefore:

$$q"_{min} = \frac{(T_{melt} - T_o)}{\frac{L_{ice}}{k_{ice}} + \frac{1}{h_o}} \qquad \text{Eq. 3.16}$$

where T_o is the ambient temperature, L_{ice} is the ice thickness and T_o is the ambient temperature. If the heat flux is less than $q"_{min}$, the de-icing system will reach steady state before the adhesion layer reaches the melting point and the blade will be unable to be de-iced.

When the heater is turned on, heat is lost by conduction into the ice. If the ice is thin enough and the heater is on long enough, heat will also be lost at the ice surface due to convection. However if heat does not significantly penetrate through the ice, convection will not affect the time required to de-ice the blade. The heater power density for convection losses to be considered negligible can be approximated from the steady state analysis by specifying that the outer ice surface temperature must be equal to the ambient temperature, $T(L_{ice}) = T_o$.

$$q"_{mod} = \frac{(T_{melt} - T_o)k_{ice}}{L_{ice}} \qquad \text{Eq. 3.17}$$

where $q"_{mod}$ will represent a moderate heater power density that is between low heater power densities (where convection is significant) and high heater power densities. If the heater power density is very high (>> $q"_{mod}$), the convection and conduction losses will not be significant. In this region, the time required to de-ice the blade will asymptotically approach the time required to melt the adhesion layer, which can be approximated as:

$$t_{min} = \frac{\delta \cdot h_{fl}\rho_{ice}}{q''_{high}} \qquad \text{Eq. 3.18}$$

where δ is the thickness of the adhesion layer and heat capacity of the ice is negligible compared to h_{fl}, the latent heat of fusion. The required de-icing time has been mapped out for a range of expected ambient temperatures and potential heater power densities. The one dimensional results will be applicable to any commercial scale wind turbine within the range of the heat transfer coefficients used in this analysis (section 3.1.1). The time required to remove ice from the blade of the wind turbine for the base case conditions is presented in Figure 3.13 below.

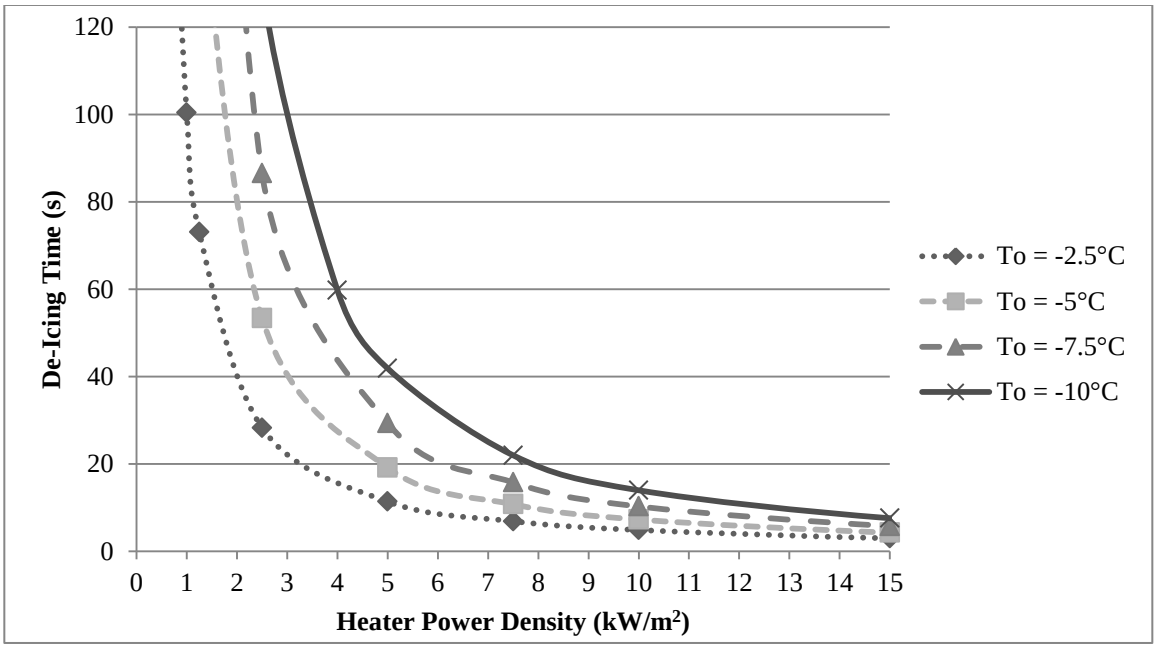

Figure 3.13: Effect of heater power density and ambient temperature on the base case (Table 3.2)

From Figure 3.13 it can be observed that increasing the heater power density has compounding gains. When the heater power density is low, the time required to de-ice the blade asymptotically approaches infinity based on the ambient conditions. At T_o = -10°C the time required to de-ice the blade approaches the infinity as the heater power density approaches q''_{min} = 0.920 kW/m^2. At slightly higher power densities, where de-icing is possible but requires a long time to do so, the energy from heater has a

chance to penetrate through the ice layer where heat is lost due to convection. If the power density is high, the penetration front never reaches the surface of the ice and the convection has no effect on the de-icing time. At -10°C, with 10 mm of glaze ice, the heater power density required in order for convection losses to be neglected is q''_{mod} = 1.9 kW/m^2. Therefore the heat flux due to convection will not affect de-icing time for the majority of the heater power densities (and for all practical de-icing times), presented in Figure 3.13.

With increasing heater power density the de-icing time will approach the time required to melt the adhesion layer (Equation 3.18). For example, the proportion of time required to heat the adhesion layer to the melting temperature (0°C) decreases from 34% to 21% of the total time to melt the adhesion layer when the heater power density is increased from 5 kW/m^2 to 15 kW/m^2 (Figure 3.14).

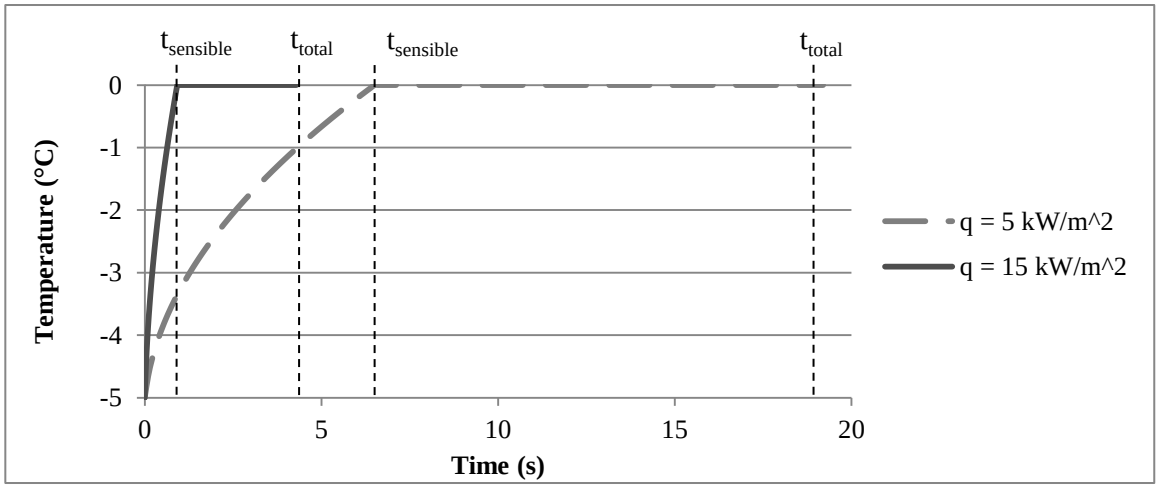

Figure 3.14: Temperature of the adhesion layer with time showing the proportion of sensible heating time to total de-icing time. Initial temperature is -5°C, the ice accretion is a 10 mm thick layer of glaze ice and the heat transfer coefficient is 180 W/m^{2}K. $t_{sensible}$ is the time required to heat the adhesion layer to the melting point and t_{total} is the total time required to de-ice the blade.

Insulating the blade from the heater will reduce the amount of heat that is lost into the substrate (insulation if present, otherwise the blade wall) and a rime ice accretion (instead of glaze ice) will reduce the amount of heat that is lost to the ice due to conduction. Additionally, increasing the heater power density will reduce the amount of heat that is

lost due to conduction to the ice and the substrate. The effect of insulating the heater from the blade is investigated in the next chapter section.

3.2.2.3 Effect of Insulation Backing

The base case scenario considers the time required to de-ice the blade with the heater mounted directly on the blade surface. A layer of insulation between the heater and the blade will increase the proportion of heat that is used to melt the adhesion layer. An effective insulator will have a low thermal inertia compared to the ice (Appendix B.4); Table B.2 compares the thermal inertia of different insulating materials. The optimum insulation thickness can be determined by calculating the percent decrease in de-icing time with decreasing insulation (0% increase corresponds to the maximum useful insulation thickness). Thicker insulation is required at colder temperatures and lower heater power densities due to the longer de-icing time. Figure 3.15 presents the effect of insulation at -10°C, which is expected to be the coldest temperature at which significant

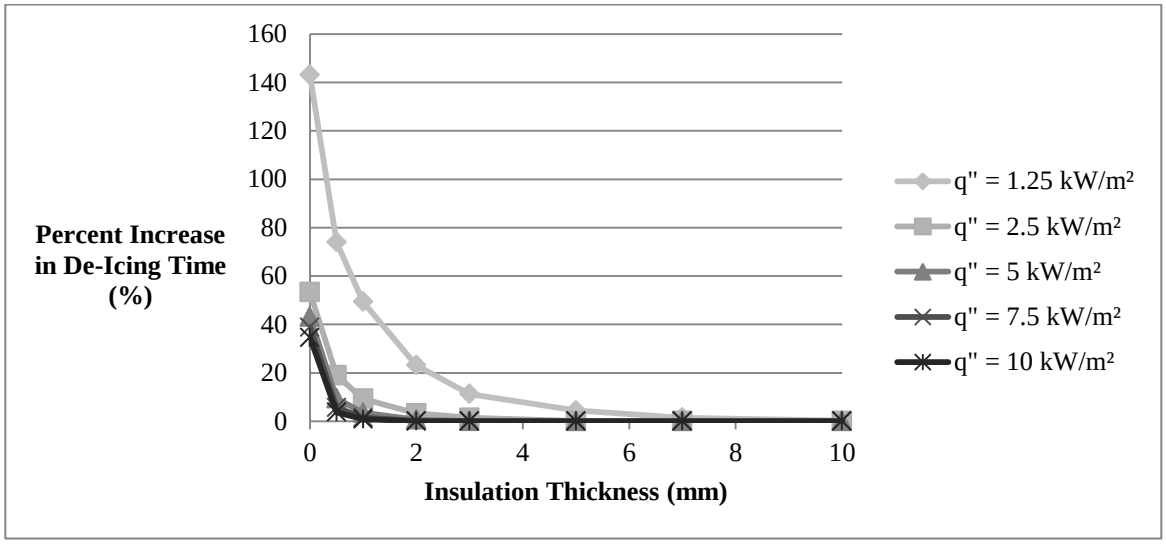

Figure 3.15: The effect of insulation backing on electro-thermal de-icing time. The ambient temperature is -10°C and the outside heat transfer coefficient, h_o is 180 W/m^{2}K. The ice layer is 10 mm of glaze ice.

icing will occur. The conductivity of insulting materials is approximately an order of magnitude smaller than the conductivity of fibreglass (typical blade skin material). The low conductivity of the insulation allows more of the heat to penetrate into the ice instead

of the substrate. For a practical range of heater power densities (2.5 to 10 kW/m^2), 1 – 2 mm of insulation will reduce the de-icing time by 25% or more (Figure 3.15). Further increasing the thickness (> 2mm) of the insulation layer in this range of heater power densities has no significant effect on the time required to de-ice. However if the heater power density is below 2.5 kW/m^2 the time to de-ice is longer and a thicker layer of insulation will be effective. Between 0.75 and 2.5 kW/m^2, 2-5 mm of insulation is sufficient. The subsequent results in this analysis will be presented based on the assumption that the heater is separated from the blade by 2 mm of insulation for heater power densities greater than 2.5 kW/m^2 and 5 mm of insulation for heater power densities below 2.5 kW/m^2.

3.2.2.4 Effect of External Convection

For the base case scenario, it was observed that for a heater power density of 5 kW/m^2 (q">q"$_{mod}$), the temperature rise at the outer surface would only increase by 0.7°C. For this heater power density, convection will not have a significant influence on de-icing time. However, if the heater power density is less than q"$_{mod}$ (Equation 3.17), there is enough time for a significant rise in surface temperature and convection will influence the de-icing time. For low to moderate heater power densities, the time required to de-ice the

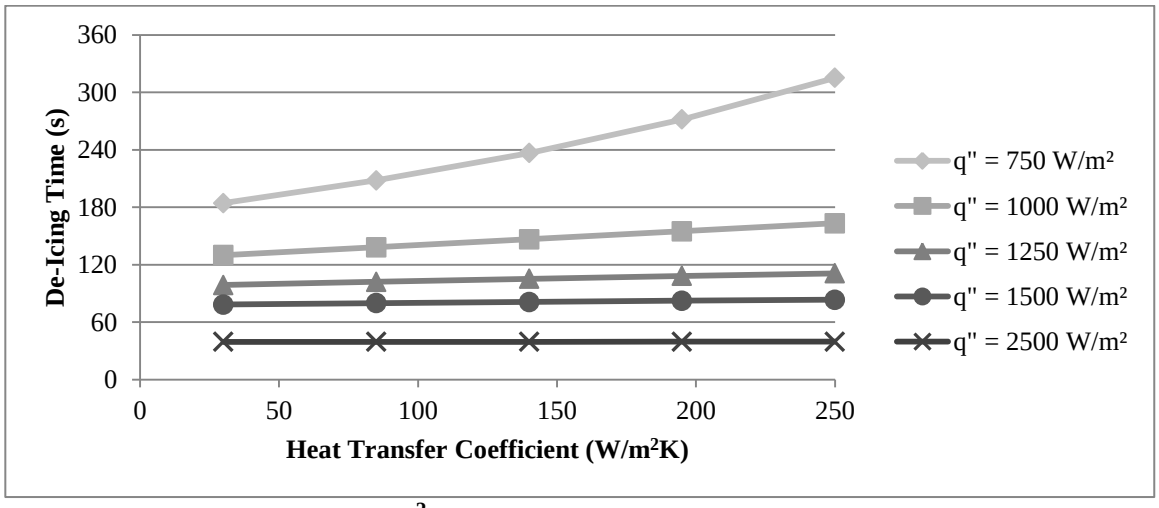

a) T_o = -5°C, q"$_{mod}$ = 940 W/m^2

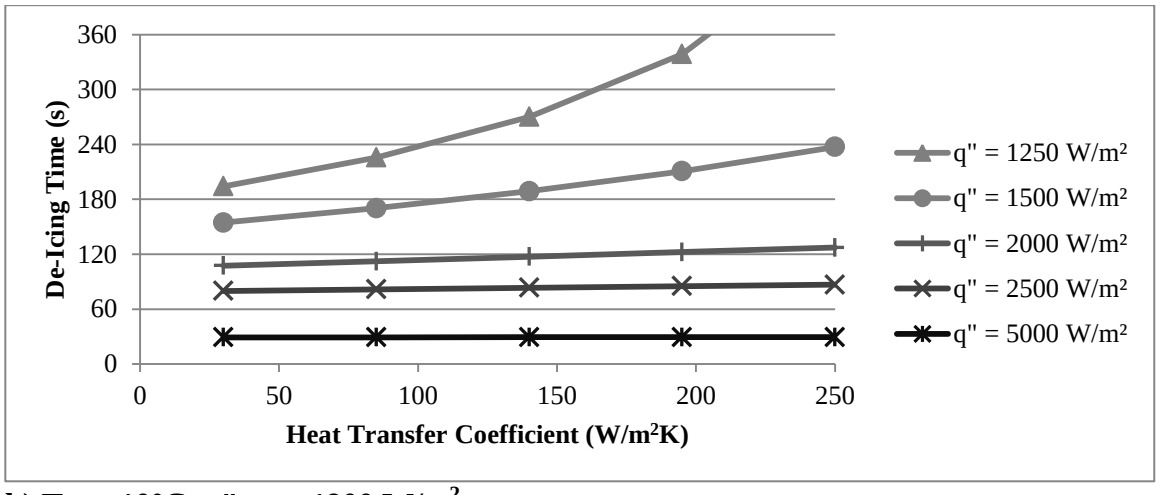

b) T_o = -10°C, q"$_{mod}$ = 1900 W/m^2

Figure 3.16: The effect external convection on de-icing time for 10 mm thick glaze ice accretion. The heater is mounted on 2 mm of insulation.

blade is presented in Figure 3.16 for a 10 mm glaze ice accretion at T_o = -5°C and T_o = -10°. For low heater power densities (q" < q"$_{mod}$), an increase in the external heat transfer coefficient will rapidly increase the time required to de-ice. A 5 mm layer of glaze ice with T_o = -10°C (the lowest temperature for which significant icing will occur) is a practical worst case de-icing scenario. As previously discussed, if heater power density is less than q"$_{min}$ (Equation 3.16), the blade will be unable to be de-iced. For a range of external heat transfer coefficients, the de-icing time is presented in Figure 3.17.

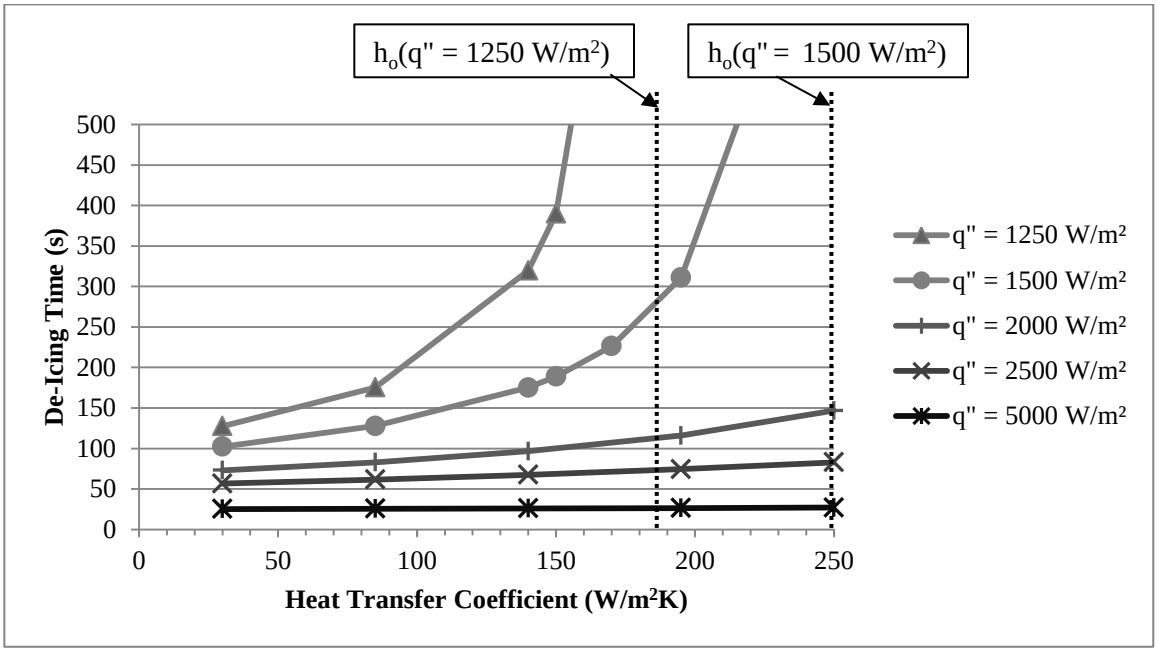

Figure 3.17: The effect external convection on de-icing time. The ambient temperature is -10°C and the heater is mounted on 2 mm of insulation. The thickness of the glaze ice is 5 mm. q"$_{mod}$ = 3800 W/m^2

When the effects of convection are significant (q"< q"$_{mod}$), the time required to de-ice the blade will asymptotically approach infinity when q" is proportional to q"$_{min}$. This is possible when the thickness of the glaze ice is 5 mm, T_o = -10°C and the heater power density is less than 2000 W/m^2. The effects of convection will not affect the time required to de-ice when q" is greater than q", which is dependent upon the ambient temperature, ice type and thickness.

3.2.2.5 Effect of Ice Type and Thickness

In this section the influence of ice type and thickness on de-icing time is investigated. As described previously, the properties of ice that accumulate on the leading edge of the blade can vary dramatically. A rime ice accretion contains trapped air which lowers the conductivity and density of the ice layer. Additionally the nature of a rime ice allows it to form a thicker layer. The lower conductivity and thicker nature provide an improved insulation barrier compared to glaze ice and the lower density means that a smaller mass of ice has to be melted in the adhesion layer. For these reasons a glaze ice layer is considered a worst case scenario.

The thickness of the ice layer also has a significant effect on de-icing. A minimum ice is required for de-icing if the heater power density is below the heat flux required to prevent ice from forming on the blade. If the ice layer is thick and the de-icing time is small, the penetration of heat will not reach the outer surface of the ice and external convection will not be significant.

The minimum ice thickness can be calculated from the steady state analysis, in the same way that q''_{min} (Equation 3.16) was determined. For a given heater power density, the minimum ice thickness required for de-icing can be approximated as:

$$L_{min} = (T_{melt} - T_o)\frac{k_{ice}}{q''} - \frac{k_{ice}}{h_o} \qquad \text{Eq. 3.19}$$

Equation 3.19 can be rearranged to show that a minimum ice thickness is not required when:

$$q'' \geq q''_{A/I} = h_o(T_{melt} - T_o) \qquad \text{Eq. 3.20}$$

where T_{melt} is the melting temperature of ice and T_o is the ambient temperature. $q''_{A/I}$ is exactly equal to heater power density required for anti-icing (with $T_s=T_{melt}$), as mentioned in section 3.1. When the heat transfer coefficient is small, the thermal resistance of the ice layer is relatively unimportant. If the heat transfer coefficient is large, a minimum ice thickness is relevant, this is represented in Figure 3.18:

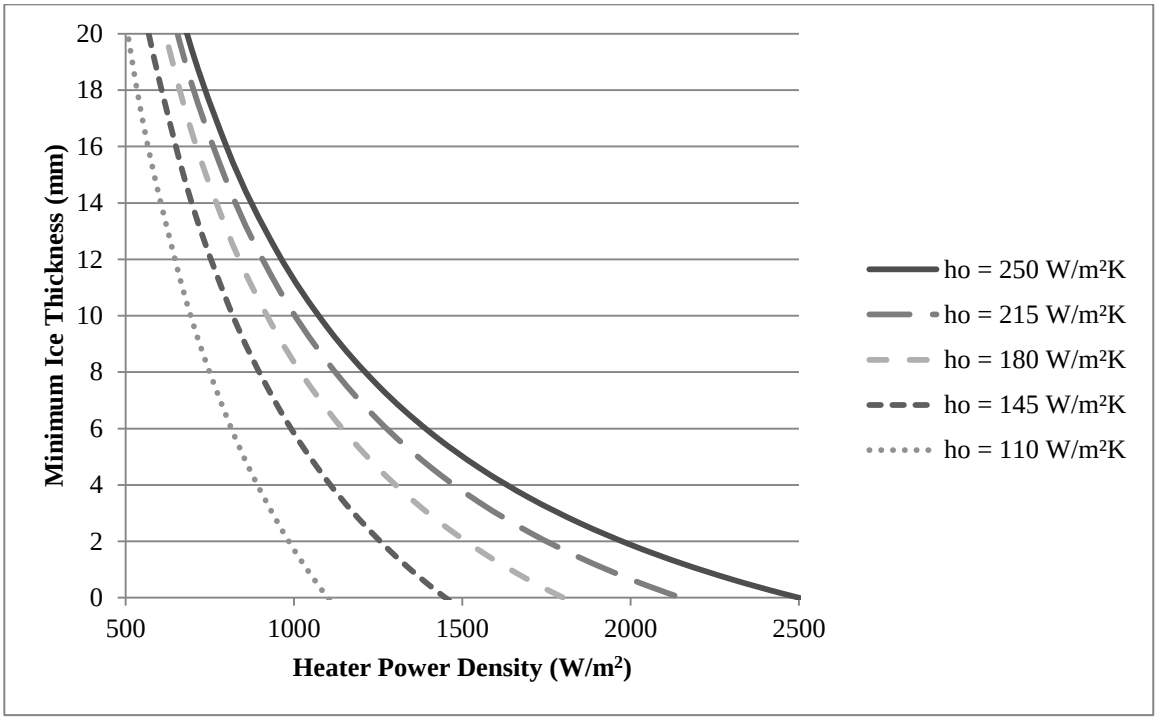

Figure 3.18: Minimum ice thickness required for de-icing. Ambient temperature, To is -10°C, and the type of ice is glaze.

If the depth of the ice is less than the minimum thickness presented in Figure 3.18, the interface temperature will not reach 0°C. For a practical range of ambient conditions (to T_o = -10°C, h_o = 250 W/m^{2}K), a minimum ice thickness is not required for electro-thermal heaters with a power density greater than 2500 W/m^2.

The minimum ice thickness for the effects of convection to be considered negligible can be approximated by rearranging $q"_{mod}$. The ice thickness required for external convection to be considered negligible for a given heater power density is approximated as:

$$L_{conv} = (T_{melt} - T_o)\frac{k_{ice}}{q"} \qquad \text{Eq. 3.21}$$

The required ice thickness for convection to be negligible is always equal to or less than the minimum ice thickness required for de-icing to be possible. For a range of ice thicknesses, external heat transfer coefficients and heater power densities, the time to de-ice a glaze ice accretion is determined using numerical analysis and presented in Figure 3.19:

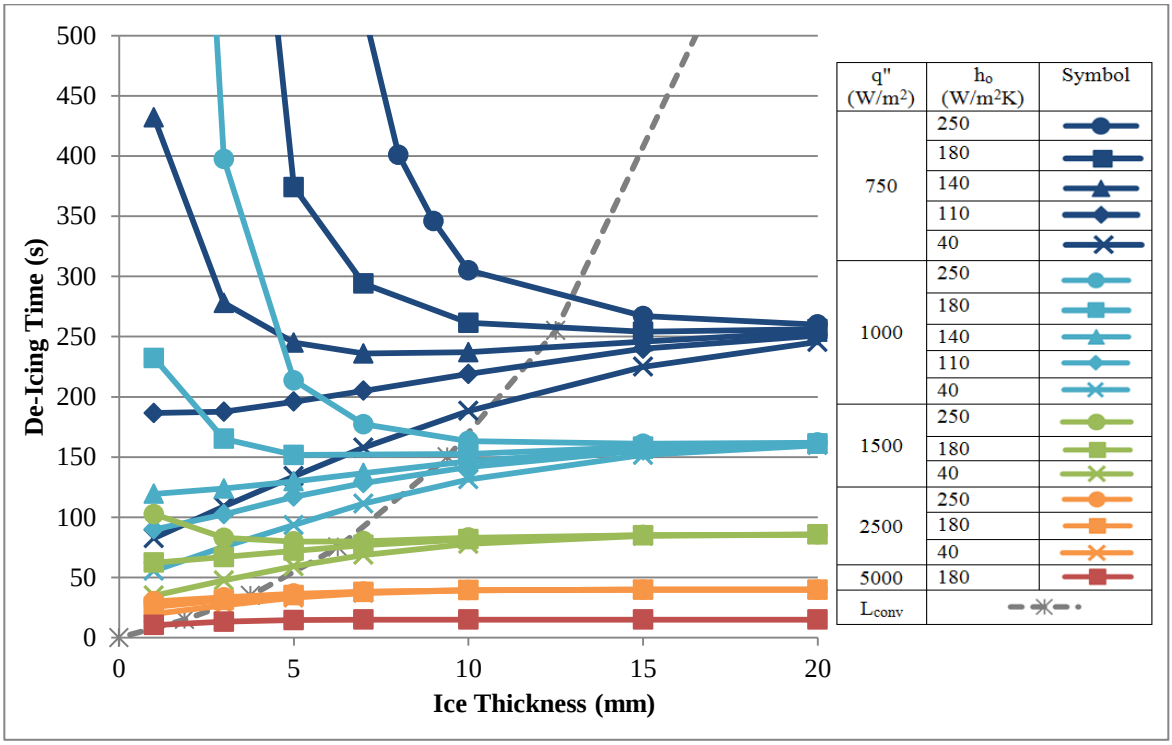

Figure 3.19: The effect of ice thickness on de-icing time. The ambient temperature is -5°C. L_{conv} is the approximation (Eq. 3.21) of ice thickness required for convection at the ice surface to be significant.

For each heater power density presented in Figure 3.19, the dependence of de-icing time on ice thickness and external heat transfer coefficient can be separated into three regions:

1. In the right hand region ($q'' > q''_{mod}$), where the ice thickness is greater than L_{conv}, a minimum ice thickness is not required and the effects of convection will not significantly influence the time required to de-ice the blade. In this region the heat loss is almost entirely dominated by conduction.
2. In the upper left region ($q'' < q''_{A/I}$ & $q'' < q''_{mod}$), convection losses from the blade are significant. A lower ice thickness and higher external heat transfer coefficient will increase the amount of heat that is lost due to convection which will increase the time required to de-ice the blade. In the upper left region, a minimum ice thickness is required for de-icing to be possible ($q'' < q''_{A/I}$).
3. In the lower left had region ($q''_{A/I} < q'' < q''_{mod}$), the external heat transfer coefficient is low and convection at the ice surface effectively acts as insulation;

this allows the surface temperature to increase substantially, further reducing the heat lost by conduction. In this region if the ice thickness is increased more heat is lost by conduction and the de-icing time increases. As the external heat transfer coefficient goes to zero, the insulation provided by convection increases. This effect is illustrated by comparing the temperature profiles of two case scenarios (in this region) with different ice thicknesses (Appendix B.6).

The de-icing time for a practical worst case scenario is considered, in which the external heat transfer coefficient is 250 W/m^{2}K and the ambient temperature is -10°C. The de-icing time for this scenario is presented in Figure 3.20 below:

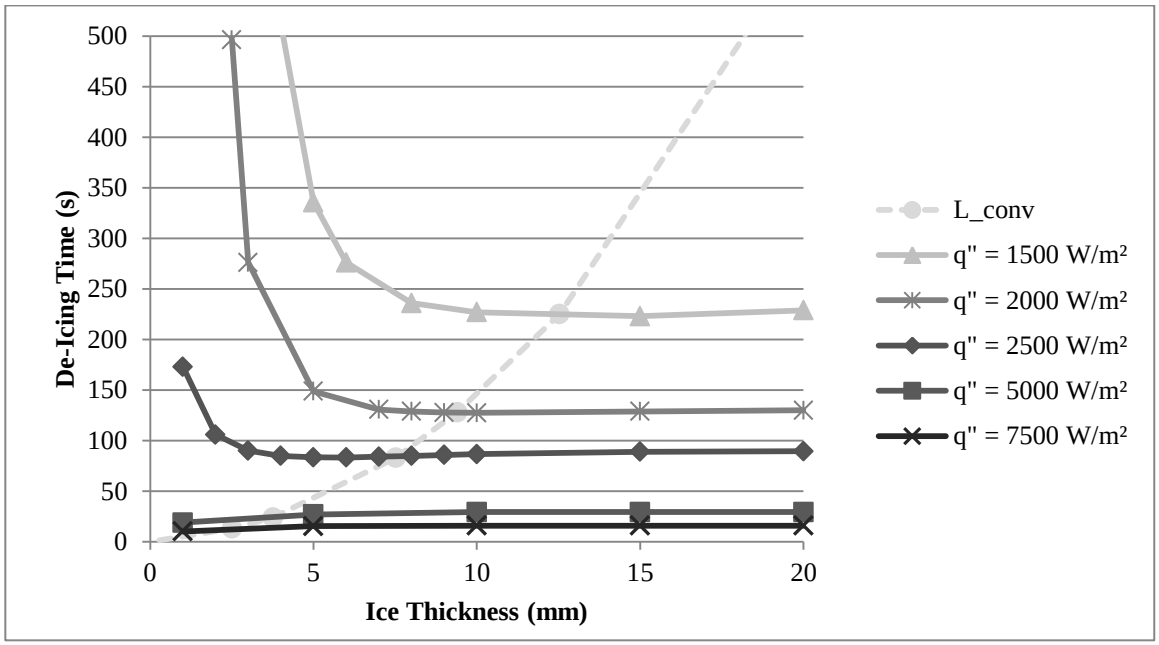

Figure 3.20: The effect of ice thickness on de-icing time. The ambient temperature is -10°C and the outside heat transfer coefficient, ho is 250 W/m^{2}K. L_conv is the approximation (Eq. 3.21) of the ice thickness required for convection at the ice surface to be significant.

Similar to the previous figure, the time required to de-ice can be separated into regions. In the left hand region ($L_{ice} < L_{conv}$), the ice thickness will affect the time required to de-ice. If q" is less than $q"_{A/I} \cong 2500$ W/m^2 (upper left), then increasing the ice thickness will decrease the time to de-ice and a minimum ice thickness is required to de-ice. If q"

is greater than $q''_{A/I} \cong 2500$ W/m^2 (lower left), then increasing the ice thickness will decrease the time to de-ice. If L_{ice} is greater than L_{conv}, convection losses will not be significant.

From the results of this analysis, guidelines for the operation of an electro-thermal de-icing system can be established: If the ice layer is initially thin and the external heat transfer coefficient is high ($q'' < q''_{mod}$ & $q'' < q''_{A/I}$), then the operator should wait until sufficient ice has accumulated before sending power to the heaters. If the ice layer is initially thin and the heat transfer coefficient is low ($q'' < q''_{mod}$ & $q'' > q''_{A/I}$), then de-icing will be most efficient for thin layers of ice, however the total heating in time must be considered in this scenario if multiple heating cycles are required for a single icing event. If the ice thickness is already thick ($q'' > q''_{mod}$), then the time to de-ice will be independent of convection.

3.2.3 Power Application Strategies

High local power densities will reduce the penetration of heat into the ice, maximizing the amount of useful energy that is required to melt ice within the adhesion layer. Therefore higher local power densities give more efficient de-icing (Figure 3.21). Figure 3.21

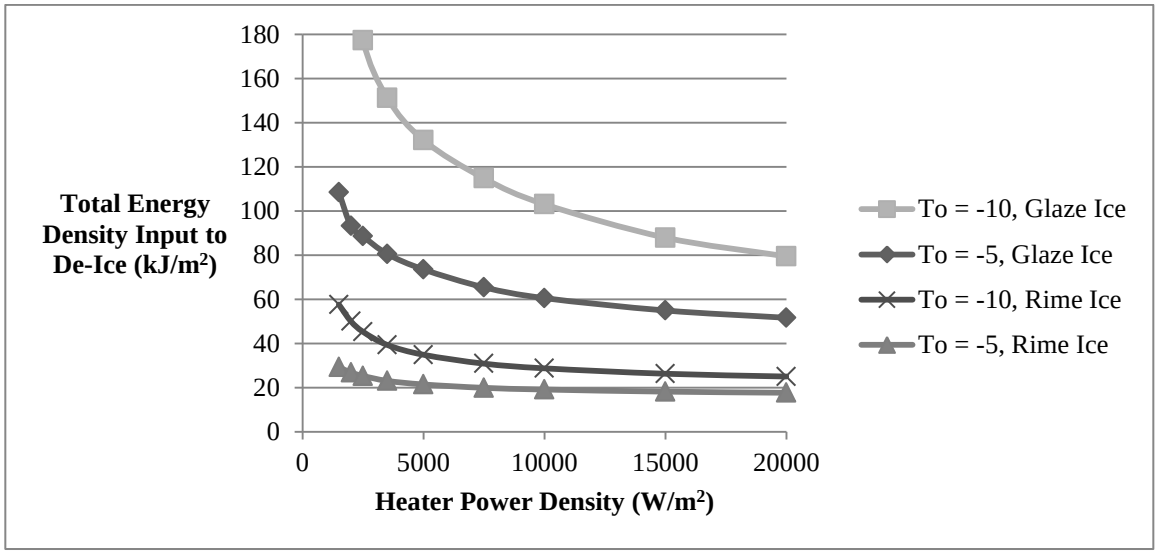

Figure 3.21: Total energy density input required for de-icing. Outside heat transfer coefficient is 180 W/m^{2}K.

shows that the total energy input required to de-ice will decrease with increasing heater power density. However it is impractical to provide these sorts of power densities over large areas simultaneously. In order to provide the desired heater power density, heat can be applied sequentially to panels.

In this thesis, two power application strategies are proposed for de-icing the blade in sections. The first strategy is to separate the blade into zones that would be heated in overlapping groups, with the break off section in the overlapping zone(s). A section that is separated into five zones is depicted in Figure 3.22. A sequential de-icing strategy

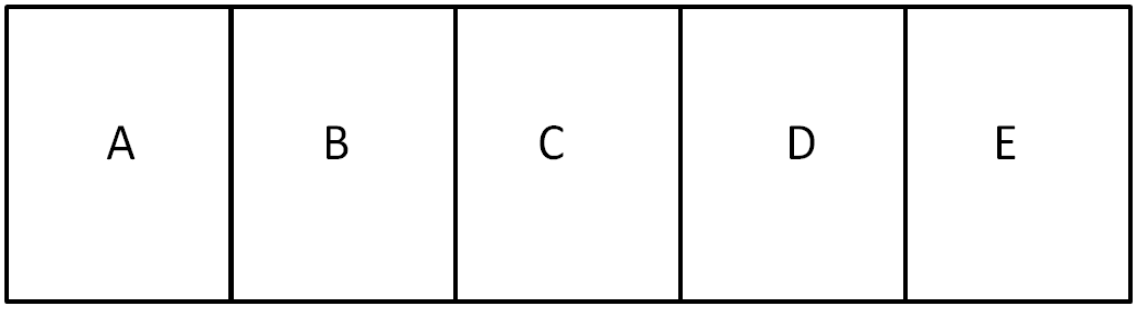

Figure 3.22: Separation of zones for de-icing

would heat zones D-E, then C-D, then B -C then sections A-B so that there is always an overlap between the zones being heated. In typical operating conditions, normal loading will not be sufficient to overcome the structural strength of the ice. Heating the blade will remove the adhesion strength of the ice, creating a stress concentration between the heated zones. Due to the irregularity of leading edge ice accretion, an overlap area will compensate for the uncertainty in the point of maximum stress concentration. The heater overlap area can be optimized by increasing or decreasing the number of zones and heating C-D-E, then A-B-C so that the overlap zone is equal to or greater than the distance that the ice can break without leaving structurally sound remnant ice. The total area that can be de-iced is determined from the power available to the operator, which can be provided directly from the wind turbine itself or can be taken from the grid.

The second proposed strategy heats a strip continuously, between the sections that are to be de-iced; this eliminates the need to overlap the blade sections. The continuously

heated strip has been previously suggested for aircraft electro-thermal de-icing systems and is referred to as a separation strip [56]. The separation strip operates in an anti-icing mode so that a thin strip is kept ice free between neighbouring sections. The remaining power can then be used to de-ice the individual sections.

3.3 Electro-Thermal Heating Summary

An electro-thermal heating system can be operated in either an anti-icing mode, to prevent ice accretion, or in a de-icing mode, to remove ice accretion once it has formed. The power requirements of an anti-icing system was simplified down to the main parameters involved and has been mapped out for a range of large wind turbines. It was found that the required power increases linearly with blade length, ambient temperature and nearly linearly with ambient wind speed and fraction of heater area to total area.

It was observed that the efficiency of the electro-thermal de-icing increased with higher heater power densities. In order to deliver a large power density, the heating can be applied sequentially to individual sections of the blade at a time. To overcome the structural strength of neighbouring sections, two power application systems are proposed; sequential heating and separation strips. Efficient de-icing of the blade surface to overcome the adhesion strength of the ice, coupled with a power application strategy will optimize the delivery of energy to where it is needed.

The time required to electro-thermally de-ice the blade is affected by the heater power density, the ambient temperature, the ice type and in some cases the thickness of the ice and the external heat transfer coefficient. Additionally heat is lost by conduction into the blade itself. It was found that if 1 to 2 mm of insulation backing is placed between the heater and the blade, the de-icing time will be reduced by 25% or more. Glaze ice was determined to represent the worst case scenario in both de-icing time and heat penetration depth. Figure 3.23 represents a flow chart in order to determine the relative importance

of the remaining parameters (L_{ice}, h_o, q", T_o). The heater power density is proportional to the power that is available, divided by the area of each heating panel. If the heater power density is less than $q"_{min}$ the blade will be unable to be de-iced and the number of panels must be increased. If the heater power density is greater than $q"_{mod}$, then the effects of convection will be insignificant and Figure 3.13 can be used to determine the time required to de-ice the blade. If the heater power density is greater than $q"_{min}$ but less than $q"_{mod}$ the thickness of the ice accretion and the heat flux due to convection will be significant. In this region a minimum ice thickness is required in order to de-ice the blade if the heater power density is less than $q"_{A/I}$. When ice thickness and convection are significant Figures 3.19 and 3.20 can be used to approximate the time required to de-ice the blade.

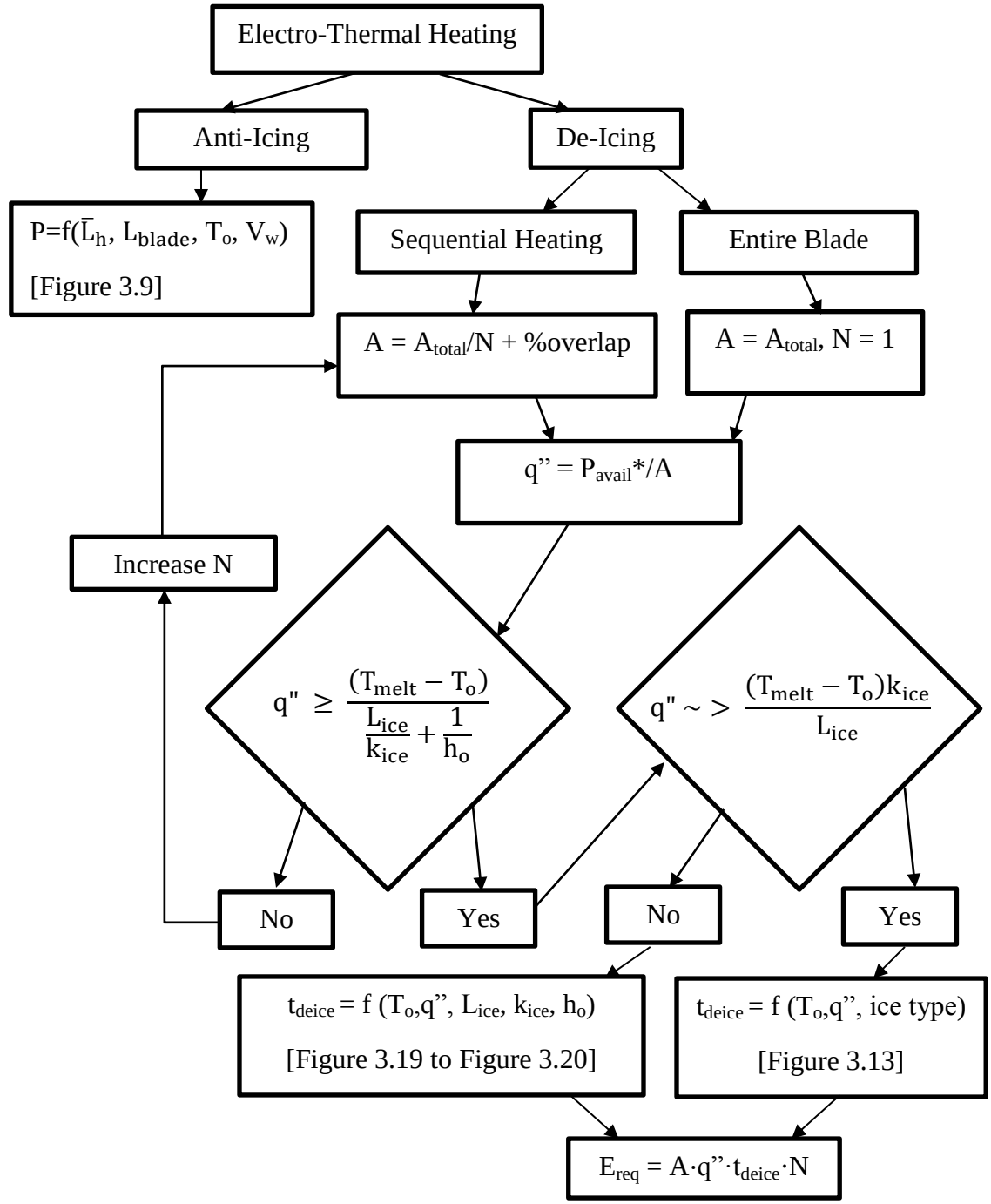

Figure 3.23: Flow diagram of an electro-thermal heating system for removing ice on wind turbine blades

4 Hot-Air Heating

An alternative heating strategy to electro-thermal heating is hot air anti-icing and de-icing. Previously described in Chapter 2, hot-air anti-icing and de-icing works by installing a heater and blower in the root of the turbine blade which blows heated air through a channel that spans the leading edge of the blade. Once the air reaches the tip of the blade it is recirculated back to the root where it is reheated. The system (Figure 4.1) is available for Enercon wind turbines [66]. In Enercon blades the channels to direct the hot air are part of the pre-existing construction. Blades that are manufactured without a channel along the leading edge can have one built into the design of the hot air heating system. A custom channel will be more expensive but will have the ability to direct the heat where it is needed most.

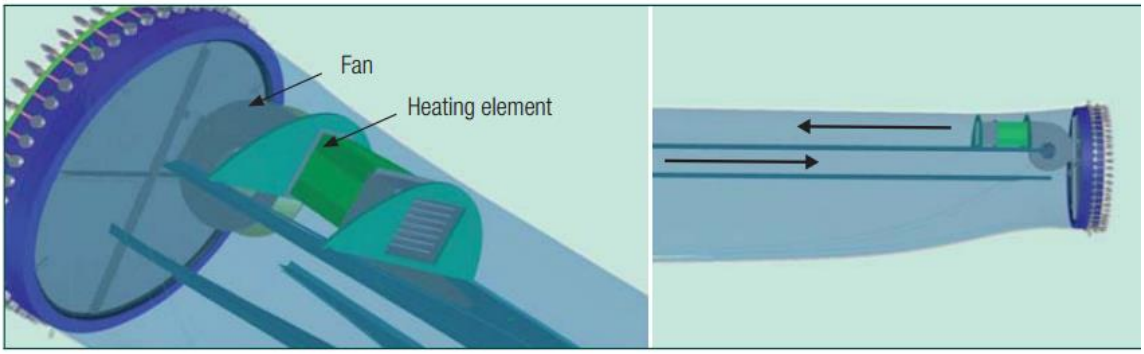

Figure 4.1: Functional principle of rotor blade de-icing system [66]

The main advantages of hot air icing mitigation systems are the inexpensive cost of installation, low maintenance costs, inherent lightning protection and no aerodynamic penalties caused by installation of the system [66]. However the efficiency of hot air de-icing and anti-icing is reduced due to the indirect heating.

As previously discussed, wind turbine blades are constructed so that the wall of the blades are thickest at the root and taper towards the tip. Consequently the thermal resistance of the wind turbine blade wall varies considerably along the span of the blade. In this thesis, the hot air heating system will be analysed for a range of blade wall thicknesses.

Initially, steady state heat transfer between the hot air and ambient temperature is explored, with and without ice accumulation. Anti-icing is represented by the steady state heat transfer without ice and the blade surface temperature kept above freezing. With ice on the blade, the steady state heat transfer case represents the limiting scenario, in which de-icing will not be possible.

In order to determine the required heating time to de-ice the blade, a transient analysis is required, which is done numerically. The differential heat transfer equations and phase change problem are solved using a finite volume approach.

The blade sections are analysed separately in order to observe the effect of wall thickness on the heat transfer process. Special attention is given to the outer third of the blade, where ice accumulation is most likely to occur and will have the greatest impact on energy production. In order to gain useful insight into hot air de-icing, the number of variables involved will be simplified per case scenario. The internal heat transfer can be analysed based on the limiting case scenario where the inside surface temperature is equal to the hot air temperature as it will be shown that the resistance due to convection on the inner surface is small relative to conduction through the wall. The range of expected heat transfer coefficients represent variation in the ambient wind speed, operating condition (at stand-still or during operation of the turbine) and geometry of the blade. The remaining variables are: the inside hot air temperature, blade wall resistance, ice thickness, ice type, external heat transfer coefficient and ambient temperature. Simplification of the ice type, ice thickness and external heat transfer coefficient is possible into harsh and favourable case scenarios in order to focus on the effects of hot air temperature, blade wall resistance and ambient temperature.

4.1 Hot Air Heating Model Description

The setup for the single blade analysis of a hot air de-icing system is presented in Figure 4.2 below:

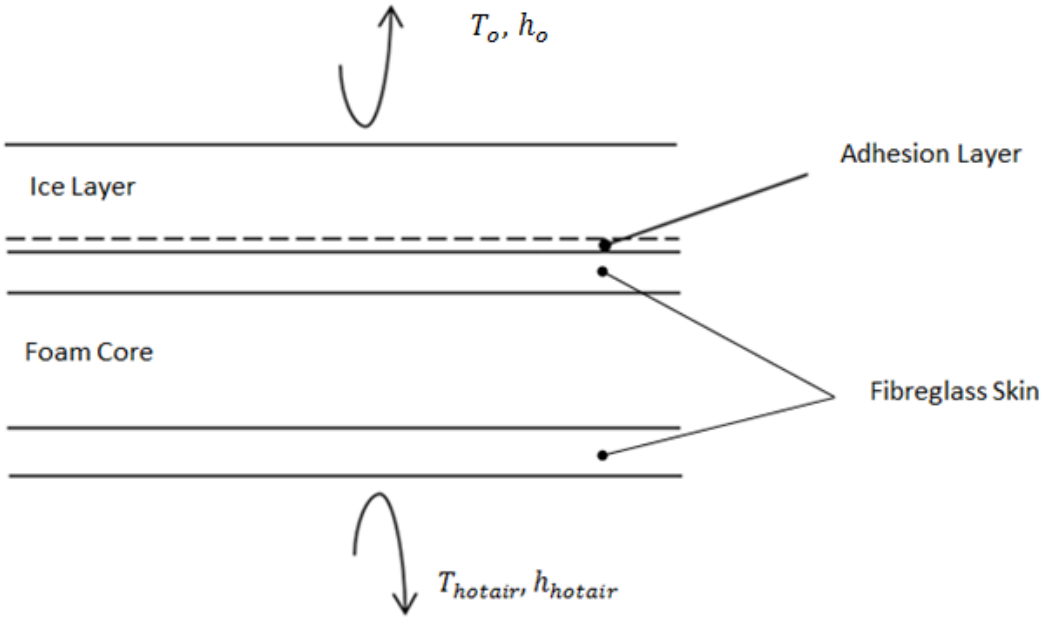

Figure 4.2: Section profile of the hot air de-icing system

Heat is provided at the inner side of the blade wall by convection of hot air through a channel that runs along the leading edge. T_{hotair} is the temperature of the hot air and h_{hotair} is the heat transfer coefficient on the inside of the blade. Heat is then conducted through the composite blade wall and ice layer. At the ice surface, heat is dissipated into the ambient environment due to external forced convection. The purpose of a de-icing system is to melt a thin layer of ice, referred to as the "adhesion layer", at the blade/ice interface.

The effectiveness of a hot air de-icing system to transfer heat to the adhesion layer is dependent on the thermal conductivity, heat capacity, density and thickness of the blade wall. However, only the thermal resistance of the blade wall is important for steady state heat transfer. For these scenarios, the thermal resistance of the composite blade wall is calculated as:

$$R_{wall} = \frac{2 \cdot L_{skin}}{k_{skin}} + \frac{L_{core}}{k_{core}} \qquad \text{Eq. 4.1}$$

neglecting any skin-core interface resistance. The thermal resistance of the blade wall is part of the larger thermal resistance network which is presented below:

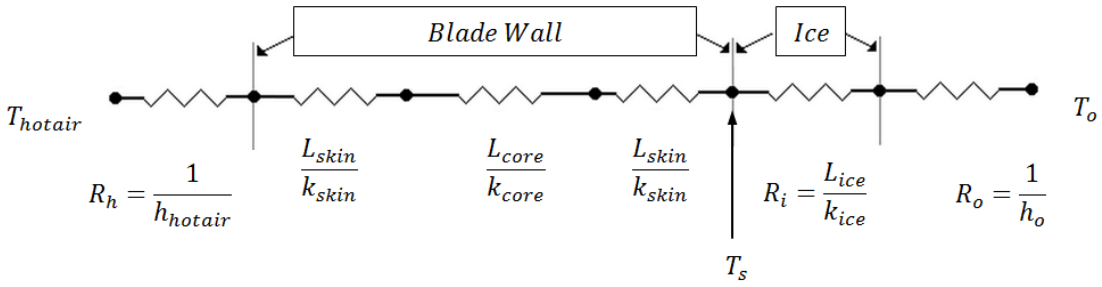

Figure 4.3: Resistance diagram of the hot air de-icing system

where h_{hotair} and h_o are the heat transfer coefficients of the hot air side and the ambient, respectively.

Along the outer third of the blade, the total thickness of the inner and outer blade skin is typically between 6 and 12 mm (3-6 mm per skin). At the root of the blade, the fibreglass skin thickness may increase significantly in order to fasten the blades to the nacelle. However the primary concern of icing is the outer third of the blade. As described earlier, the thickness of the core tapers towards the tip of the blade. At the outer third position of the blade, the core thickness is typically between one and four centimetres thick. For this range of skin and PVC core thicknesses, the thermal resistance of the blade is calculated in Table 4.1 below:

		Total Skin Thickness (mm):				
		4	6	8	10	12
Core Thickness (cm)	0	0.022	0.033	0.044	0.056	0.067
	0.5	0.178	0.190	0.201	0.212	0.223
	1	0.335	0.346	0.357	0.368	0.379
	1.5	0.491	0.502	0.513	0.524	0.535
	2	0.647	0.658	0.669	0.681	0.692
	2.5	0.803	0.815	0.826	0.837	0.848
	3	0.960	0.971	0.982	0.993	1.004
	3.5	1.116	1.127	1.138	1.149	1.160
	4	1.272	1.283	1.294	1.306	1.317

Table 4.1: Thermal resistance of the blade wall (m^2K/W) with PVC foam (k_{core} = 0.032 W/mK) as the core material and E-glass (k_{skin} = 0.18 W/mK) as the skin material

It can be clearly seen that when a PVC foam core is present, the core resistance dominates the total skin-core composite thermal resistance.

4.2 Hot Air De-Icing Steady State Analysis

Investigating the simple scenario of hot air de-icing at steady state will provide insight into the limitations of a hot air icing mitigation system. The minimum hot air temperature required for de-icing can be calculated from the steady state case. The forced hot air on the inside of the blade must, at the very least, be able to raise the adhesion layer of ice to 0°C. With the adhesion layer at 0°C, the minimum hot air temperature can be calculated from the steady state analysis. The maximum hot air temperature is limited by the operating range of the blade material.

In this section, the limit of a hot air de-icing system is determined for a range of blade wall resistances that are representative of the outer third of commercial wind turbine blades. The range of external heat transfer coefficients represent the wind turbine at a standstill and during operation. The effect of the ice accretion on de-icing is simplified into two case scenarios; a rime ice example and a glaze ice example. Considering Figure

4.3, the required hot air temperature in order for the adhesion layer to reach melting at steady-state is:

$$T_h - T_s = (T_s - T_o)\frac{(R_h + R_{wall})}{(R_i + R_o)} \qquad \text{Eq. 4.2}$$

where T_h is the temperature of the inside air, T_s is the adhesion layer temperature at melting (0°C), T_o is the ambient temperature, R_h, R_{wall}, R_i and R_o are the thermal resistances of the hot air, blade wall, ice layer and outside air, respectively. For scenarios where R_h is small compared to R_{wall} (see section 4.3.2), T_h is essentially the inside temperature of the blade wall. For these cases, Eq. 4.2 becomes:

$$T_h - T_s = (T_s - T_o)\frac{R_{wall}}{(R_i + R_o)}$$

For a given R_{wall} and h_o, the minimum inner blade temperature required to maintain T_s at 0°C, under two typical ice coatings (0.5 cm of glaze and 1.5 cm of rime) are plotted in Figure 4.4 a-f. For example with 0.5 cm of glaze ice at T_o = -10°C, values of h_o = 50 W/m^{2}K and R_{wall} = 0.4 m^{2}K/W, it can be seen from Figure 4.4 b) that an inner blade wall temperature of 180°C would be required to maintain T_s at 0°C.

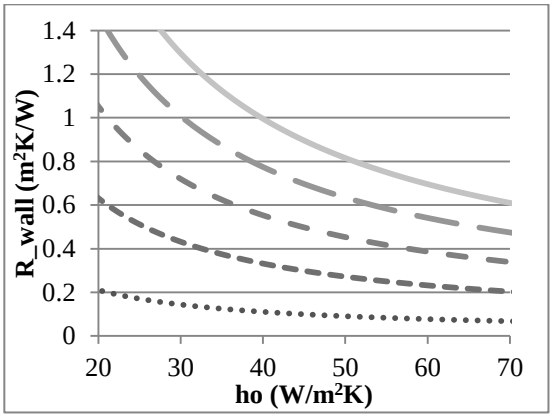

a) T_o = -5°C, 0.5 cm glaze ice

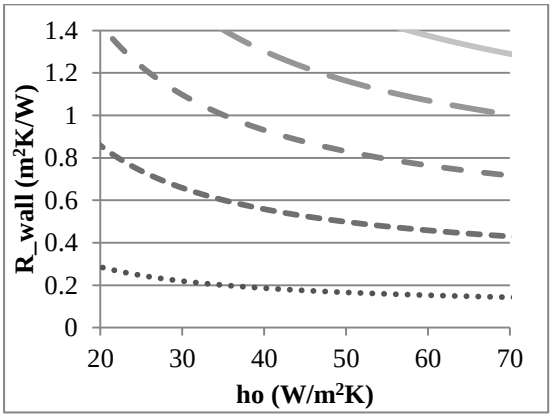

d) T_o = -5°C, 1.5 cm rime ice

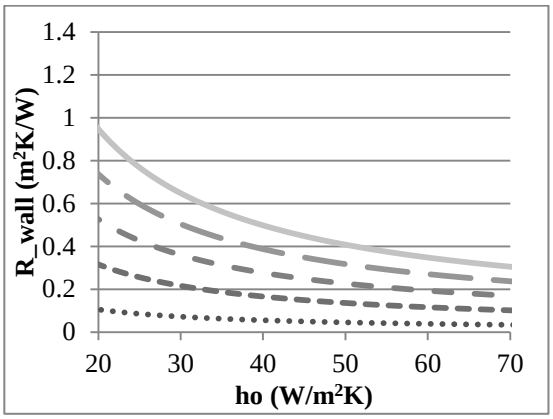

b) T_o = -10°C, 0.5 cm glaze ice

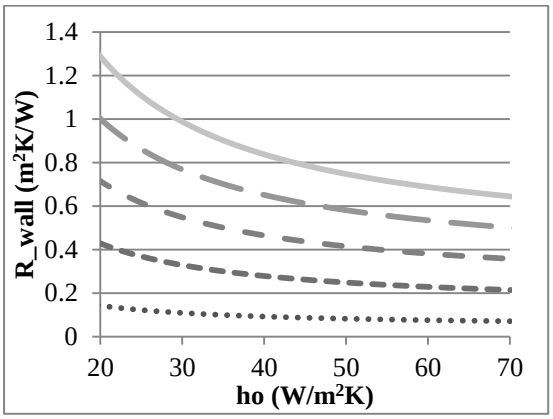

e) T_o = -10°C, 1.5 cm rime ice

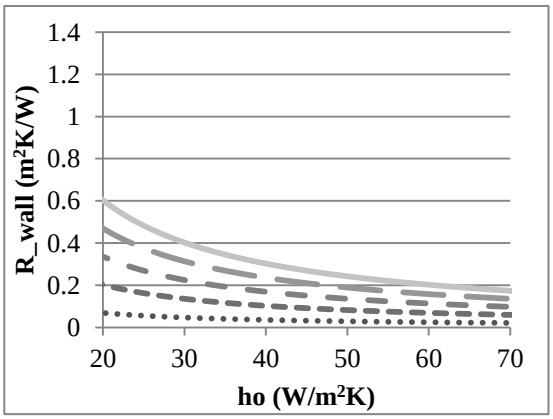

c) T_o = -15°C, 0.5 cm glaze ice

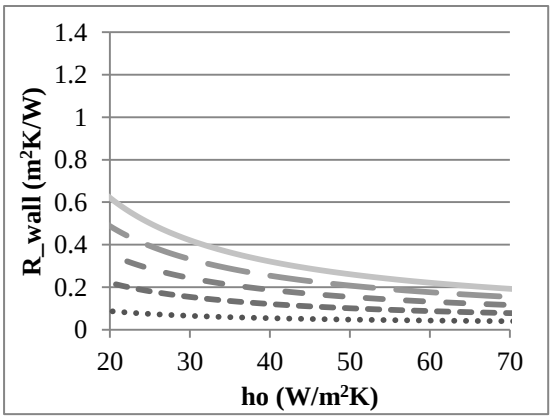

f) T_o = -15°C, 1.5 cm rime ice

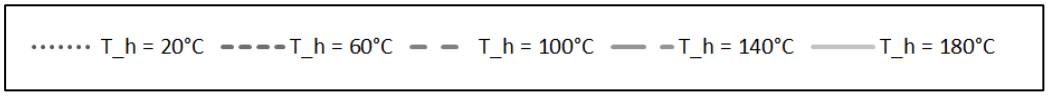

Figure 4.4: The inner blade surface temperature to provide T_s = 0°C for a range of R_{wall} and h_o. Subfigures a)-c) are for 0.5 cm of glaze ice (R_i = 0.003 W/m^{2}K) while subfigures d)-f) are for 1.5 cm of rime ice (R_i = 0.02 W/m^{2}K) and external temperatures T_o = -5°C, -10°C and -15°C.

Higher blade wall resistances and external heat transfer coefficients correspond to the top right corner of each graph. If a wind turbine blade is to be de-iced in this region a higher inner blade temperature will be required. Inner blade wall temperatures between 20 and 180°C are presented; the operating limit of fibreglass is typically 150°C, beyond which it begins to lose strength. A reasonable margin of safety would limit the operating temperature to 100°C. Considering Figure 4.4.a (T_o = -5°C and 0.5 cm glaze ice), with h_o = 60 W/m^{2}K, a hot air de-icing system would be unable to maintain the adhesion layer at 0°C for a wind turbine blade with a PVC foam core thicker than 1 cm, which would be a significant portion of the outer third of the blade.

The outside heat transfer coefficient of 60 W/m^{2}K represents an approximate local maximum heat transfer coefficient of the blade at stand still with a wind speed of approximately 7 m/s. During operation, the relative velocity, as seen by the blade can reach upwards of 60 m/s. Consequently the heat transfer coefficient near the blade tip will be on the order of 200 W/m^{2}K or more. The required hot air temperature for de-icing and anti-icing for a range of heat transfer coefficients, representative of the blade during operation are presented in Figure 4.5 below:

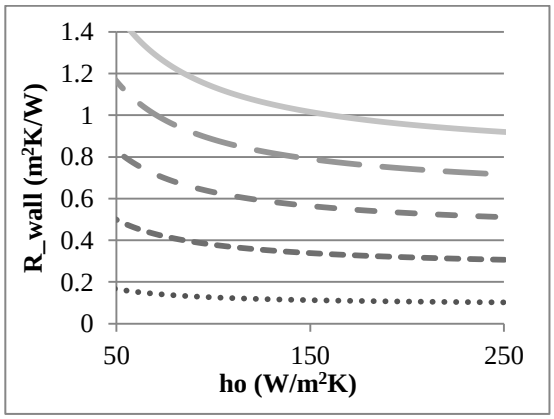

a) T_o = -5°C, 1.5 cm rime ice

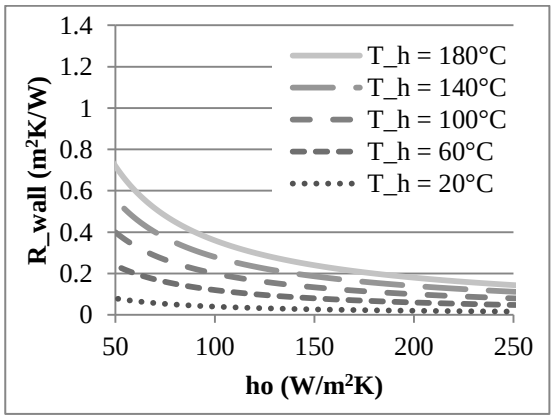

b) T_o = -5°C, anti-icing (no ice present)

Figure 4.5: The inner blade surface temperature to provide T_s = 0°C for a range of R_{wall} and h_o typical of the wind turbine in operation

During operation of the wind turbine, when the heat transfer coefficient is large, the de-icing of the wind turbine is severely limited, even under the relatively mild conditions considered in Figure 4.5.a). For a scenario where the maximum hot air temperature is 100°C, the maximum thermal resistance of the blade wall is 0.6 m^2K/W or less (i.e. $\leq$ 1.7 cm PVC core), in order to **de-ice** the blade during operation ($h_o \geq 100$ W/m^2K, see section 3.1.1). At stand-still, a portion of the blade at the tip can be de-iced under a restricted range of conditions. For the range of conditions that de-icing is possible, the time required can be determined using a numerical analysis.

At operating speeds, the outside heat transfer coefficient, h_o is high and the external thermal resistance is very low. To provide enough heat for **anti-icing**, the thermal resistance of the blade wall would have to be less than 0.2 m^2K/W (i.e. only solid fibreglass blades without any core). This makes it impractical to operate a hot air heating system in an anti-icing mode.

4.3 Hot-Air <u>De-Icing</u> Transient Analysis

The steady state analysis of hot air de-icing provides a framework for understanding the limitations and relative importance of the parameters involved. However the time required for de-icing to occur can only be determined from a transient analysis. In order to determine the amount of time required to de-ice a wind turbine using a hot air heating strategy, a numerical model using a finite volume approach is used.

4.3.1 Hot Air De-Icing Numerical Analysis

The heat transfer analysis is essentially the same as the electro-thermal scenario in Chapter 3. Equation 3.14 is the governing equation for the diffusion of heat for a one dimensional, transient analysis. At the inside of the blade, the boundary condition is convection of the hot air at temperature T_{hotair}, which is transferred to the inner wall of the blade through a heat transfer coefficient, h_{hotair}. The boundary condition at the surface of the ice is also due to convection of the ambient temperature, T_o with a heat

transfer coefficient, h_o. The heat transfer coefficient, h_o is determined by the same process as described in Chapter 3. Heat is transferred from the hot air, T_{hotair} to the inner blade wall through convection. The hot air is forced through some sort of duct work with an associated heat transfer coefficient, h_{hotair}. One typical configuration is to pass the hot air through the passage between the main spar and the leading edge blade wall. The Nusselt number for this configuration is approximated with the Dittus-Boelter correlation for internal forced convection:

$$Nu_h = \frac{h_{hotair} D_{hyd}}{k_h} = 0.023 {Re_h}^{0.8} {Pr_h}^{0.33} \quad \text{Eq. 4.3}$$

where the subscript h, indicates the hot air side of the blade wall. The Reynolds number, Re_h can be approximated as a half cylinder with a diameter equal to the chord thickness:

$$Re_h = \frac{\rho_h V_h D_{hyd}}{\mu_i} \quad \text{Eq. 4.4}$$

where D_{hyd} is the hydraulic diameter that is calculated using Eq. 4.5, which is the equivalent diameter for a semi-circular cross-section:

$$D_{hyd} = \left(\frac{\pi}{\pi+2}\right) \mathrm{D} \quad \text{Eq. 4.5}$$

4.3.2 Internal Heat Transfer

The blower in a hot air de-icing system forces hot air through the leading edge of the blade. The blower size must be selected so that the frictional effects of the recirculated air are overcome and to ensure good heat transfer on the hot air side of the channel. With increasing heat transfer on the inside of the blade, the temperature of the inside wall approaches the temperature of the hot air. In reference to Equation 4.2, the importance of the thermal resistance between the hot air and the inner blade wall, R_h, is relative to the resistance of the blade wall, R_{wall}. From Equation 4.3 and a range of duct sizes and hot air velocities that would be typical of wind turbines, a range of internal heat transfer convective resistances can be determined (Figure 4.6).

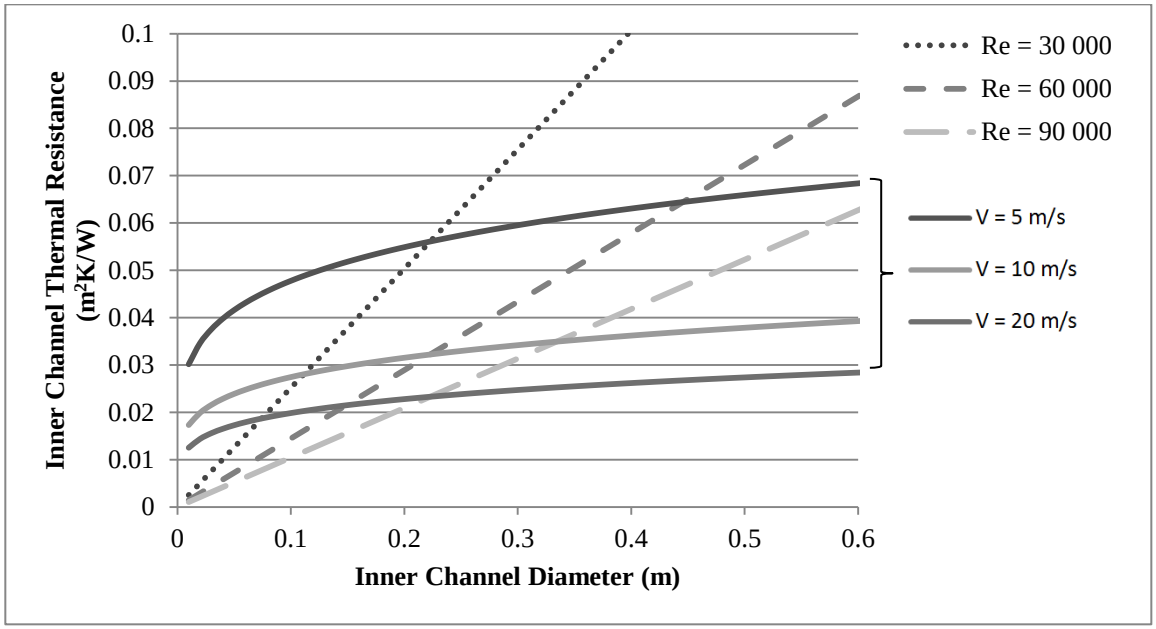

Figure 4.6: Thermal resistance between the hot air and the inner blade wall for a range of flow rates and channel diameters

These internal convective heat transfer resistances are much less than the overall resistance (see Table 4.2), especially when matched with the real spanwise changes in blade cross sections. The cross sectional area of the channel is the smallest at the tip of the blade and gets larger towards the root. This causes the blade channel to act as a nozzle so that as the cross sectional area decreases towards the tip, the local velocity increases. For an example wind turbine blade, the thermal resistance for different sections along the length of the blade are calculated and presented in Table 4.2. A hot air flow rate of 0.2 m^3/s is assumed for the calculation, giving a range of velocities that would not produce excessive pressure drop losses (these velocities and corresponding h_{hotair} values proportional to $\frac{1}{R_{hotair}}$ are relatively low for forced air applications).

Wall Thickness (cm)	Core Thickness (cm)	R_{wall} (m^2K/W)	D_{hotair} (cm)	V_{hotair} (m/s)	Nu_{hotair}	R_{hotair} (m^2K/W)
5.0	4.0	1.306	53	1.8	68.8	0.152
4.5	3.5	1.149	34	4.4	98.1	0.068
3.5	2.5	0.837	25	8.2	126	0.039
3.0	2.0	0.681	23	9.6	134	0.034
2.5	1.5	0.524	21	12	144	0.029
2.0	1.0	0.368	19	14	156	0.024
1.5	0.5	0.212	17	18	171	0.02
1.0	0.0	0.056	16	20	179	0.018

Table 4.2: Thermal resistance of an example blade and hot air. Channel diameter assumed to be equal to the blade thickness and the cross sectional area is approximated as a semi-circular area.

For a moderately sized blower (0.2 m^3/s), the resistance on the hot air side is between 4 - 10% of the thermal resistance between the hot air and the adhesion layer, except for the very tip of the blade, where the foam core tapers off to nothing. It can also be noted that root-to-tip variation in wall core thickness (decreasing thickness and wall thermal resistance) will often match the root-to-tip decrease in hot air ducting area (increasing hot air velocity and decreasing R_{hotair}). Therefore improving the heat transfer on the inside of the blade will have little benefit in terms of reducing the time required to melt the adhesion layer. For the rest of the analysis, a large inside heat transfer coefficient is considered in order to give the limiting case scenario, with near perfect heat transfer in order to focus on the remaining variables.

4.3.3 Ambient Conditions

From the time that the hot air de-icing system is turned on, the heat from inside the blade must penetrate through the fibreglass and foam core before it can reach the adhesion layer. This forces a much slower melting process than for electro-thermal de-icing, where the heat is being applied directly to the adhesion layer. The longer de-icing time for hot air systems also means that the heat is able to penetrate through the ice layer and convection becomes a significant factor at the ice surface. Therefore a large number of variables influence the time required to de-ice a turbine blade using a hot air based

heating method. For this reason the potential ice accretion and ambient conditions are simplified into "harsh" and "favourable" case scenarios in this thesis.

Previously mentioned in Chapter 2, rime ice formations freeze quickly, trapping air into the ice as it freezes, while glaze ice forms slower and is closer to being pure ice. The trapped air in the rime ice increases the ability of the ice to insulate the adhesion layer from the free stream temperature. Due to the trapped air, rime ice is usually thicker than glaze ice formations. Typical rime ice formations are 1 to 2 cm thick while glaze ice is usually less than 1 cm. A thin layer of glaze ice is considered as a harsh case scenario and a thick layer of rime ice is considered as a favourable scenario. The "favourable" and "harsh" conditions considered for the analysis are presented in Table 4.3.

	Favourable Conditions (F – Condition)	Harsh Conditions (H – Condition)
Type of ice accretion	Rime Ice	Glaze Ice
Thickness of ice accretion	1.5 cm	0.5 cm
Density of Ice	333 kg/m^3	920 kg/m^3
Heat capacity	1380 J/kgK	2040 J/kgK
Conductivity	0.696 W/mK	1.88 W/mK
Thermal resistance of ice, R_i	0.0216 m^{2}K/W	0.00266 m^{2}K/W
Outside heat transfer coefficient	30 W/m^{2}K	60 W/m^{2}K
Outside heat transfer thermal resistance, R_o	0.0333 m^{2}K/W	0.0167 m^{2}K/W

Table 4.3: Conditions for favourable and harsh case scenarios

The limitations of a hot air de-icing and anti-icing system are dependent on the thermal resistance network. A summary of the thermal resistances is provided in the next section.

4.3.4 Thermal Resistance Summary

The thermal resistance network consists of four separate sections: the thermal resistance due to internal forced convection on the inside of the blade; the thermal resistance of the blade wall; the layer of ice and the thermal resistance due to external forced convection on the exterior of the ice. The range of thermal resistances for a hot air heating system are summarised in Table 4.4:

Section	Thermal Resistance (m^2K/W)
Inner surface convection, R_h	0.02 – 0.04
Blade wall (core thickness: 5 mm – 25 mm), R_{wall}	0.21 – 0.84
Ice (thin glaze – thick rime), R_i	0.003 – 0.022
Outer surface convection, R_o	0.02 – 0.05

Table 4.4: Summary of thermal resistances

As previously shown, the thermal resistance of the blade wall is much more significant than the thermal resistance of convection from the hot air to the inner wall surface. Therefore improving the heat transfer on the inside of the blade will provide little benefit to de-icing the blade. The ice layer provides a certain amount of insulation between the adhesion layer and the ambient temperature, depending on the thickness and type of ice. The benefit of the ice layer is larger if the layer of ice is thicker and is rime ice (lower conductivity). The maximum thermal resistance of the blade wall can be approximated using the same approach used in the steady state analysis section, but re-arranging for R_{wall}. The maximum resistance of the blade wall is:

$$R_{wall} = \frac{T_h - T_s}{T_s - T_0}(R_i + R_o) \qquad \text{Eq.4.6}$$

where T_s is adhesion layer temperature at melting (0°C). The maximum thermal resistance of the blade wall is determined for the two, harsh and favourable case scenarios at different temperatures. With T_h = 100°C, the maximum thermal resistance that the blade wall can have is presented in Table 4.5:

	-5°C, Favourable	-10°C, Favourable	-5°C, Harsh	-10°C, Harsh
R_{ice} (m^2K/W)	0.0216	0.0216	0.00266	0.00266
$R_{outside}$ (m^2K/W)	0.0333	0.0333	0.0167	0.0167
Maximum R_{wall} (m^2K/W)	**1.1**	**0.55**	**0.4**	**0.2**

Table 4.5: Maximum thermal resistance of the blade wall in order to succeed in de-icing, with T_h = 100°C

When the thermal resistance of the blade wall is greater than the maximum, presented in Table 4.5, the de-icing time is effectively infinite. To de-ice a blade in harsh conditions

when the ambient temperature is -10°C and the hot air temperature is limited to 100°C, the maximum thermal resistance of the blade wall cannot exceed 0.2 m^2K/W. This maximum is exceeded with a PVC foam core thickness of only 0.5 cm.

With these limitations in consideration, the transient behaviour of the hot air de-icing system is analysed for the range of thermal wall resistances and ambient conditions where de-icing is possible. In addition to the favourable and harsh conditions that are presented in Table 4.3, the hot air de-icing system will also be analysed for a series of sections and ambient temperatures. The blade sections are analysed independently in order to quantify the effect of the varying core thicknesses. Due to the nature of the tapering thickness of the blade skin, the results of this analysis will be applicable to a range of blade constructions. The single section analysis will show the dependence of de-icing time on the primary factors under favourable and harsh conditions.

4.3.5 Hot Air De-Icing Results

The ambient temperatures of -5°C and -10°C were considered in combination with the harsh and favourable case scenarios. At temperatures below -10°C the hot air de-icing system is ineffective at de-icing the composite blade with PVC foam. An example of the transient behaviour of internal hot air heating can be seen in Figure 4.7. The steep temperature gradient through the core section illustrates the high resistance of the core material. For the example in Figure 4.7, the adhesion layer has melted after 20 minutes.

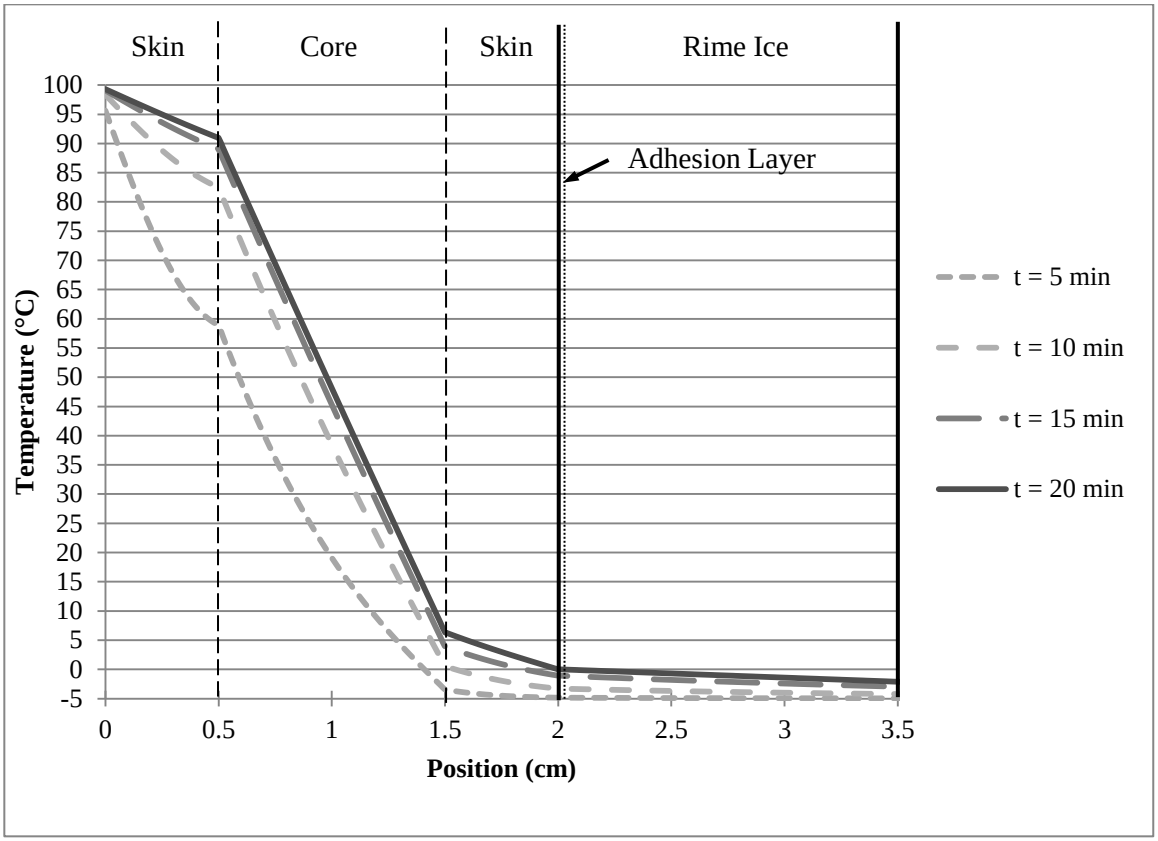

Figure 4.7: Temperature profile through the blade and ice with time. The initial temperature is equal to the ambient temperature of -5°C. The inner blade wall is maintained at 100°C. The fibreglass skins are 5 mm thick each and have a conductivity and heat capacity of 0.18 W/mK and 1600 J/kgK, respectively. The foam core is 10 mm thick and has a conductivity and heat capacity of 0.032 W/mK and 1500 J/kgK. The ambient conditions are favourable (Table 4.3).

As mentioned previously, the hot air de-icing system is sensitive to changes in the ambient conditions and the section of the blade that is to be de-iced. The de-icing time using hot air heating is presented in Figure 4.8 for a range of PVC core thicknesses,

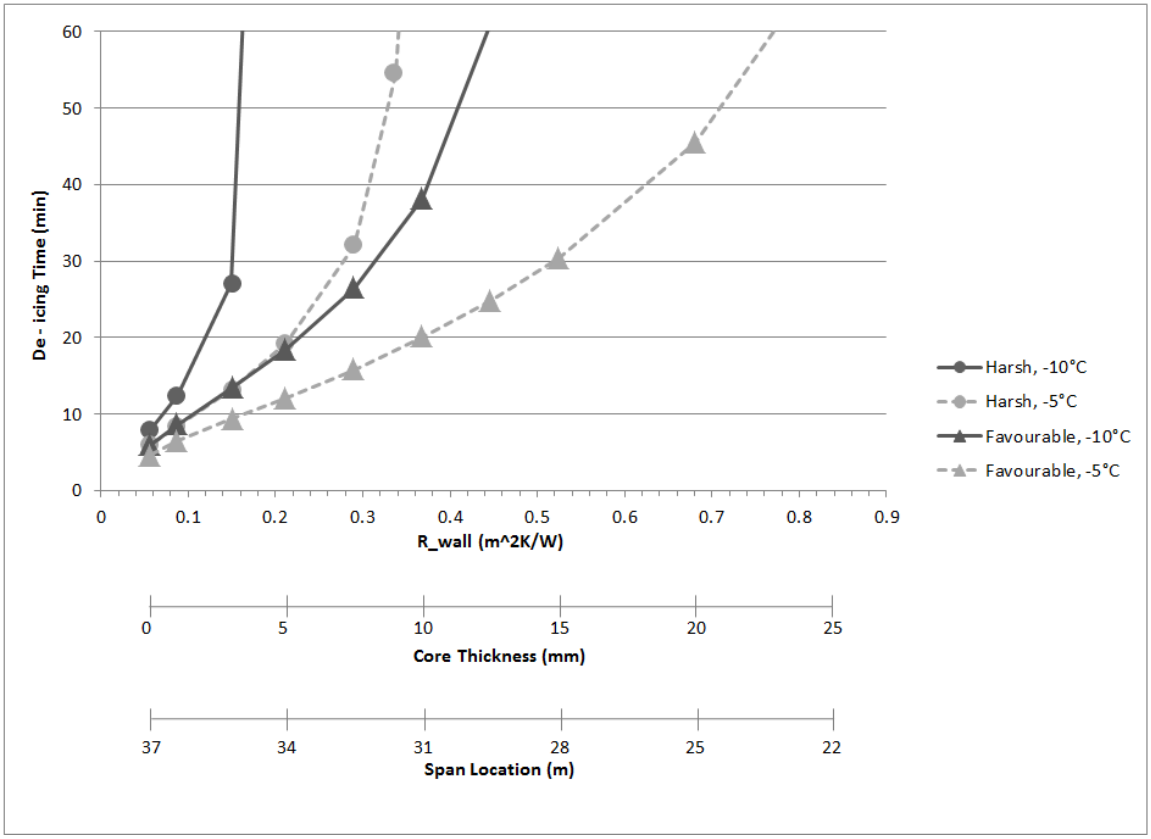

Figure 4.8: Required de-icing time for a hot air heating system for different PVC foam core thicknesses. The fibreglass skin is 5 mm thick. The hot air and blade inner surface are 100°C

corresponding to the thermal resistance of the blade, R_{wall} and spanwise location for the example 38 m long blade. Each line corresponds to a specific combination of ambient temperature and harsh/favourable case scenarios. From Figure 4.8 it can be observed that the time required to de-ice the blade increases quickly as the thermal resistance of the wall increases. For each combination, the vertical asymptote is where the hot air de-icing system will reach steady state with $T_s < 0°C$ and the blade will be unable to be de-iced. This agrees with the maximum thermal resistance for de-icing outlined in Table 4.5.

The summary of thermal resistances presented in Table 4.4 suggests that a bottleneck in the heat transfer process is created by the high thermal resistance of the blade wall. When the thermal wall resistance of the blade is greater than the maximum presented in Table

4.5, the hot air de-icing system will be ineffective. Therefore alternative modifications must be considered for hot air de-icing to be effective in a broad range of conditions.

4.3.6 Modifications to Improve Hot-Air De-Icing

The majority of the power produced from a wind turbine comes from the outer third of the blade, because of the larger swept area. This section of the blade is also the most prone to icing due to the high relative velocity of the blade. Therefore it is important to keep the outer third of the wind turbine blade free of ice.

As previously shown, the thermal insulation of the core material in the wind turbine blade limits the effectiveness of hot air de-icing systems. Alternative constructions of the wind turbine blades can be considered in order to increase the efficiency of hot air de-icing systems. The blade of a wind turbine is designed so that it has a high strength to weight ratio. Alternative core materials that have similar strength to weight ratios are listed in Table 4.6, along with their respective conductivities.

Material		Density (kg/m^3)	Conductivity (W/mK)
PVC foam core		150	0.032
Balsa wood		140	0.055
Nomex honeycomb	(3/8" cell)	48	0.094
	(1/4" cell)	50	0.081
	(3/16" cell)	48	0.074
	(1/8" cell)	48	0.065
Aluminum honeycomb	(3/8" cell)	48	4.68
	(1/4" cell)	54	5.00
	(3/16" cell)	50	4.76
	(1/8" cell)	50	4.76

Table 4.6: Potential core materials and their conductivity [12, 67]

Previously it was shown that in harsh conditions with T_o = -10°C, the hot air de-icing system would be ineffective if the thermal resistance of the blade exceeded 0.2 m^2K/W. Table 4.7 presents the thermal resistance of alternative core materials that can be substituted into the design of the blade.

Core Material:	PVC Foam	Balsa Wood	Nomex Honeycomb	Aluminum Honeycomb
Core Conductivity (W/mK)	0.032	0.055	0.08	5
Wall Thickness (cm)	R_{wall} (m^2K/W)			
4.0	1.306	0.783	0.556	0.063
3.5	1.149	0.692	0.493	0.063
3.0	0.993	0.601	0.431	0.062
2.5	0.837	0.510	0.368	0.061
2.0	0.681	0.419	0.306	0.060
1.5	0.524	0.328	0.243	0.059
1.0	0.368	0.237	0.181	0.058
0.5	0.212	0.146	0.118	0.057
0	0.056	0.056	0.056	0.056

Table 4.7: Thermal resistance of the blade with different core materials

Nomex honeycomb, which is commonly used in fibreglass reinforced plastic components, has approximately half the thermal resistance of PVC foam. A composite blade with a Nomex honeycomb core exceeds a thermal resistance of 0.2 m^2K/W with a core thickness greater 1 cm, as can be seen in Table 4.7. A Nomex core would be an improvement over PVC foam however it would not be sufficient for all conditions. From Table 4.7 it can also be observed that the thermal resistance of the blade wall with an aluminum honeycomb core would not exceed 0.2 m^2K/W, even for core thicknesses much greater than those used in blades. Therefore a hot air heating system would be able to de-ice a blade with an aluminum honeycomb core without exceeding 100°C. The time required to de-ice a wind turbine blade with alternative core materials is presented in Figure 4.9. It can be observed that de-icing a wind turbine blade with a Nomex honeycomb core will be significantly improved over a blade constructed with a PVC core. However in harsh conditions and temperature below -5°C the effectiveness of a hot air de-icing system will be limited to the tips of the blade, where the core of the blade is thinner.

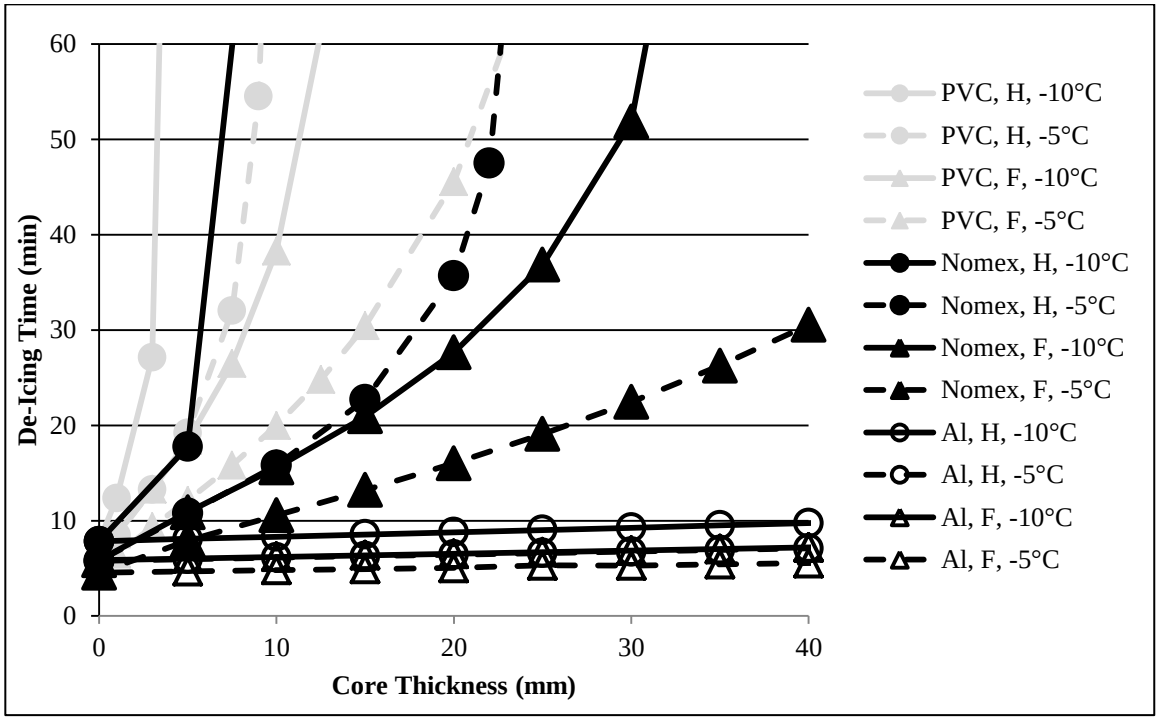

Figure 4.9: Time required to de-ice a wind turbine blade with hot air for a range of core thicknesses and an inner blade wall temperature, T_h = 100°C. Harsh (H) and favourable (F) operating conditions are represented with circles and triangles, respectively. Ambient temperatures of -10°C and -5°C are represented with solid and dashed lines, respectively. Alternative core materials are represented with different marker colours; a PVC core (k_{core} = 0.032 W/mK) is represented by the light grey markers; a Nomex honeycomb core (k_{core} = 0.08 W/mK) is represented by solid black markers and an aluminum honeycomb core (k_{core} = 5 W/mK) is represented by white markers.

Alternatively the blade can be built using an aluminum honeycomb core. The thermal resistance of even a thick 4 cm aluminum honeycomb core would represent approximately 10% of the thermal resistance of the blade wall with the fibreglass skin, the remaining fibreglass blade skin that sandwiches the core would represent nearly 90% of the thermal resistance of the blade wall. The de-icing time is then short for all of the cases considered in Figure 4.9 and is essentially independent of core thickness. It should be noted that this large reduction in wall resistance means that the internal hot air convection is no longer entirely negligible. However the typical hot air resistances (0.02 – 0.04 W/m^2K), seen in Table 4.2 are still considerably less than the skin and core conductive resistance.

4.3.7 Hot Air De-Icing Summary

In this chapter a hot air de-icing system for wind turbine blades was investigated. The analysis was presented for a general range of conditions so the designer of a de-icing system can apply the results presented here to their particular application. This analysis investigated the limitations of a hot air de-icing system from both an analytical, steady state analysis and a numerical, transient analysis.

The analysis showed that the thermal resistance of the foam core creates a bottleneck in the hot air de-icing system. Combined with the temperature limitation on the inner surface of the wall means that the practicality of a hot air anti-icing and de-icing system is limited. With the temperature limitations of the fibreglass and the high thermal resistance of the blade wall, it was shown that for sections with a thick core, the blade wall would reach steady state (with $T_s > 0°C$) before the system could be de-iced.

Hot air for anti-icing a blade with a foam core is not feasible due to the high external heat transfer coefficient. De-icing with its much higher outer thermal resistance (insulation of the ice layer and lower h_o) is possible but again is limited by core resistance due to the temperature limit and is only possible for thin cored sections with PVC foam. For the cases that de-icing was possible, it was shown that a de-icing cycle would typically take 30 min or longer.

If more conductive materials that have similar strength to weight ratios are used, a hot air de-icing system can be effective over a wider range of core thicknesses. The use of Nomex honeycomb effectively halves the core resistance and allows de-icing to be used for realistic core thicknesses depending on the external conditions. Aluminum honeycomb has a conductivity approximately 2 orders of magnitude higher than PVC foam. With an aluminum honeycomb core, the blade wall resistance is dominated by the thin fibreglass reinforced plastic skins. This range of resistances will allow a hot air de-icing system to de-ice the blade in less than ten minutes.

The thermal properties of the blade must be taken into account before a hot air de-icing system is retro-fitted into the design of the turbine blade. If proper care is not taken, the hot air de-icing system could over-heat the fibreglass beyond its recommended limit. Alternatively, if the inside air is not heated sufficiently, the heat transfer through the blade and ice will reach steady state and energy provided from the de-icing system will be wasted.

5 Conclusions and Future Work

The objective of this research was to analytically and numerically investigate heat applications strategies that prevent or remove ice accretion on wind turbine blades. This thesis will provide results and tools to benefit designers of anti-icing and de-icing heating systems for wind turbine blades. An effective anti-icing or de-icing strategy for wind turbines will prevent or remove build-up of ice on the blades to increase energy production and improve the service life by preventing loading imbalance. To date, the usefulness of various icing mitigation strategies for wind turbines have not been proven. In this thesis, electro-thermal and forced hot air heating methods were analysed for a range of expected conditions in order to determine the relative importance of the parameters associated with each method.

Electro-thermal anti-icing and de-icing was analysed analytically and numerically. External convection from the blade surface was recognized as the dominant form of heat loss in icing conditions. The importance of convection at the blade surface can be reduced with a heater power density large enough that the heat does not penetrate through the ice before the adhesion layer has melted. The effectiveness of the insulation provided by the ice layer is dependent upon the type and thickness of the ice formation, with a rime ice accretion providing a more significant layer of insulation than glaze ice. Here, the minimum power density for the effects of external convection to be considered negligible have been mapped out for a range of ambient temperatures and ice conditions. The total de-icing time in this region is relatively fast, between 5 and 60 seconds for heater power densities between 4 and 15 kW/m^2. When the heater power density is lower, a significant amount of heat is able to penetrate through the ice layer before the blade can be de-iced. In this region, the effects of convection and ice thickness are important and have been mapped out for both a base and practical worst case scenario. In this region the total de-icing time is typically between 60 and 500 seconds for heater power densities between 2 and 4 kW/m^2.

It was shown that insulating the heater from the blade can reduce the energy required for de-icing. For heater power densities between 2.5 and 10 kW/m^2, 1 to 2 mm of insulation would reduce the energy consumed by 25% or more. Increasing the thickness of the insulation beyond 2 mm had little effect on de-icing time in this region. Between a heater power density of 0.75 and 2.5 kW/m^2, the time required to de-ice is longer and 2 to 5 mm of insulation is required to prevent significant heat loss into the blade.

The anti-icing power required is linearly proportional to the blade length and ambient temperature and nearly linearly proportional to the ambient wind speed and heated length from the leading edge, which is a predetermined fraction of the chord length. The required anti-icing power was mapped out for a range of common wind turbine constructions.

With electro-thermal de-icing, heat can be applied directly to the adhesion layer so that little energy is wasted. This allows an electro-thermal heating system to de-ice the blades while the wind turbine is in operation. However, in order to provide a large, instantaneous heating density, a power application strategy is required. In this thesis, a sequential heating strategy is described that would allow high heater power densities to be achieved. It is left to the designer to use the information within this thesis to design a de-icing system based on the available power, blade geometry, ambient temperature and icing conditions specific to their application.

An alternative heating strategy to electro-thermal de-icing is to force hot air through the leading edge of the blade. Potentially, heat can be applied in an anti-icing or de-icing mode when the blade is at a standstill or during operation of the wind turbine. This thesis analysed a combination of these different strategies using analytical and numerical methods. It was observed that when removing or preventing ice accretion with hot air heating, the system is sensitive to the ambient conditions. For conventional, composite PVC foam and fibreglass blade wall constructions, heating with convected hot air could, in some cases be practical in a de-icing scenario at standstill.

A steady state analysis of hot air de-icing suggests that the important parameters in the de-icing procedure are: blade construction, hot air temperature, ice characteristics, external heat transfer coefficient and ambient temperature. The minimum hot air temperature for de-icing a wind turbine blade is presented in terms of the thermal resistance of the blade wall and the external heat transfer coefficient for a series of icing conditions. These results are applicable to any wind turbine blade within the wide range of thermal resistances presented. It was observed that the thermal resistance of the blade wall is largely controlled by the thickness of the core. For conventional wind turbine constructions with PVC foam cores, the hot air de-icing system is only effective over a limited range of operating conditions. In certain conditions the high thermal resistance of the blade wall requires a prohibitively high hot air temperature. This effectively creates a bottleneck in the hot air heating system, which cannot be overcome without altering the construction of the blade.

The limitations of a hot air de-icing system are confirmed by the transient numerical analysis, with the inner blade wall temperature set to 100°C, a reasonable materials-based limit. The de-icing time approaches infinity as the thickness of the blade wall is increased due to the system not being able to de-ice the blade before a steady state is reached with the adhesion layer un-melted. For a practical worst case scenario, the hot air heating system would be unable to de-ice the blade with a PVC foam core thickness greater than 5 mm. In favourable conditions, the hot air heating system would require between 10 and 70 minutes for PVC foam core thickness between 5 and 35 mm, corresponding to an average heat flux of 1500 W/m^2.

Nomex and aluminum honeycomb were considered as alternative blade core materials due to their relatively higher thermal conductivity over PVC foam and similar strength to weight ratios. From the steady state analysis, it is shown that the hot air heating system can de-ice the blade if the core is replaced with a Nomex honeycomb over a wider range of operating conditions. However, even with this configuration, the hot air heating system wouldn’t be able to de-ice the blade over the entire range of expected icing conditions without the inner blade wall exceeding 100°C. Aluminum honeycomb is an alternative,

non-conventional material with high thermal conductivity that can be used as a core material of the blade. The time required to de-ice a wind turbine blade with a hot air heating system is mapped out for a blade wall construction with PVC foam, Nomex honeycomb and aluminum honeycomb cores. A hot air heating system would be able to de-ice a blade with an aluminum honeycomb core over the entire range of anticipated operating conditions. The potential for a hot air de-icing system to be successful on a blade with an aluminum honeycomb core construction is promising.

5.1 Future Work

Icing on wind turbine blades is a relatively new problem with an extensive amount of new and useful research that can be done, including but not limited to: development of heating strategies to prevent or remove ice accretion, prediction of ice accretion and ice mapping, improving ice detection mechanisms and reducing surface coating adhesion strength while improving coating durability. This thesis focused on analytical and numerical methods to provide the framework for designers of hot air and electro-thermal anti-icing and de-icing systems.

With an adequate heater power density, electro-thermal de-icing can be an effective strategy to mitigate ice accretion on wind turbine blades. However, reliability and operational maintenance concerns such as: lightning protection, cleaning, fouling, blade flex and degradation of electro-thermal heating panels are ongoing issues for electro-thermal heaters.

Hot air de-icing of conventional, PVC foam cored blade sections was only effective over a restricted range of ambient conditions, based on a limiting inner blade wall temperature of 100°C. It was shown that with a hot air temperature of 100°C, an aluminum cored blade can effectively de-ice for a range of core thicknesses and that the hot air temperature is no longer the limiting factor as it was with a PVC foam core. With an

aluminum honeycomb core, a range of other air supply systems can then be considered, including a simple channel down the leading edge. The total power consumption of a hot air de-icing system can be determined from a multi-sectional analysis, an example of which is provided in Appendix C.2. However this analysis is left to the designer using the tools and results presented here, applied to their specific geometry

Heating strategies are a promising method to mitigate against ice accretion on the blades. \However the technology has so far not proven to be successful. Maximizing the efficiency over the range of expected icing conditions is critical to the success of a heating strategy in order to increase the net gain in energy production and ultimately the viability of a heating system. This thesis has analytically and numerically investigated hot air and electro-thermal de-icing and anti-icing to provide insight into the fundamental heat transfer involved. Additionally, the results of this analysis will provide necessary framework for the design of a wind turbine blade heating system to mitigate ice accretion.

References

[1] Global Wind Energy Council, "Wind in Numbers", Retrieved September 9th, 2013 from: http://www.gwec.net/global-figures/wind-in-numbers/.

[2] Canadian Wind Energy Association, (2013), "Wind by the Numbers: Economic Benefits of Wind Energy". Retrieved September 9th, 2013 from: http://www.canwea.ca/pdf/canwea-factsheet-economic-web-final.pdf.

[3] Jasinski, W.J., Noe, S.C., Selig, M.S., Bragg, M.B., Bragg, M.B. (1998), "Wind Turbine Performance Under Icing Conditions", Transactions of the ASME, Journal of solar energy engineering. New York, NY, USA. February, Vol. 120, pp 60-65.

[4] Homola, M. C. (2005), "Impacts and Causes of Icing on Wind Turbines". *Narvik University College*.

[5] Laakso, T., Baring-Gould, I., Durstewitz, M., Horbaty, R., Lacroix, A., Peltola, E., Ronsten, G., Tallhaug, L., Wallenius, T. (2009), "State-of-the-art of Wind Energy in Cold Climates". *IEA Wind Task 19.*

[6] Maissan, J., (2001), "Wind Power Development in Sub-Arctic Conditions with Severe Rime Icing", *Circumpolar Climate Change Summit and Exposition*.

[7] Laakso, T., Holttinen, H., Ronsten, G., Tallhaug, L., Horbaty, Baring-Gould, R., Lacroix, A., Peltola, E., Tammelin, B. (2003), "State-of the art of Wind Energy in Cold Climates". *IEA Wind Task 19.*

[8] Tammelin, B., Cavaliere, M., Holttinen, H. Morgan, C. Seifert, H. Santti, K., Wind Energy Production in Cold Climate, Meteorological Publications No, 41, Finnish Meteorological Institute, Helsinki. 41 p., 2000

[9] COST-727, Atmospheric Icing on Structures: 2006, Measurements and data collection on icing: State of the Art Publication of MeteoSwiss, 75, 110 pp.

[10] Lamraoui, F., Fortin, G., Benoit, R., Perron, J., Masson, C. (2013). "Atmospheric icing severity: Quantification and mapping", *Atmospheric Research,* Vol. 128, pp.57-75.

[11] Wallenius, T., Antikainen, P., Peltola, E., Dilingh, J. (2012), "Design principles of VTT ice prevention system", *VTT Technical Research Centre Finland.*

[12] Cengel, Y., (2006). "Heat and Mass Transfer", New York; New York: McGraw-Hill.

[13] Petrovic, J., (2003), "Mechanical Properties of Ice and Snow", *Journal of Materials Science,* Vol. 38, pp 1-6.

[14] Bragg, M., Broeren, A., Blumenthal, L., (2003), "Iced-Airfoil and Wing Aerodynamics", *SAE Technical Paper*.

[15] Bragg, M., (2005), "Iced-Airfoil Aerodynamics", *Progress in Aerospace Sciences,* Volume 41, Issue 5, pp 323-362.

[16] Seifert, H., Richert, F., (1997), "Aerodynamics of Iced Airfoils and Their Influence on Loads and Power Production", *European Wind Energy Conference*.

[17] Homola, M.C., Nicklasson, P.J., Sundsbø, P.A., (2006), "Ice Sensors for Wind Turbines", *Cold Regions Science and Technology,* Vol. 46, pp. 125-131.

[18] Loughborough, D. L., (1952), "The Physics of the Mechanical Removal of Ice From Aircraft", *Aeronautical Engineering Review,* Vol. 11, No. 2, pp. 29-34.

[19] Xian, X., Chu, M.L., Scavuzzo, R.J., Srivatsan, T.S., (1989), "An experimental evaluation of the tensile strength of impact ice", *Journal of Materials Science Letters,* Vol. 8, pp. 1205-1208.

[20] Gouni, R., (2011), "A New Technique To Study Temperature Effects on Ice Adhesion Strength for Wind Turbine Materials", *Case Western Reserve University.*

[21] Makkonen, L., (1984), "Atmospheric Icing of Sea Structures", *U.S. Army Cold Regions Research & Engineering Laboratory,* pp. 102.

[22] Bibeau, L., Kraj, A., (2010), "Measurement Method and Results of Ice Adhesion Force on The Curved Surface of a Wind Turbine Blade", *Renewable Energy*, Vol. 35, pp 741-746.

[23] Finstad, K., Makkonen, L., (1996), "Modeling of Rime Icing on Wind Turbine Blades", *BOREAS III, Proceedings of the 3rd Conference on Wind Energy Production in Cold Climates*, Finnish Meteorological Institute, Helsinki.

[24] Kimura, S. et al., (2008), "Icephobic coating for prevention of secondary icing", *Proceedings of the Winterwind Conference*, Norrköping, Sweden.

[25] Walsh, M. (2010), "Accretion and Removal of Wind Turbine Icing in Polar Conditions", *Aalto University*.

[26] Makkonen, L., (2012), "Ice Adhesion – Theory, Measurements and Countermeasures", *Journal of Adhesion Science and Technology*. Vol. 26, pp. 413-445.

[27] Makkonen, L., Lehmus, E., (1988), "Studies of Ice Adhesion to Structures", *VTT – Technical Research Centre of Finland, Laboratory of Structural Engineering*, pp. 200.

[28] Panjushin, V.B. et al., (1974), "Experimental Investigation of Ice Adhering to Construction Materials", *U.S. Cold Regions Research and Engineering Laboratory*, pp. 71-77.

[29] Bascom, W.D., (1969), "Ice Adhesion to Hydrophilic and Hydrophobic Surfaces", *Journal of Adhesion*, Vol 1, pp.246-263

[30] Oksanen, P., (1983), "Friction and Adherence of Ice", *VTT – Technical Research Centre of Finland*, pp. 36.

[31] Dalili, N., Edrisy, A., Carriveau, R., (2009), "A Review of Surface Engineering Issues Critical to Wind Turbine Performance", *Renewable and Sustainable Energy Reviews*, Vol. 13, pp. 428-438.

[32] Ilinca, A., Parent, O., (2011), "Anti-Icing and De-Icing, Techniques for Wind Turbines: Critical Review", *Cold Regions Science and Technology*, Vol. 65, pp. 88-96.

[33] Seifert, H., (2003), " Technical Requirements for Rotor Blades Operating in Cold Climates", *BOREAS VI – Proceedings of the 6th Conference on Wind Energy Production in Cold Climates*.

[34] Lacroix, A., Manwell, J., (2000), "Wind Energy: Cold Weather Issues", *University of Massachusetts, Amhers Renewable Energy Research Laboratory*.

[35] Maissan, J., Weis, T., (2003), "The Effects of Black Blades on Surface Temperatures of Wind Turbines", *Pembina Institute.*

[36] Albers, A., (2011), "Summary of a Technical Validation of Enercon's Rotor Blade De-Icing System, *Deutsche WindGuard Consulting GmbH*.

[37] Gray, V. H., Bowden, D. T., Von Glahn, U., (1952), "Preliminary results of cyclical de-icing of a gas-heated airfoil", *National Advisory Committee for Aeronautics*.

[38] Thomas, F., Gelder, G., Lewis, P., Koutz, S., (1953), "Icing Protection For a Turbojet Transport Airplane: Heating Requirements, Methods of Protection, and Performance Penalties", *National Advisory Committee for Aeronautics, TN 286.*

[39] Battisti, L., Baggio, P., Fedrizzi, R., (2006), "Warm-Air Intermittent De-Icing System of Wind Turbines", *Wind Engineering*, Vol. 30, No. 5, pp. 361-374.

[40] Gelder, T., Lewis, J., (1951), "Comparison of Heat Transfer From Airfoil in Natural and Simulated and Icing Conditions", *National Advisory Committee for Aeronautics*.

[41] Wang, X., Bibeau, E., Naterer, G.F., (2007), "Experimental Correlation of Forced Convection Heat Transfer from a NACA airfoil", *Experimental Thermal and Fluid Sciences*, Vol. 31, 1073-1082.

[42] Kelly Aerospace Thermal Systems, "Wind Turbine Ice Protection System", Retrieved June 21st, 2013 from: http://www.kellyaerospace.com/wind_turbine_deice.html.

[43] Petrenko, V., et. al., (2011), "Pulse Electro-Thermal De-Icer (PETD)", *Cold Regions Science and Technology*, Vol. 65, pp. 70-78.

[44] Seifert, H., (1996), "Technical Requirements for Rotor Blades Operating in Cold Climate", *BOREAS VI,* 9.

[45] Roeseler, B., (2006), "Composite Wings and Wind Power", *WIGO Open Session*.

[46] Severino, C., Abedian, B., (2012), "Effect of Lightning Strikes on Wind Turbine Blade Life", *Tufts University*.

[47] Wright, W., (2002), "User Manual for The NASA Glenn Ice Accretion Code LEWICE", *National Aeronautics and Space Administration.*

[48] Myers, T. (2001), "Extension to the Messinger Model for Aircraft Icing", *AIAA Journal*, Vol. 39 (2), pp. 211-218.

[49] Makkonen, L. (2001), "Modelling and Prevention of Ice Accretion on Wind Turbines", *Wind Engineering*, Vol. 25 (1) pp. 3-21.

[50] Myers, T. (2004), "A Mathematical Model for Atmospheric Ice Accretion and Water Flow on a Cold Surface", *International Journal of Heat and Mass Transfer*, Vol. 47 (25) pp 5483-5500.

[51] Beaugendre, H., Morency, F., Habashi, G., (2003), "FENSAP-ICE's Three-Dimensional In-Flight Ice Accretion Module: ICE3D", Journal of Aircraft, Vol. 40 (2), pp. 239-247

[52] Messinger, B.L., (1953), "Equilibrium Temperature of an Unheated Icing Surface as a Function of Air Speed", *Journal of Aeronautical Science,* Vol. 27 (1): pp. 29-42.

[53] Poinsatte, P., Fossen, J.V., (1990), "Convective Heat Transfer Measurements From a NACA 0012 Airfoil in Flight and in The NASA Lewis Icing Research Tunnel", *NASA Technical Memorandum 102448*.

[54] Meier, O., (2010), "A Handbook Method for The Estimation of Power Requirements for Electrical De-Icing Systems", *Hamburg University of Applied Sciences*.

[55] Homola, M., et. al., (2009), "The Dependence of Icing Severity on Chord Length", *Presented at EWEC*.

[56] Gelder, T., Lewis, J., Koutz, S, (1953), "Icing Protection For a Turbojet Transport Airplane: Heating Requirements, Methods of Protection, and Performance Penalties", *National Advisory Committee for Aeronautics*.

[57] N. Froessling, (1940), *Verdunstung, Wärmeubertragung und Geschwindigkeitverteilung bei zweidimensionaler und rotationssymmetricher Grenzschichtströmung*, Lunds Univ. Arrsskrift. N. F. 2, 36, Nr. 4

[58] Poinsatte, P., (1989), "Heat Transfer Measurements From a NACA 0012, Airfoil in Flight and in The NASA Lewis Icing Research Tunnel", *NASA Contractor Report 4278*.

[59] Boelter, L.M.K., Grossman, L.M., Martinelli, R.C., Morrin, E.H., (1948), "Comparison of Several Methods of Calculating Heat Losses from Airfoils". *National Advisory Committee for Aeronautics TN 1453*.

[60] Spalding, D.B., Pun, W.M., (1962), "A Review of Methods For Predicting Heat-Transfer Coefficients For Laminar Uniform-Property Boundary Layer Flows*", International Journal of Heat and Mass Transfer*, Vol. 5, pp. 239-249.

[61] Mayer, C., Ilinca, A., Fortin, G., Perron, J., (2007), "Wind Tunnel Study of Electro-Thermal De-Icing of Wind Turbine Blades", *The International Society of Offshore and Polar Engineers*, Vol. 17 (3).

[62] Kraj, A., Bibeau, E., (2010), "Phases of Icing on Wind Turbine Blades Characterized by Ice Accumulation", *Renewable Energy*, Vol. 35, pp. 996-972.

[63] Lewis, J., Bowden, D., (1952), "Preliminary Investigation of Cyclical De-Icing of an Airfoil Using an External Electric Heater", *National Advisory Committee for Aeronautics RM E51J30*.

[64] Patankar, S.V., (1980), "Numerical Heat Transfer and Fluid Flow", Washington; New York: Hemispher Pub. Corp.

[65] Date, A., (2005), "Introduction to Computational Fluid Dynamics", Cambridge; New York: Cambridge University Press.

[66] (2011), "Technical Description Enercon Wind Energy Converters Rotor Blade De-Icing System", Aurich; Germany: ENERCON GmbH.

[67] HEXCEL, (2006), "CR III 5052 & 5056 Corrosion Resistant Specification Grade Aluminum Data Sheet", Retrieved September 15th, 2013 from: http://www.hexcel.com/Resources/DataSheets/Honeycomb-Data-Sheets/CR3_us.pdf.

[68] Smith, F. (2001), "Carbon Fibre Based Heating Elements", *The A to Z of Materials*, Retrieved September 3rd, 2013 from: http://www.azom.com/article.aspx?ArticleID=1624.

Appendix A

A.1 Wind Turbine Blade Geometry

An example wind turbine blade geometry is based upon the dimensions in a previous study, conducted by Severino [46]. Severino investigated the heat transfer associated with turbine blades when they are struck by lightning. The wind turbine examined in the study is a horizontal axis, 1.5 MW, 38 m blade radius wind turbine.

The thickness of the fibreglass skin is 80 mm thick from the root of the blade until the widest chord length at about 5m. From this point until the tip of the blade the fibreglass skin has a constant thickness of 5 mm (two layers on either side of the core). The PVC foam core has a constant thickness of 40 mm from a span position of 5 m until 13 m. From a span position of 13 m until 37 m the PVC foam decreases in thickness from 40 mm and tapers off to zero. For the last metre the blade wall is entirely comprised of fibreglass and is 10 mm thick. The thickness of the foam core and the fibreglass skin at different span positions is outlined in Table A.1.

Span Position (m)	Eglass Thickness (mm)	PVC Foam Core Thickness
Root	80	0
5	5 x2	40
13	5 x2	40
19	5 x2	30
25	5 x2	20
31	5 x2	10
37	5 x2	0
Tip (38 m)	10	0

Table A.1: Thickness of the fibreglass skin and the foam core for a typical 38 m 1.5 MW wind turbine [46]

The blade shape is based upon the NACA 64(3)-618 standard profile. The shape of this profile along with the nodal points of a cross section of unit length 1 can be observed in Figure A.1 and Table A.2, respectively.

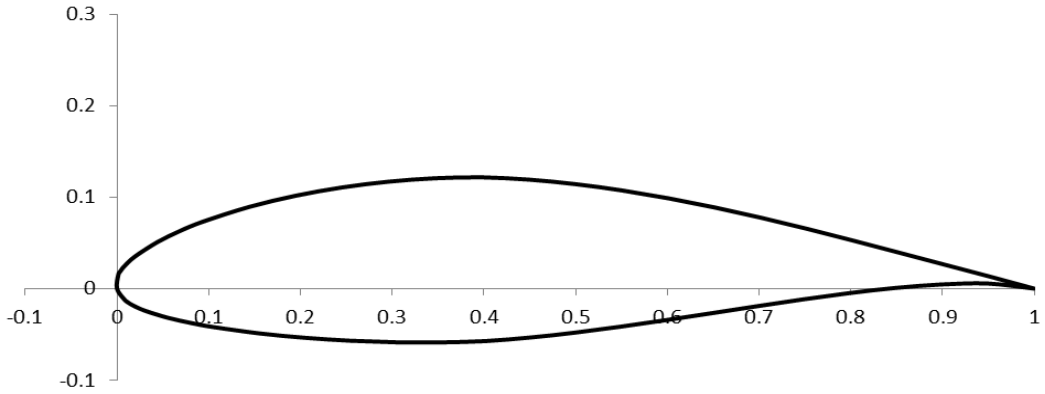

Figure A.1: NACA 64(3)-618 blade profile with a chord unit length

NACA 64(3) - 618			
Chord (x)	Height (y)	Chord (x)	Height (y)
1	0	0	0
0.95056	0.01344	0.0085	-0.01234
0.90115	0.02646	0.01141	-0.01465
0.85161	0.03963	0.01695	-0.0181
0.80191	0.0527	0.03018	-0.02402
0.75203	0.06544	0.05583	-0.03197
0.70196	0.07754	0.08105	-0.03769
0.65171	0.0887	0.10605	-0.0422
0.60129	0.0987	0.15573	-0.04899
0.55071	0.1073	0.20514	-0.05377
0.5	0.11423	0.2544	-0.05695
0.44917	0.11915	0.30355	-0.05866
0.39827	0.12163	0.35265	-0.05885
0.34735	0.12065	0.40173	-0.05737
0.29645	0.11698	0.45083	-0.05345
0.2456	0.11065	0.5	-0.04805
0.19486	0.10153	0.54929	-0.0416
0.14427	0.08937	0.59871	-0.0344
0.09395	0.07322	0.64829	-0.0269
0.06895	0.06312	0.69804	-0.01922
0.04417	0.05093	0.74797	-0.01174
0.01982	0.03518	0.79809	-0.00494
0.00805	0.02452	0.84839	0.00075
0.00359	0.01885	0.89885	0.00456
0.0015	0.01534	0.94944	0.00552

Table A.2: Nodal points for a NACA 64(3)-618 standard blade profile

The chord length of the wind turbine blade has a maximum length of 3.92 m close to the root and decreases to a minimum length of 0.85 m at the blade tip. The chord length at various sections along the length of the blade is presented in. The profile of the blade at each section is scaled to the chord thickness using the NACA 64(3)-618 blade profile. With this information the blade skin can be full recreated in three dimensions.

The chord lengths at various span locations are recorded in Table A.3.

Span Position (m)	Chord Length (m)	Span Position (m)	Chord Length (m)
0	2	23.75	1.32
4.75	3.92	26.13	1.2
6	3.57	28.5	1.12
7.13	3.25	30.88	1.04
11.5	2.57	33.25	0.98
16.63	1.77	35.63	0.91
18.85	1.64	36.75	0.88
21.38	1.43	38	0.85

Table A.3: Chord length at various span positions of a 1.5 MW wind turbine

The profile of the blade is then scaled to the chord length at different span locations in order to build a geometry that is representative of a typical 1.5 MW, 38 m, horizontal axis wind turbine blade.

A.2 Blade Material Properties

The blade skin consists of a foam core that is sandwiched between two layers of fibreglass. The thermal properties of the respective materials are presented in Table A.4:

	Eglass (Skin Material)	PVC Foam (Core Material)
Density (kg/m^3)	2100	150
Conductivity (W/mK)	0.18	0.032
Heat Capacity (J/kgK)	1600	1500

Table A.4: Thermal properties of the blade materials [46]

A.3 Thermal Electric Heater

The heater selection for a de-icing and anti-icing operation is crucial to the success of the ice removal strategy. Ideally, the heater will be as thin as possible with a high thermal diffusivity. This will minimize the amount of energy stored in the heater and a high conductivity will reduce the temperature gradient that exists within the heater. Additionally the heater should be able to flex with the blade. There have been recorded instances where the operational flex of the turbine has caused the heater to delaminate, damaging the skin of the turbine blade [44]. The adhesive bond of the heater must also be able to endure the thermal cycling that occurs throughout de-icing. Finally it is crucial that the profile of the heater does not affect the aerodynamics of the turbine blade. A small increase in the drag will have costly effects on the performance of the wind turbine over its life cycle.

For the purpose of our analysis we can assume that the coating is negligible and the thickness of the heater is 0.5 mm thick with a 2% volume fraction of nickel. The thermal properties of the heater are available in Table A.5.

	Nickel coated carbon fibre heater thermal properties
Density (kg/m^3)	1700
Conductivity (W/mK)	18.4
Heat Capacity (J/kgK)	705

Table A.5: Thermal properties of a nickel coated carbon fibre heater. The volume fraction of the nickel is 2% [68]

Appendix B

B.1Analytical Approximation of Penetration Depth of Heat

The assumption that the substrate and the ice are semi-infinite is only valid if the thickness is greater than the penetration depth of the heat. The penetration depth is defined as the thickness beyond which the temperature remains significantly unchanged. In this thesis we define the penetration depth as the thickness beyond which the non-dimensional temperature is 99% of its original value.

Throughout a de-icing cycle the interface condition changes from a constant heat flux condition during the sensible heating, to a constant temperature condition throughout the latent heating phase. Assuming the temperature distribution throughout the heater is uniform, the maximum temperature at the heater interface remains at or below the melting temperature. Therefore we can use a conservative approach and calculate the penetration depth based upon a constant heat temperature at the interface throughout the de-icing cycle.

For a constant temperature at the interface, the temperature distribution through a semi-infinite slab can be calculated from equation B.1:

$$\frac{T(x,t)-T_i}{T_s-T_i} = erfc\left(\frac{x}{2\sqrt{\alpha t}}\right) \qquad \text{Eq. B.1}$$

For the penetration depth, $D_{0.99}$ the non-dimensional temperature is:

$$\frac{T(D_{0.99},t)-T_i}{T_s-T_i} = 0.01$$

$$\mathbf{0.01} = \boldsymbol{erfc}\left(\frac{\boldsymbol{D_{0.99}}}{\boldsymbol{2\sqrt{\alpha t}}}\right)$$

Solving the complimentary error function for which erfc(η) = 0.01, the penetration depth is then:

$$D_{0.99} = 3.6\sqrt{\alpha t} \qquad \text{Eq. B.2}$$

where α is the thermal diffusivity and t is the time required for the heater to be on. From Equation B.2 it can clearly be seen that the penetration depth is entirely controlled by the thermal diffusivity and the length of time. The thermal diffusivity of blade materials and ice types is presented in Table B.1 below:

	Eglass	PVC Foam	Glaze Ice	Rime Ice
k (W/mK)	0.18	0.032	1.88	0.68
ρ (kg/m^3)	2100	150	920	333
C (J/kgK)	1600	1500	2040	738
α (m^2/s)	5.36E-08	1.42E-07	1.00E-06	2.77E-06

Table B.1: Thermal diffusivity of common blade materials and ice types [12], [46]

The penetration depth at which the temperature has risen by 1% of its original value for different materials is presented in Figure B.1.

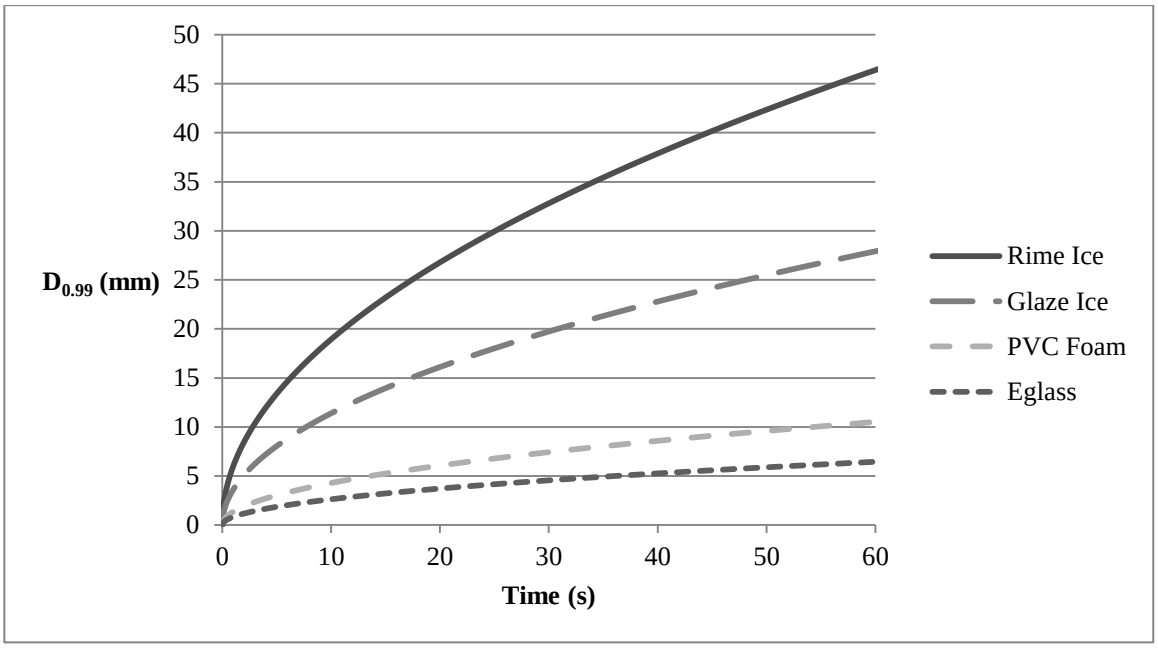

Figure B.1: Penetration depth at which the temperature has risen by 1%

From Figure B.1, the temperature through 5 mm of E-glass skin would require the heater to be on for a minimum of 35 seconds. This is significantly longer than the typical de-icing cycle.

Additionally, the heat will have to penetrate through the core and another layer of fibreglass skin before any significant temperature rise will reach the inner blade wall. Therefore it is safe to assume that any convection at the inner blade wall is negligible.

B.2 Analytical Analysis of One-Directional De-Icing

The one dimensional transient heat conduction equation without energy generation, which is representative of the diffusion of heat through the skin and ice surfaces, is:

$$\frac{\partial^2 T}{\partial x^2} = \frac{1}{\alpha}\frac{\partial T}{\partial t}$$

which assumes that the heating element in thin (a typical heating element in only 0.5 mm thick).

Assuming that the ice is thick enough that it can be treated as semi-infinite and that the heat flux is constant and diffuses in one direction only, the solution to the above equation is of the form:

$$T(x,t) - T_o = \frac{q''}{k}\left[\sqrt{\frac{4\alpha t}{\pi}}\, exp\left(-\frac{x^2}{4\alpha t}\right) - x erfc\left(\frac{x}{2\sqrt{\alpha t}}\right)\right] \qquad \text{Eq. B.3}$$

with the interface at position x=0. The temperature at the interface with time is:

$$T(0,t) - T_o = \frac{q''}{k}\left[\sqrt{\frac{4\alpha t}{\pi}}\right] \qquad \text{Eq. B.4}$$

The time required to reach the melting temperature ($\Delta T = T_{melt} - T_{initial}$) can be calculated simply as:

$$t_{sens} = \left(\frac{k\Delta T}{q''}\right)^2 \frac{\pi}{4\alpha} \qquad \text{Eq. B.5}$$

with a total energy per unit area:

$$Q_{sens} = q''t_{sens} = \frac{1}{q''}(k\Delta T)^2 \frac{\pi}{4\alpha} \quad \text{Eq. B.6}$$

Notice that in the above equation that the energy is inversely proportional to the power of the heater. Therefore the energy to heat the interface to the melting temperature can be minimized by increasing the power density of the heater.

The limiting case for the minimum energy requirement to melt a film of water at the interface is:

$$Q = \delta \rho h_{fl} \quad \text{Eq. B.7}$$

where δ is the required thickness of ice to be melted and is equal to the surface roughness of the interface. A generous estimate of the surface roughness of a wind turbine blade is 100 μm. This translates to an energy density of about 30 kJ/m^2 for glaze ice and 11 kJ/m^2 for rime ice. However in reality there will be loses both into the portion of the ice that does not melt and into the blade. The minimum energy requirement for de-icing provides a target to optimize towards.

B.3 Electro-Thermal De-Icing Numerical Validation

The computational model was compared with the possible analytical solutions to confirm that they are in agreement. For the simple scenario with no losses into the blade and before the ice begins to melt, the numerical results can be compared with the analytical solution. Equation B.3 defines the temperature profile through the ice at a specific time, t and the variation of temperature at a specific point through time.

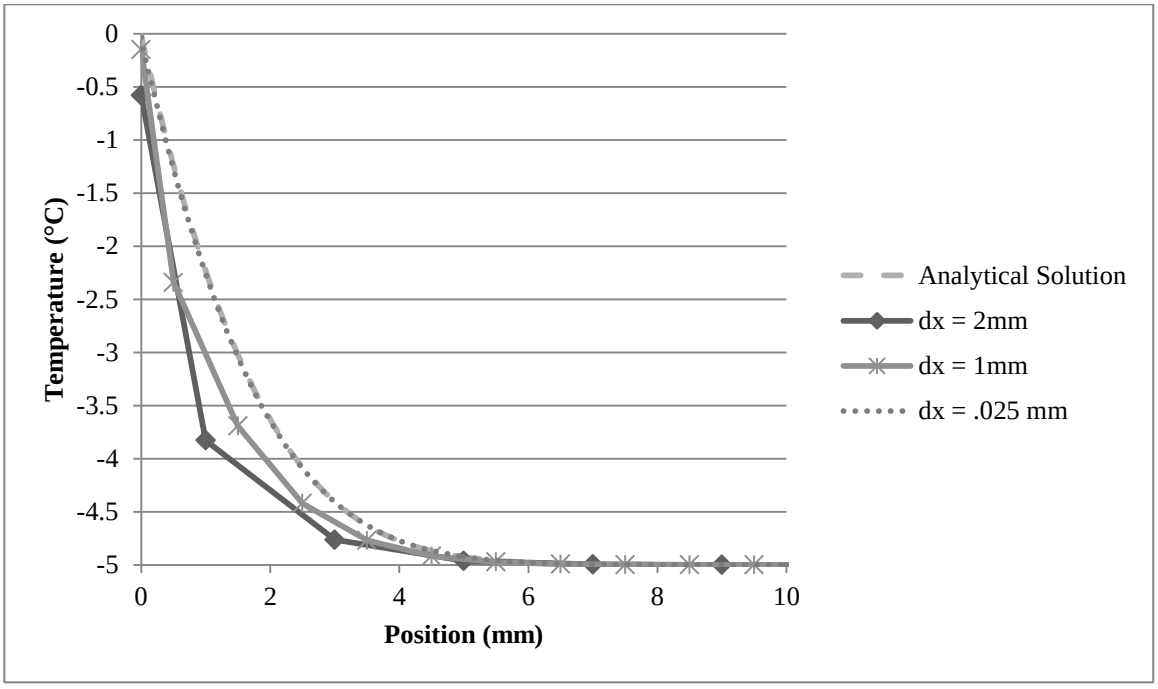

Figure B.2: Comparison of the numerical result with the analytical solution. The heater power is 5000 W/m^2, the thickness of the glaze ice is 2cm and the initial temperature is -5°C. Temperature profiles are at t=2.75s.

As the grid size decreases the numerical solution approaches the analytical result. When the grid size is .025 mm the numerical solution is nearly identical to the analytical result.

The algebraic formula used to determine the node-coordinates is:

$$\frac{x(i)}{L} = \left[\frac{i-1}{N}\right]^{inf} \qquad \text{Eq. B.8}$$

where i is the integer node location, N is the number of nodes, L is the length and inf is the inflation factor used to increase the number of nodes towards a certain side. For example, the insulation domain which is before the heater has an inflation factor of 0.5. The ice domain, which is after the heater, has an inflation factor of 2. This refines the grid spacing on either side of the heater, which is the expected location of steep temperature gradients. In order to effectively demonstrate the effect of grid refinement, the inflation factor in Figure B.2 is equal to 1.

B.4 Fraction of Heat Diffusion

It is useful to quantify the proportion of heat that is lost into the blade in order to make an educated decision as to whether or not to insulate the heater from the blade surface. As discussed in chapter 2 the blade is comprised of a PVC foam core that is sandwiched by a 5mm layer of E-glass on either side. The E-glass is a moderate insulator with a conductivity of 0.18 W/mK while the PVC is an excellent insulator with a conductivity of 0.032 W/mK.

The fraction of heat that is diffused into the blade rather than into the ice can be determined by comparing the thermal inertia of the ice to that of the interface. Assuming that the heater is at uniform temperature so that the temperature of the heater/ice and heater/blade interfaces are equal:

$$\left(\frac{k\Delta T}{q"}\right)^2 \frac{\pi}{4\alpha}\bigg|_{ice} = \left(\frac{k\Delta T}{q"}\right)^2 \frac{\pi}{4\alpha}\bigg|_{blade} \qquad \text{Eq. B.9}$$

The ratio of heat flux into the ice and blade is then:

$$\frac{q"_{ice}}{q"_{blade}} = \frac{\sqrt{k_{ice}\rho_{ice}C_{ice}}}{\sqrt{k_{blade}\rho_{blade}C_{blade}}} \qquad \text{Eq. B.10}$$

The energy in the heater itself can be approximated with the following equation:

$$Q_{heater} = \rho_{heater}\, C_{heater} L_{heater}\, \Delta T \qquad \text{Eq. B.11}$$

For the duration of the heating process the temperature of the heater does not rise significantly above the temperature of the adhesion layer. If the initial temperature is -5°C, the temperature rise is approximately 5°C.

Q_{heater} = (1700 kg/m^3)(705 J/kgK)(.0005m)(5K)

Q_{heater} = 3 kJ/m^2

which is negligible compared to total energy consumed by the heater. The total amount of heat input is equal to the sum of the heat going into the ice and into the blade. The fraction of heat going into the ice is then:

$$f = \frac{q"_{ice}}{q"_{tot}} = \frac{1}{\sqrt{\frac{k_{blade}\rho_{blade}C_{blade}}{k_{ice}\rho_{ice}C_{ice}}}+1} \qquad \text{Eq. B.12}$$

where $\sqrt{k_{ice}\rho_{ice}C_{ice}}$ and $\sqrt{k_{blade}\rho_{blade}C_{blade}}$ are the thermal inertias of the ice and the substrate material, respectively. The thermal inertia of potential ice and substrate materials are compared in Table B.2:

Material	Conductivity (W/mK)	Density (kg/m^3)	Heat Capacity (J/kgK)	Thermal Inertia $\left(\frac{J}{m^2 K s^{1/2}}\right)$
PVC foam	0.032	150	1500	85
Cellular glass (insulation)	0.058	144	1000	91
Expanded rubber (insulation)	0.032	72	1.68	62
Eglass	0.18	2100	1600	780
Glaze Ice	1.88	920	2040	1900
Low Density Rime Ice	0.696	333	1380	570

Table B.2: Thermal inertia of blade materials and ice of different types [12, 46]

Using Equation B.12, the heat flux fraction is determined for each substrate/ice combination.

Fraction of Useful Heat		
Surface\Ice type	Glaze Ice	Rime Ice
PVC foam (insulator)	0.96	0.87
Standard blade skin material (Eglass)	0.71	0.42

Table B.3: Approximation of the fraction of heat going into the ice for different insulator/ice combinations

The high thermal inertia of glaze ice means that approximately 71% of the heat goes into heating the ice, even with the standard blade skin. Insulating between the heater and the blade skin with PVC foam will increase the amount of useful energy by approximately 25%.

B.5 Refreezing time

Once the heater power has been turned off the ice layer continues to diffuse heat and there is the potential risk that the ice may refreeze to the blade. The refreezing time can be approximated using the one dimensional transient heat conduction equation with a constant surface temperature. The heat flux from the adhesion layer is then:

$$q_{out}(t) = \frac{k_i \Delta T}{\sqrt{\pi \alpha_i t}} + \frac{k_s \Delta T}{\sqrt{\pi \alpha_s t}} \qquad \text{Eq. B.13}$$

where the subscript i denotes the ice, s is the substrate, k is the conductivity, α is the thermal diffusivity and t is the time, once the heater has been turned off.
$\Delta T = T_{melt} - T_o$ is the temperature difference and T_o is the ambient temperature.

From conservation of energy, the refreezing time, t_f can be calculated based on the continuous diffusion of heat once the heater has been turned off. The approximation is based on the assumption that the ice and the substrate can be represented as semi-infinite.

$$t_f = \frac{\left(\rho_i \delta * h_{fl}\right)^2}{4\Delta T^2 \left(\sqrt{k_i \rho_i C_i} + \sqrt{k_s \rho_s C_s}\right)^2} + \frac{\rho_i \delta * h_{fl} \sqrt{\pi} \sqrt{t_m}}{\Delta T \left(\sqrt{k_i \rho_i C_i} + \sqrt{k_s \rho_s C_s}\right)} \qquad \text{Eq. B.14}$$

where $t_m$is the duration of time that the heater is turned on and δ is the thickness of the adhesion layer.

From the previously determined de-icing times, the refreezing time has been calculated for the associated heater power density and ambient condition, the results are recorded in Table B.4 below:

Refreezing time (s)				
q" (kW/m^2)	T_o = - 2.5°C	T_o = - 5°C	T_o = - 7.5°C	T_o = - 10°C
1	130	78.1	65.0	60.3
1.25	116	66.8	54.4	49.1
2.5	84.5	42.7	32.5	28.2
5	65.8	29.2	20.6	17.0
7.5	58.3	24.1	16.2	13.0
10	54.1	21.4	13.9	10.9
15	49.3	18.3	11.4	8.65
20	46.6	16.6	10.1	7.45

Table B.4: Refreezing time calculated from Equation B.14. The ice thickness is 2 cm and the ice type is glaze. Substrate is fibreglass.

The refreezing time is proportional to the de-icing time. A high heater power density will have a relatively short penetration depth of heat, i.e. a shorter de-icing time. For sequential heating applications the adjacent heaters will have to be left on for an additional time period so that the neighbouring sections do not refreeze.

B.6 Description of Secondary Effect

Typically, a thicker layer of ice will reduce the amount of time required to de-ice the blade, by limiting the heat loss due to convection. However a secondary effect is observed when the ice is thin enough that convection effects the de-icing time and the heater power density is below $q''_{A/I} = h_o(T_{melt} - T_o)$. In this region a slightly thicker section of ice allows the ice to remain in the initial, highly transient time domain. This means that the ice will see a steeper temperature gradient for longer so that there is increased overall conduction. A larger conduction heat flux causes more heat loss from the adhesion layer hence a longer de-icing time.

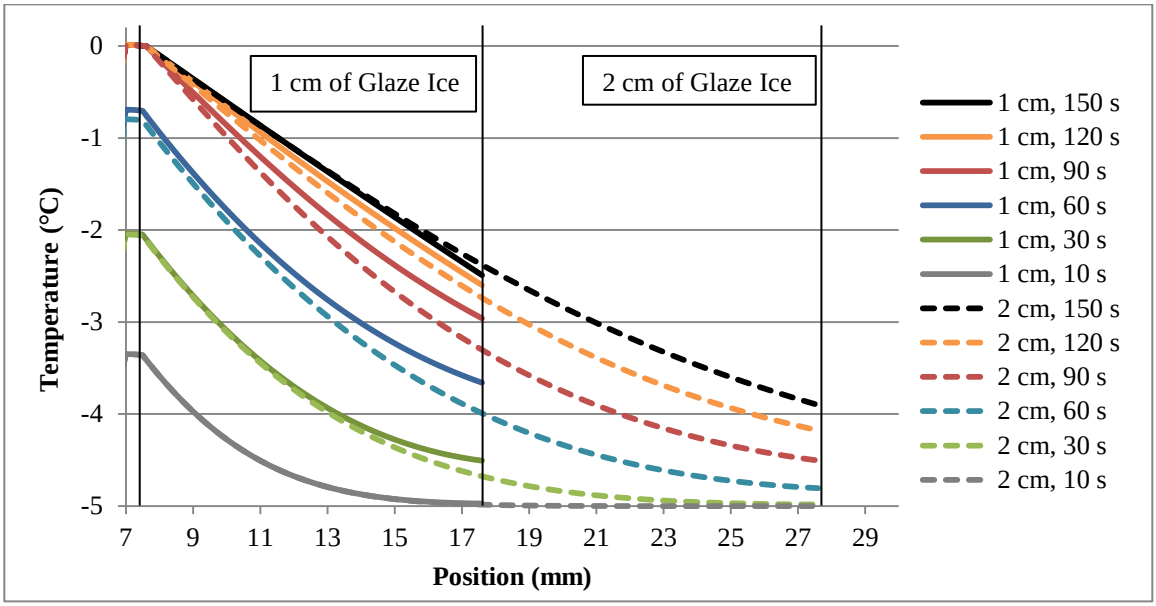

Figure B.3: Temperature profiles through 1cm (solid lines) and 2cm (dashed lines) of glaze ice. Heater power density is 1000 W/m^{2}K, ambient temperature is -5°C and the external heat transfer coefficient is 180 W/m^{2}K

From Figure B.3 it can be observed that initially the temperature profile of the 1 cm and 2 cm thick glaze ice accretions are the same (10 s contour line). However after this point the temperature profiles of the thinner (1 cm) layer of glaze ice will flatten out at the outer ice surface/air interface. Due to conservation of energy, convection at the outer ice surface must equal the heat flux due to conduction at this point. When the outer ice surface temperature is close to the ambient temperature, convection at the outer ice/air interface is very low. This causes the temperature profile of the thinner ice layer to flatten out, reducing the amount of conduction that is lost from the adhesion layer.

If the icing time where longer, conduction from the 1 cm ice layer would surpass the amount of conduction from the adhesion layer for the 2 cm layer of ice, this effect is observed at the 150 s temperature profile line. The thicker layer of ice increases the resistance between the adhesion layer, which will reduce the steady state conduction heat flux (primary relationship). However the total de-icing time of the 1 cm and 2 cm ice layer is approximately 160 and 170 seconds, respectively. Therefore the secondary effect has a greater influence in this case scenario than the primary relationship between ice thickness and de-icing time.

Appendix C

C.1 Steady State Solution

When the resistance of the blade wall is large, the heating from the hot air de-icing system will reach steady state heat transfer with the convection from the blade surface and de-icing will not occur. An example of this is presented in Figure C.1:

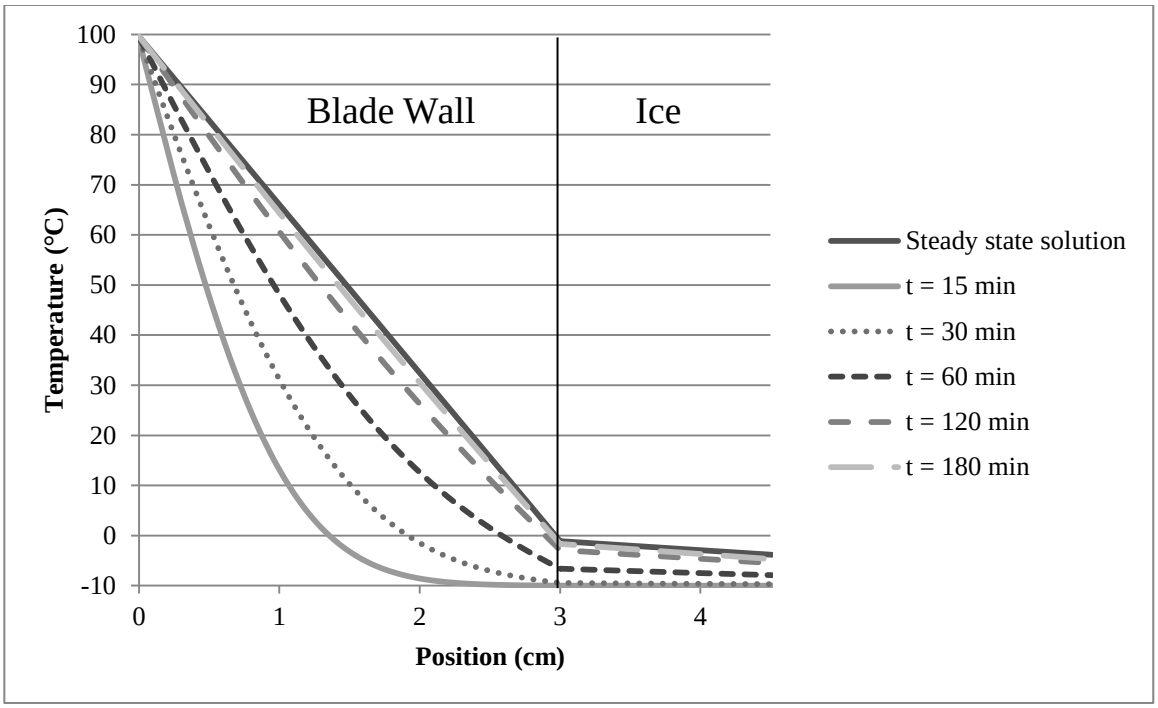

Figure C.1: Numerical solution of hot air de-icing approaching the steady state solution. Ambient temperature is -10°C and the inner blade wall is fixed at 100°C. The equivalent conductivity of the blade wall is 0.044 W/mK and the icing conditions are favourable. The blade wall is homogenous and has a thermal resistance of 0.68 m^2K/W.

The steady state solution is obtained analytically for conduction through a homogenous wall and ice. The inner surface temperature is 100°C while the heat loss at the ice surface is due to external forced convection with a heat transfer coefficient of 23 W/m^2K. The fact that the numerical analysis approaches the analytical steady state solution suggests that the model is working properly.

C.2 Multi-Sectional Analysis

To determine the power requirement of a hot air de-icing system, a multi-sectional analysis is required. The multi-sectional analysis is essentially the same as the single sectional analysis however the hot air temperature is calculated from the heat lost and the temperature of the preceding section. Once the air reaches the tip of the blade, the air is recirculated to the root and the air is re-heated. The amount of re-heat is dependent upon the power input from the heater. For a range of heater powers the temperature at the two third's span position of a 38 m, example wind turbine is presented below:

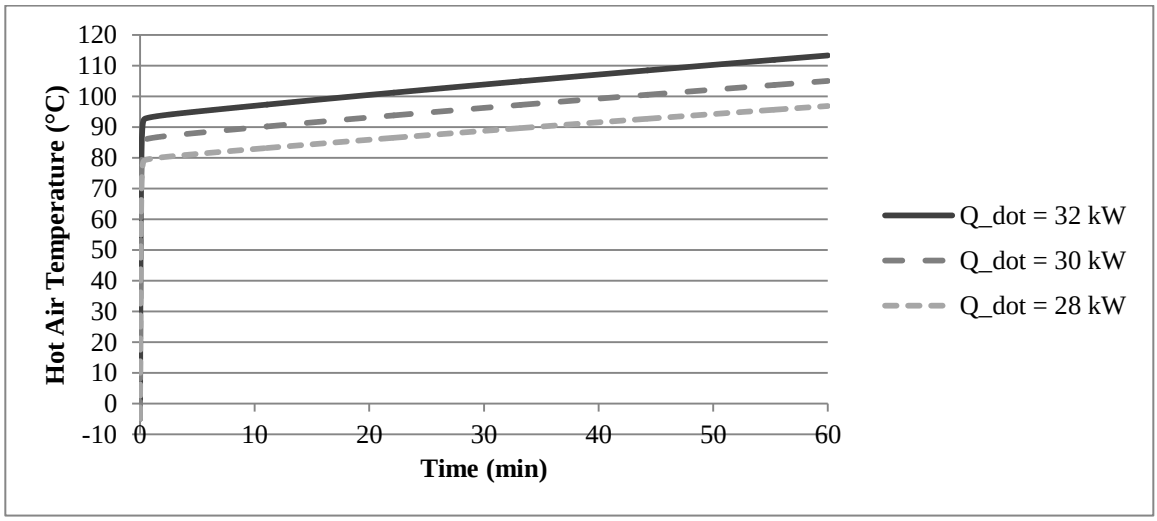

Figure C.2: Numerically determined inner air temperature of a hot air de-icing system. The span position is two third's the blade radius of a 38 m, 1.5 MW wind turbine blade. 1.5 cm of glaze ice has formed on the outside of the blade, the ambient wind speed is 5 m/s and the ambient temperature is -5°C.

From Figure C.2 it can be observed that for a 30 kW heater, the hot air temperature of the blade increases to approximately 100°C. Initially the air temperature heats up quickly however after this initial phase the hot air temperature begins to level off. The hot air temperature is dependent upon the construction of the wind turbine blade, the ambient temperature, the type and thickness of the ice accretion, the power of the heater, the flow rate that the blower can provide and the design of the hot air channel. Therefore the results of this specific case scenario are only to provide an example of the heater power requirement of a hot air de-icing system.